A Study of Models of Nucleon Structure Functions

Baishali Saikia

Department of Physics

Gauhati University

This thesis is submitted to

Gauhati University as requirement for the degree of

Doctor of Philosophy

Faculty of Science

January 2018

Certificate

This is to certify that the thesis titled "A Study of Models of Nucleon Structure Functions" is the result of research work of Baishali Saikia, carried under our supervision, submitted to Gauhati University for the award of the degree of Doctor of Philosophy in Physics.

This thesis conforms to the standard of PhD Thesis under Gauhati University including the standard related to plagiarism and has a similarity index not more than 20% (twenty percent), excluding the bibiliography.

(Retd.)
29.01.2018

Prof. Dilip Kumar Choudhury, Supervisor

Professor
Department of Phys.
Gauhati University

29.01.2018

Dr. Kushal Kalita, Co-Supervisor

January 2018

Assistant Professor
Department of Physics
Gauhati University

Declaration

I hereby declare that this thesis is the result of my own research work which has been carried out under the guidance of Prof. Dilip Kumar Choudhury and Dr. Kushal Kalita, of Gauhati University. I further declare that this thesis as a whole or any part thereof has not been submitted to any university (or institute) for the award of any degree or diploma.

This thesis contains less than 90,000 (ninety thousand) words excluding bibliography and captions.

Baishali Saikia
29.01.2018

Baishali Saikia

January 2018

To my loving parents
&
my beloved elder sister *$\mathscr{L}$ate Panchali Saikia* ...

Acknowledgements

First of all, I would like to express my deep gratitude to my respected supervisor Prof. Dilip Kumar Choudhury, Gauhati University, for his invaluable guidance. But for his unstinted help and continuous encouragement for perfection and hard work, it would not have been possible for me to complete the thesis within the stipulated time.

I would also like to extend my sincere gratitude to my co-supervisor Dr. Kushal Kalita, for his valuable suggestions and encouragement in different aspects.

I would also like to convey my sincere gratitude to the Head of the Department Prof. Madhurjya P Bora, as well as Prof. Ngangkham Nimai Singh and Prof. Anurup Gohain Barua (former HODs during my research period) for providing me with all the necessary research facilities.

I am extremely grateful to all the faculty members of the Department, specially to Prof. Buddhadeb Bhattacharjee, Dr. Kalpana Bora and Dr. Sanjeev Kalita, for their valuable suggestions and immense encouragement.

I am very much thankful to my friends and seniors, specially to Sashikant bhaiya, Satyanand bhaiya, Kalyan dada, Dr. Subhankar Roy, Dr. Akbari Jahan, Dr. Nabaratna Bhagawati, Dr. Chandan Duarah, Dr. Debajyoti Dutta, Dr. Neelakshi N K Borah, Dr. Tapan Rajbongshi, Dr. Paragjyoti Chutia, Mausumi, Mintu, Tapashi, Luxmi, Jugal, Gayatri, Kuldeep, Murchana, Ruby, Angana and also Dipjyoti Deka for their unfailing support and encouragement.

I would like to place on record my sincere gratitude to the University Grand Commission for providing me the necessary financial support for my research work.

I would also like to place on record my gratitude to the Gauhati University office staff for their help extended to me in various matters.

I would also like to offer my sincere thanks to one and all, who have directly or indirectly lent their hand in this venture.

Last but not the least, I have no words to express my gratitude to my loving parents for their unceasing supports, encouragement and attention. Their unfailing appreciation has given me a strong motivation to carry on with the work diligently.

Above all, I am grateful to the God for granting me good health and well-being to complete my thesis.

Abstract

The research work of this thesis is “A Study of Models of Nucleon Structure Functions". In this thesis, we will study several models of structure functions of the proton specially at small x from the point of view based on the concept of self-similarity [1]. We will introduce the definition of self-similarity and its application in Unintegrated Parton Distribution Functions (uPDF), Parton Distribution Functions (PDFs) and structure function of proton. The predictions of the models will be compared with most recent experimental data as well as other phenomenological and QCD based models. We will also give outlines of the following topics in chapter 1: (1) QCD evolution equations: Dokshitzer-Gribov-Lipatov-Altarelli-Parisi (DGLAP) and BFKL with the kinematics of Deep Inelastic Scattering (DIS) and Semi-Inclusive Deep Inelastic Scattering (SIDIS).

(2) Transverse Momentum Dependent Parton Distributions Functions (TMDs) with the kinematics of DIS and SIDIS and its evolution equation.

(3) Froissart bound and its applicability in DIS.

In chapter 2, we will study the self-similarity based model of proton structure function suggested in Ref. [1], fitted by H1 and ZEUS data [57, 58] which will be again refitted by recent HERA data [59] to verify the changes in defining parameters and phenomenological ranges of validity.

In chapter 3, we will study the limitations of the models described in chapter 2 and redefine a model which is free from singularity in the entire x-range : $0 < x < 1$.

In chapter 4, we will improve the earlier models of chapters 2 and 3 such that they are singularity free and have got a wider phenomenological ranges of validity.

In chapter 5, we will outline the method of incorporation of Froissart-Martin bound in the self-similarity based models of proton structure functions discussed in chapter 4.

In chapter 6, we will calculate the momentum fractions carried by quarks and gluons in the models described in chapters 2 to 5. We will compare the results with the predictions of Perturbative QCD, Lattice QCD and Ads/QCD models.

In chapter 7, we will discuss how Transverse Momentum Dependent Parton Distributions Functions (TMDs) can be introduced in the self-similarity based models of proton structure functions discussed in chapter 2 and 4.

In Chapter 8, we will outline the change of the structure of the TMDs discussed in chapter 7 if Froissart compatibility is also additionally introduced. We will discuss the difference between the two in this chapter.

Chapter 9 contains the conclusion of the thesis along with the future outlook of it.

Table of contents

List of figures

List of tables

1
INTRODUCTION

The research work of this thesis is “A Study of Models of Nucleon Structure Functions". In this thesis we study several models of structure functions of the nucleon specially at small x from the point of view based on the concept of self-similarity [1]. The predictions of the models are then compared with most recent experimental data as well as other phenomenological and QCD based models. We will also study Transverse Momentum Dependent Parton Distribution Functions (TMDs) in later part of the work.

1.1 Self-similarity and its application

The self-similarity is an inherent property of fractal geometry invented by Benoit Mandelbrot [2] in 1975. When an object is subdivided into many parts and if the shape of each part is equal to the original shape of the object then each small part will be called the self-similar to the original one.

For self-similar objects, the dimension can be measured by using the formula :

$$D = \frac{\log M^D}{\log M} = \frac{\log(\text{number of self-similar objects})}{\log(\text{magnification factor})} \tag{1.1}$$

where D is the fractal dimension. For every fractal object, D must be expressed in terms of fraction. Thus a fractal may have two inherent properties: One that is self-similarity and the other is dimension that should be in fraction i.e fractal dimension. This is true for ideal mathematical objects like Koch curve (D=1.26), Sierpinski gasket (D=1.58), Cantor set (D=0.63) etc.

The definition of dimension can be generalized for the case of non-discrete fractals. In this generalization, the magnification (scaling) factor is real number z and the number of self-similar objects is $f(z)$. Taking into account that the dimension may change with scaling, a local dimension is defined as [1]

$$D(z) = \frac{\partial \log f(z)}{\partial \log z} \tag{1.2}$$

For ideal mathematical fractals, $D(z)$ is constant for the whole fractal. If an object have a fractal structure for a certain region of magnification, then the dimension is approximately constant, $D(z) = D$ and

$$f(z) = D.\log z + D_0 \tag{1.3}$$

D_0 is normalization of $f(z)$, which thus has power law behavior, $f(z) \propto z^D$.

In general, fractals may have two independent magnification factors, z and y. In this case, the density function $f(z,y)$ will be [1]

$$\log f(z,y) = D_{zy}.\log z.\log y + D_z.\log z + D_y.\log y + D_0 \tag{1.4}$$

D_{zy} represents the dimensional correlation relating the z and y factors. The function $f(z,y)$ satisfies a power law behavior in z for fixed y and in y for fixed z. In such approach, however, there is a certain freedom in relating the magnification factors. Using this approach, the concept of self-similarity can be applied to self-similar Unintegrated Parton Distribution Function (uPDF) as well as Parton Distribution Functions (PDFs) and Structure Functions [1].

1.2 self-similar Unintegrated Parton Distribution Functions (uPDF), Parton Distribution Functions (PDFs) and Structure Functions

In QCD, parton model deals with Deep Inelastic Scattering (DIS: $lN \to lX$ in Fig. 1.1) from which one can obtain the information about the structure of nucleons (proton and neutron), basically about the partonic quark-gluon structure of the nucleon or how partons carry nucleon momentum inside it. The inclusive process like DIS can give only the longitudinal component of nucleon momentum; the Bjorken x. This kind of momentum information is enclosed in parton distribution functions (PDFs) $q_i(x,Q^2)$; which is a function of both x and Q^2, where Q^2 is the four momentum transfer square from the initial to the final lepton. This PDFs give the number density of partons inside the nucleon.

The unintegrated Parton Distribution Function (uPDF) $f_i(x,Q^2)$ is unintegrated over the virtual momentum Q^2. It is related to the conventional quark density by

$$q_i(x,Q^2) = \int_0^{Q^2} f_i(x,Q^2)dQ^2 \tag{1.5}$$

Using Eq. 1.5, one can define the structure function of the nucleon as follows:

$$F_2(x,Q^2) = x\sum_i e_i^2 \left(q_i(x,Q^2) + \bar{q}_i(x,Q^2)\right) \tag{1.6}$$

which involves both quarks and anti quarks.

When the proton is probed at very high energy, there will be a high probability of emissions and splittings of gluons which may help in the formation of sea quark densities from the level of valence quarks. The deeper the proton is probed, the more gluon-gluon interactions can be observed which leads to the formation of more number of sea quarks densities and therefore this may follow the self-similarity property. The behavior of unintegrated quark density w.r.t x and Q^2 in log-log scale can be tested and found to have linearity. Hence one can suggest that the x and Q^2 can be treated as the magnification factors.

Next comes the proper choice of magnification factors: they should be positive, non-zero and have no physical dimension. $\frac{Q^2}{Q_0^2}$ and $\frac{1}{x}$ satisfy all these conditions. But based on the notion that for small x, the partons should show more self-similarity behavior, $\frac{1}{x}$ shows it, which is also inconsistent with Glück-Reya-Vogt (GRV) [3] parameters. To avoid $Q^2 = 0$, the author then use $1 + \frac{Q^2}{Q_0^2}$ as a reasonable magnification factor but alternate choice of $\frac{Q^2}{Q_0^2 + Q^2}$ is also equally possible.

Choosing the 1st choice, the following general form of unintegrated quark density was suggested by Lastovicka (Eq. 6 of Ref. [1]):

$$\log f_i(x, Q^2) = D_1 . \log \frac{1}{x} . \log \left(1 + \frac{Q^2}{Q_0^2}\right) + D_2 . \log \frac{1}{x} + D_3 . \log \left(1 + \frac{Q^2}{Q_0^2}\right) + D_0^i \qquad (1.7)$$

leading to

$$f_i(x, Q^2) = e^{D_0^i} \left(\frac{1}{x}\right)^{D_1 \log\left(1+\frac{Q^2}{Q_0^2}\right)} \left(\frac{1}{x}\right)^{D_2} \left(1 + \frac{Q^2}{Q_0^2}\right)^{D_3} \qquad (1.8)$$

Integrating over the virtuality of the quark

$$q_i(x, Q^2) = \int_0^{Q^2} f_i(x, Q^2) dQ^2 \qquad (1.9)$$

or

$$q_i(x,Q^2) = \frac{e^{D_0^i}\, Q_0^2 \left(\frac{1}{x}\right)^{D_2}}{\left(1+D_3+D_1\log\left(\frac{1}{x}\right)\right)} \left(\left(\frac{1}{x}\right)^{D_1 \log\left(1+\frac{Q^2}{Q_0^2}\right)} \left(1+\frac{Q^2}{Q_0^2}\right)^{D_3+1} - 1\right) \tag{1.10}$$

In that work, virtuality of the quark (Q^2) and not the transverse momentum (k_t^2) was the integrating variable.

Using Eqn 1.8 in the usual definition of the structure function $F_2(x,Q^2)$ (Eq. 1.6), one can get

$$F_2(x,Q^2) = \frac{e^{D_0}\, Q_0^2\, \left(\frac{1}{x}\right)^{D_2-1}}{\left(1+D_3+D_1\log\left(\frac{1}{x}\right)\right)} \left(\left(\frac{1}{x}\right)^{D_1 \log\left(1+\frac{Q^2}{Q_0^2}\right)} \left(1+\frac{Q^2}{Q_0^2}\right)^{D_3+1} - 1\right) \tag{1.11}$$

where

$$e^{D_0} = \sum_{i=1}^{n_f} e_i^2 \left(e^{D_0^i} + e^{\bar{D}_0^i}\right) \tag{1.12}$$

Eq. 1.12 involves both quarks and anti-quarks.

1.2.1 Improvement to take into account the correct dimensionality of uPDF, PDF and structure function

In Eq. 1.9, the definition of integrated parton distribution functions, there is a dimension anomaly: the left hand side of the equation is dimensionless while the right hand side has got the dimension of energy square. To make the integrated PDF ($q_i(x,Q^2)$) and unintegrated PDF ($f_i(x,Q^2)$) dimensionless in Eq.1.9, we will introduce a mass parameter M^2(=1 GeV^2) [80] in the equation such that both $q_i(x,Q^2)$ and $f_i(x,Q^2)$ becomes dimensionless.

Therefore, we have redefined uPDF , PDF and structure function as follows:

uPDF

$$\log[M^2.f_i(x,Q^2)] = D_1.\log\frac{1}{x}.\log\left(1+\frac{Q^2}{Q_0^2}\right)+D_2.\log\frac{1}{x}+D_3.\log\left(1+\frac{Q^2}{Q_0^2}\right)+D_0^i \quad (1.13)$$

leading to

$$f_i(x,Q^2) = \frac{e^{D_0^i}}{M^2}\left(\frac{1}{x}\right)^{D_1\log\left(1+\frac{Q^2}{Q_0^2}\right)}\left(\frac{1}{x}\right)^{D_2}\left(1+\frac{Q^2}{Q_0^2}\right)^{D_3} \quad (1.14)$$

Therefore PDF

$$q_i(x,Q^2) = \frac{e^{D_0^i}\,Q_0^2\left(\frac{1}{x}\right)^{D_2}}{M^2\left(1+D_3+D_1\log\left(\frac{1}{x}\right)\right)}\left(\left(\frac{1}{x}\right)^{D_1\log\left(1+\frac{Q^2}{Q_0^2}\right)}\left(1+\frac{Q^2}{Q_0^2}\right)^{D_3+1}-1\right) \quad (1.15)$$

and Structure function

$$F_2(x,Q^2) = \frac{e^{D_0}\,Q_0^2\left(\frac{1}{x}\right)^{D_2-1}}{M^2\left(1+D_3+D_1\log\left(\frac{1}{x}\right)\right)}\left(\left(\frac{1}{x}\right)^{D_1\log\left(1+\frac{Q^2}{Q_0^2}\right)}\left(1+\frac{Q^2}{Q_0^2}\right)^{D_3+1}-1\right) \quad (1.16)$$

1.3 QCD evolution equations

1.3.1 (Dokshitzer-Gribov-Lipatov-Altarelli-Parisi (DGLAP) evolution equations of Singlet and Non-singlet structure functions

The DGLAP equation [4–6] basically defines the Q^2-evolution of the parton distribution functions, given a PDF at $Q^2 = Q_0^2$, one can study how it evolves with the virtuality Q^2. The distribution $q_i(x,t_0)$ is not obtained from the DGLAP equation. It is non-perturbative in origin which has different parametrization available in current literature.

A. DGLAP equation of Non-singlet structure function

The non-singlet flavor dependent contribution is defined as,

$$F_2^{NS}(x,Q^2) = x\sum_i (q_i(x,Q^2) - \bar{q}_i(x,Q^2)) \tag{1.17}$$

where q_i is the density of quark of ith flavor (PDF).

Introducing the variable $t = \ln\frac{Q^2}{\Lambda^2}$, the DGLAP evolution equation for the non-singlet structure function at LO can be written as:

$$\frac{\partial F_2^{NS}(x,t)}{\partial t} = \frac{A_f}{t}\left[\{3+4\ln(1-x)\}F_2^{NS}(x,t) + 2\int_x^1 \frac{dz}{1-z}\left\{(1+z^2)F_2^{NS}\left(\frac{x}{z},t\right) - 2F_2^{NS}(x,t)\right\}\right] \tag{1.18}$$

Here, $A_f = \frac{4}{3\beta_0}$, $\beta_0 = 11 - \frac{2}{3}N_f$, N_f being the number of flavors and $\alpha_s(t) = \frac{4\pi}{\beta_0 t}$.

B. Coupled DGLAP equations for Singlet and gluon structure functions

The DGLAP evolution equations for quark singlet $F_2^S(x,Q^2)$ and gluon $G(x,Q^2)$ densities are as follows:

For quark singlet

$$\frac{\partial F_2^S(x,t)}{\partial t} - \frac{A_f}{t}\left[\{3+4\ln(1-x)\}F_2^S(x,t) + I_1^S(x,t) + I_1^G(x,t)\right] = 0 \tag{1.19}$$

where,

$$I_1^S(x,t) = 2\int_x^1 \frac{dz}{1-z}\left[(1+z^2)F_2^S(\frac{x}{z},t) - 2F_2^S(x,t)\right], \tag{1.20}$$

$$I_1^G(x,t) = \frac{3}{2}N_f\int_x^1 dz[z^2+(1-z)^2]G(\frac{x}{z},t), \tag{1.21}$$

$F_2^S(x,t)$ is the singlet structure function of the proton which can be written as:

$$F_2^S(x,Q^2) = x\sum_i \left(q_i(x,Q^2) + \bar{q}_i(x,Q^2)\right) \tag{1.22}$$

The DGLAP evolution equation for the gluon distributions have the standard form in LO:

$$\frac{\partial G(x,t)}{\partial t} - \frac{\alpha_s(t)}{2\pi} I_1^G(x,t) = 0 \tag{1.23}$$

where,

$$\begin{aligned} I_1^G(x,t) &= 6\left\{\frac{11}{12} - \frac{N_f}{18} + \ln(1-x)\right\} G(x,t) + 6\int_x^1 dz \frac{zG(\frac{x}{z},t) - G(x,t)}{1-z} \\ &+ 6\int_x^1 dz \left\{z(1-z) + \frac{(1-z)}{z}\right\} G(\frac{x}{z},t) + \frac{4}{3}\int_x^1 dz \frac{1+(1-z)^2}{z} F_2^S(\frac{x}{z},t) \end{aligned} \tag{1.24}$$

1.3.2 BFKL equation

The BFKL equation [8–10] is basically derived for the unintegrated gluon distribution function $f(x,k_t^2)$ where k_t^2 is the transverse momentum of gluons. It is defined as

$$f(x,k_t^2) = f^{(o)}(x,k_t^2) + \bar{\alpha}_s(k_t^2)\int_x^1 \frac{dz}{z} \int \frac{dk_t'^2}{k_t'^2} \left[\frac{f(\frac{x}{z},k_t'^2) - f(\frac{x}{z},k_t^2)}{|k_t'^2 - k_t^2|} + \frac{f(\frac{x}{z},k_t^2)}{\left[4k_t'^4 + k_t^4\right]^{1/2}}\right] \tag{1.25}$$

where $f^{(o)}(x,k_t^2)$ is the unintegrated gluon distribution function at $k_t^2 = k_0^2$ and $\bar{\alpha}_s = 3\alpha_s/\pi$.

The gluon distribution function $f(x,k_t^2)$ is unintegrated over its transverse momentum k_t. It is related to the conventional gluon density $g(x,Q^2)$ by

$$xg(x,Q^2) = \int_0^{Q^2} f(x,k_t^2)\frac{dk_t^2}{k_t^2} \tag{1.26}$$

More recent study of transverse momentum parton distribution functions [12] has however, indicated the refinement of the above relation between unintegrated and integrated version of PDFs contains both quarks and gluons.

In more recent time, improved evolution equations like GLR [13] and JIMWKL [14] equations have also been suggested having various degrees of theoretical refinement compared to DGLAP equation. But at the phenomenological level, DGLAP equation appears to be more successful both at the HERA and LHC region. However, DGLAP equation has inherent limitations as it rests on Q^2 evolution of integrated parton distribution functions: many other important aspects of the proton structure function is not revealed by it. PDF is generally an average of all degrees of freedom except the longitudinal one. Since proton is a 3-dimensional object, other degrees of freedom like its transverse component of momentum needs to be incorporated in a proper generalization of PDFs.

In recent years, a serious systematic attempt to study the transverse structure of the proton has been done both theoretically and experimentally. The crucial aspects of this is looking for observables which are sensitive to the transverse structure of the nucleon. While the longitudinal part of the nucleon has been well studied in DIS, transverse part needs experiment of Semi Inclusive Deep Inelastic Scattering (SIDIS: $lN \to lhX$ in Fig. 1.1) in which one observes a hadron at the final stage besides the lepton.

In this case, a hadron resulting from the fragmentation of a scattered quark retains the original motion of the quark including its transverse motion. The fragmentation function is defined by $D_{h/q}$ which gives the number density of hadrons resulting from the hadronization of the partons with transverse momentum (k_t'). Using factorization theorem in QCD [15–18], the SIDIS differential cross-section can be expressed as :

$$d\sigma^{lp\to lhX} = \sum_q f_{q/p}(x,k_t;Q^2) \otimes d\hat{\sigma}^{lq\to lq} \otimes D_{h/q}(z_h,k_t';Q^2) \tag{1.27}$$

in which the non-perturbative, long-distance physics (contained in $f_{q/p}$ and $D_{h/q}$) is convoluted with the elementary, short-distance, hard-scattering interaction ($d\hat{\sigma}^{lq\to lq}$). The parton distributions (PDFs) $f_{q/p}$ and fragmentation functions (FFs) $D_{h/q}$ depend not only on Q^2 and the longitudinal momentum fraction (respectively x and z_h) but also on transverse motion of partons inside the nucleon (k_t) and of the final hadron with respect to the fragmentation parton (k_t'). These Transverse Momentum Dependent parton distributions and fragmentation functions are usually abbreviated as TMDs.

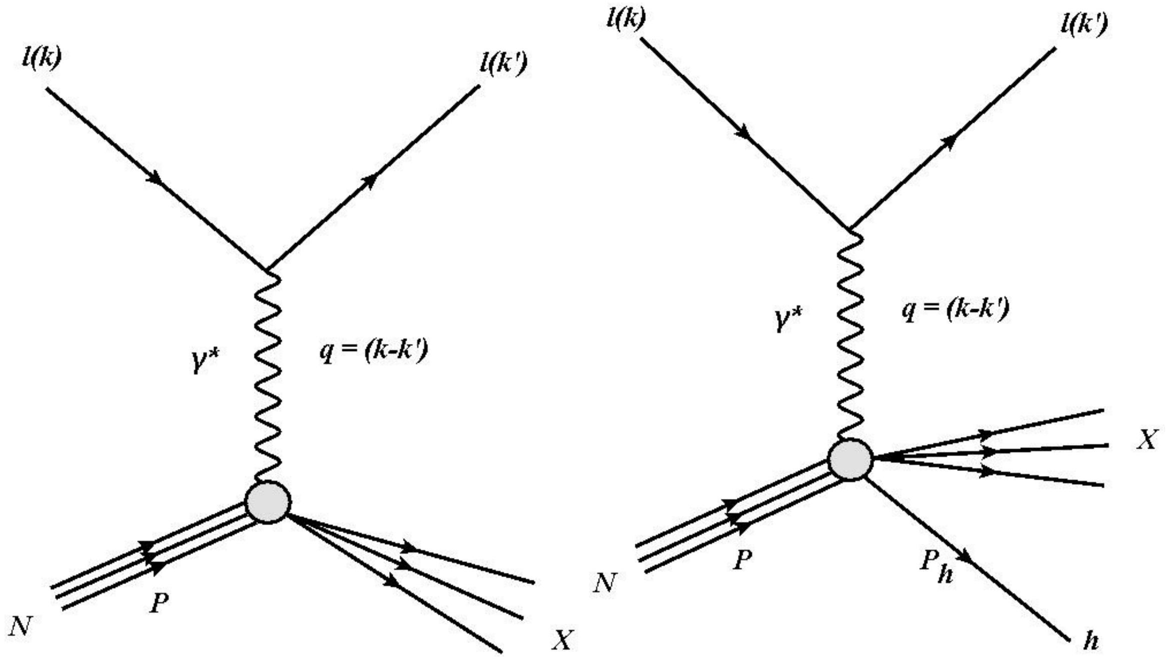

a) DIS b) SIDIS

Fig. 1.1 DIS vs SIDIS

Experimentally the semi-inclusive deep inelastic scattering (SIDIS) process can in general be expressed as the following differential cross-section [19]

$$\frac{d\sigma}{dQ^2\, dx\, dz_h\, d^2P_{ht}}\ , \tag{1.28}$$

Here x and Q^2 are well known DIS kinematics where

$$Q^2 = -q^2 = (k-k')^2\ ,$$

$$x = \frac{Q^2}{2P.q}$$

k and k' are the incoming and scattered lepton momenta respectively as shown in Fig. 1.1 and $q = k - k'$. P is the four momentum of proton. The other two variables are:

$$z_h = \frac{P.P_h}{P.q} = 2x.\ \frac{P.P_h}{Q^2}$$

where P_h is the four momentum of the observed hadron.
P_{ht} = transverse momentum of the detected hadron. Experimental data are mostly processed in terms of these 4 variables.

The factorization theorems of pQCD have been instrumental in the successful application of QCD theory to phenomenology. The standard collinear factorization formalism [15] makes use of “integrated” PDFs and FFs which depend only on a single longitudinal momentum fraction, while the small momentum components, including the transverse components, are integrated over in the definitions.

A transverse momentum dependent TMD-factorization [15–18] formalism goes beyond the standard factorization framework by allowing the PDFs and FFs to depend on intrinsic transverse momentum in addition to the usual momentum fraction variables. As such, different sets of approximations are needed in the factorization proofs. The PDFs and FFs in a TMD-factorization formalism are referred to as TMD PDFs and TMD FFs (they are also called “unintegrated” or “k_t -dependent”) collectively called as “TMDs” as mentioned above.

Specifically, Collins has found the right definition of TMD distinguishing it from uPDF [21]. The confusion over definition of TMD therefore appears to be solved.

While TMDs can potentially provide a much deeper understanding of QCD and hadron structure, the theoretical framework of TMD-factorization is much more complicated than the more standard collinear factorization.

The TMD factorization scheme has been developed by Collins, Soper and Sterman (CSS) [18, 22, 23] which provides a systematic treatment of pQCD over the full range of transverse momentum. This is however, beyond the scope of the present work.

There has been also interesting work devoted to parametrizing TMDs by assuming a parton model picture of TMD-factorization and directly fitting cross section calculations to experimental data [24–28]. This approach to TMD phenomenology is often called the generalized parton model (GPM) [29]. Only under this picture, Eq. 1.27 can be understood. This cross-section is simply a partonic sub-process, folded with TMD PDF and TMD

FF within the parton model. TMDs $f_{q/p}(x,k_t)$ and $D_{h/q}(z_h,k_t')$ have simple probabilistic interpretations: $f_{q/p}(x,k_t)$ for example is the probability density for finding a quark of flavor q with momentum fraction x and transverse momentum k_t inside the proton while $D_{h/q}(z_h,k_t')$ gives the number density of hadrons resulting from the hadronization of a parton q with momentum z_h and transverse momentum k_t'.

In SIDIS, the explicit form of hadronic tensor involving TMD PDF and TMD FF have got the form [30]

$$W^{\mu\nu} = \sum_f |\mathscr{H}(Q)^2|^{\mu\nu} \times \int d_t^k d^2k_t' f_{q/p}(x,k_t) D_{h/q}(z_h,k_t') \times \delta^{(2)}(k_t + q_t - k_t') \tag{1.29}$$

Here $|\mathscr{H}(Q)^2|^{\mu\nu}$ describes the hard partonic sub-process, $\gamma^* q \to q$, for scattering off a quark of flavor q as a function of the hard scale Q. (It also includes any overall factors needed to make the left side a proper hadronic tensor.) The size of q_t is a measure of the non-collinearity in the process. Eq. 1.29 is closely analogous to the standard collinear factorization theorem of inclusive processes [31].

In QCD, the TMD PDF and TMD FF have got two more variables: μ, ζ_f for TMD PDF and μ, ζ_D TMD FF, where μ is the usual renormalization group scaling factor. ζ_F and ζ_D are defined as [30]

$$\zeta_f = 2M_p^2 x^2 e^{2(y_p - y_s)} \tag{1.30}$$

and

$$\zeta_D = 2(M_H^2/z_h^2) e^{2(y_s - y_h)} \tag{1.31}$$

Here, x and z_h are the usual Bjorken scaling and fragmentation variables, M_p is the proton mass and M_h is the mass of the produced hadron. The rapidities of the proton and produced hadron are y_p and y_h respectively.

The evolution of TMD PDF $f_{q/p}(x,k_t;\mu;\zeta_f)$ and TMD FF $D_{h/q}(x,k_t';\mu;\zeta_D)$ are governed by the TMD evolution equations. To obtain their closed universal form is still an intense field of study. However, in specific models, like covariant parton model [32], TMD evolution equation has got the simpler form as follows:

Defining the derivative of the integrated parton distribution function ($q_i(x,Q^2)$) as $q'\left(=\frac{dq_i(x,Q^2)}{dx}\right)$, $q(x,Q^2)-xq'(x,Q^2)=\rho_q(p,Q^2)$, quark momentum $p(x)=\frac{Mx}{2}$, where M is the mass of the nucleon, $\xi=x\left(1+\left(\frac{k_t}{Mx}\right)^2\right)$, $\tilde{p}(x,k_t)=\frac{M\xi}{2}$, splitting function $P(x)$ for quark-quark of DGLAP evolution equation and TMD PDF $f_{q/p}(x,k_t;Q^2)$, one can get the exact evolution equation for TMD as below:

$$\frac{d}{d\ln Q^2}f_{q/p}(x,k_t;Q^2)=\frac{1}{4\pi\tilde{p}^2}\int_{\tilde{p}}^{M/2}\frac{d\acute{p}}{\acute{p}}P\left(\frac{\tilde{p}}{\acute{p}}\right)\rho_q(\acute{p},Q^2) \tag{1.32}$$

which is an active research field involved.

1.4 Froissart Bound

One of the cornerstones for the present strong interaction physics is the Froissart theorem [33]. It declares that the total cross sections of any two-hadron scattering cannot grow with energy faster than $(\log s)^2$ where s is the center of mass energy square. Later it was improved by Martin [34–36]. The original derivation of Froissart [33] is based on Mandelstam representation and that of Martin [34, 37] is on axiomatic field theory which could be considered as more general. The approach has led further development of the subject [38–42] as well as construction of several phenomenological models [43, 44]. it is therefore more familiar as Froissart-Martin bound.

Precession measurement of proton-proton (pp) cross-section at LHC [45–48] and in cosmic rays [49] have led the PDG group [50] to fit the data with such $\log^2 s$ term together with an additive constant $\sigma\sim A+B\log^2 s$.

However, to prove the Froissart theorem in QCD, is not yet been fully established. Recently it was shown by Greynat and Rafael [51] that in the Large-N_c limit of QCD, it is possible to construct models which a priori show no obstruction for such asymptotic behaviour of the total $\pi\pi$ cross sections.

In DIS, it is related to the hadronic structure function $F_2(x,Q^2)$ where Q^2 is the virtuality and x the longitudinal momentum fraction of quarks. This corresponds to the behavior of structure function of not rising faster than $\log^2 \frac{1}{x}$.

It is well known that the conventional equations of QCD, like DGLAP [4–6] and BFKL approaches [7–10], this limit is violated; while in the DGLAP approach, the small-x gluons grow faster than any power of $\ln\left(\frac{1}{x}\right) \approx \ln\left(\frac{s}{Q^2}\right)$ [52], in the BFKL approach it grows as a power of $\left(\frac{1}{x}\right)$ [7–11].

However, in recent years, the validity of Froissart Bound for the structure function at phenomenological level has attracted considerable attention in the study of DIS, mostly due to the efforts of Block and his collaborators [53].

It was argued in Ref. [55] that as the structure function $F_2^{\gamma p}(x,Q^2)$ is essentially the total cross section for the scattering of an off-shell gauge boson γ^* on the proton, a strong interaction process up to the initial and final gauge boson-quark couplings and Froissart bound makes sense. On this basis, one analytical expression in x and Q^2 for the DIS structure function has been suggested by them which has expected Froissart compatible $\log^2 \frac{1}{x}$ behavior and valid within the range of Q^2: $0.85 \leq Q^2 \leq 1200$ GeV^2 of the HERA data. Using this expression as input at $Q_0^2 = 4.5$ GeV^2 at DGLAP evolution equation, the validity can be increased upto 3000 GeV^2. The approach has been more recently applied in the Ultra High Energy (UHE) neutrino interaction, valid upto ultra small $x \sim 10^{-14}$ [56] . It is therefore of interest to study if such Froissart saturation like behavior can be incorporated in any other proton structure functions as well and can be tested with data.

1.5 Plan of the thesis

In chapter 2, we will study the self-similarity based model of proton structure function suggested in Ref. [1], fitted by H1 and ZEUS data [57, 58] which will be again refitted by recent HERA data [59] to verify the changes in defining parameters and phenomenological ranges of validity.

In chapter 3, we will study the limitations of the models described in chapter 2 and re-define a model which is free from singularity in the entire x-range : $0 < x < 1$.

In chapter 4, we will improve the earlier models of chapters 2 and 3 such that they are singularity free and have got a wider phenomenological ranges of validity.

In chapter 5, we will outline the method of incorporation of Froissart-Martin bound in the self-similarity based models of proton structure functions discussed in chapter 4.

In chapter 6, we will calculate the momentum fractions carried by quarks and gluons in the models described in chapters 2 to 5. we will compare the results with the predictions of Perturbative QCD, Lattice QCD and Ads/QCD models.

In chapter 7, we will discuss how Transverse Momentum Dependent Parton Distributions Functions (TMDs) can be introduced in the self-similarity based models of proton structure functions discussed in chapter 2 and 4.

In Chapter 8, we will outline the change of the structure of the TMDs discussed in chapter 7 if Froissart compatibility is also additionally introduced. We will discuss the difference between the two in this chapter.

Chapter 9 will include the summary and future outlook of this thesis.

2

Self-similarity based proton structure function and its reanalysis at small x

2.1 Introduction

Although renormalization group equation of quantum field theory [62] exhibits self-similarity [63], it is not yet established rigorously in QCD, the accepted fundamental quantum field theory of strong interaction. However, because of its wide applicability in other areas of physics [64–66] including condensed matter physics, its applicability in the study of structure of the proton is worth pursuing, at least at the phenomenological level. In the middle of 1980's, the notion of fractals has found its applicability in hadron production process [67–70] when the self-similar nature of hadron multi-particle production process was suggested.

Specifically, in 1990, Bjorken [70] highlighted the fractality of parton cascades leading to the anomalous dimension of phase space.

Relevance of these ideas in the contemporary physics of DIS has been first noted by Dremin and Levtchenko [71] in early 1990's, where it was shown that the saturation of hadron structure function at small x may proceed faster if the highly packed regions of proton have fractal structures. However, as shown in chapter 1, it was Lastovicka [1] in 2002, who first suggested the self-similarity as a possible feature of multipartons in the proton specially in the kinematical region of small Bjorken x, which in later years was pursued in Refs. [72–82]. Specifically, how quarks and gluons share the momentum fractions of the proton in self-similar way was studied in [78, 79], large x behavior of parton distribution functions (PDF) and double parton distribution functions (dPDF) in [80], and Froissart saturation in [82].

One of the apparent limitations of the phenomenological analysis of Ref. [1] is that it has a singularity at $x_0 \sim 0.019$ which is well within the kinematical range $0 \leq x \leq 1$. However, such singularity is not a common expectation from any physically viable model of proton structure function $F_2(x, Q^2)$.

In the present chapter, we therefore make a re-analysis of the model of Ref. [1] using the most recent HERA data. To that end, we will use the more recently complied HERA data [59, 92, 93], instead of analysis of Ref. [1] where as previously reported data were used Refs. [57, 58]. The difference between the two is however, not significant and still has a singularity.

In section 2.2, we outline the formalism as well as the results. Section 2.3 is the conclusion.

2.2 Formalism

2.2.1 Parton Distribution function (PDF) based on self-similarity

The self-similarity based model of the proton structure function of Ref. [1] is based on parton distribution function(PDF) $q_i(x,Q^2)$. Choosing the magnification factors $M_1 = \left(1+\frac{Q^2}{Q_0^2}\right)$ and $M_2 = \left(\frac{1}{x}\right)$, the unintegrated Parton Density (uPDF) can be written as [1, 80]

$$\log[M^2.f_i(x,Q^2)] = D_1.\log\left(\frac{1}{x}\right).\log\left(1+\frac{Q^2}{Q_0^2}\right)+D_2.\log\left(\frac{1}{x}\right)+D_3.\log\left(1+\frac{Q^2}{Q_0^2}\right)+D_0^i \tag{2.1}$$

where x is the Bjorken variable and Q^2 is the renormalization scale and i denotes a quark flavor. Here $D_1,\ D_2,\ D_3$ are the three flavor independent model parameters while D_0^i is the only flavor dependent normalization constant. M^2(=1 GeV^2) [80] is introduced to make (PDF) $q_i(x,Q^2)$ as defined below (in Eq. 2.2) dimensionless. We note that in deriving the model ansatz Eq. (2.1), one has to first generalize the definition of dimension from discrete to continuous fractals. The proper choice of magnification factors are made on the condition that they should be positive, non-zero and have no physical dimension. Whereas, in Ref. [1], choice of $\left(1+\frac{Q^2}{Q_0^2}\right)$ is made and an equivalent choice of $\left(\frac{Q_0^2}{Q^2+Q_0^2}\right)$ is also equally plausible. So is $\left(\frac{1}{x}\right)$ vs $\left(\log\frac{1}{x}\right)$. The integrated quark densities (PDF) then can be defined as

$$q_i(x,Q^2) = \int_0^{Q^2} f_i(x,Q^2)dQ^2 \tag{2.2}$$

As a result, the following analytical parametrization of a quark density is obtained by using Eq. 2.2 [79] :

Model 1

$$q_i(x,Q^2) = e^{D_0^i} f(x,Q^2) \tag{2.3}$$

where

$$f(x,Q^2) = \frac{Q_0^2 \left(\frac{1}{x}\right)^{D_2}}{M^2 \left(1 + D_3 + D_1 \log\left(\frac{1}{x}\right)\right)} \left(\left(\frac{1}{x}\right)^{D_1 \log\left(1+\frac{Q^2}{Q_0^2}\right)} \left(1 + \frac{Q^2}{Q_0^2}\right)^{D_3+1} - 1\right) \tag{2.4}$$

is flavor independent. Using Eq. 2.3 in the usual definition of the structure function $F_2(x,Q^2)$, one can get

$$F_2(x,Q^2) = x \sum_i e_i^2 \left(q_i(x,Q^2) + \bar{q}_i(x,Q^2)\right) \tag{2.5}$$

or it can be written as

$$F_2(x,Q^2) = \frac{e^{D_0}\, Q_0^2 \left(\frac{1}{x}\right)^{D_2 - 1}}{M^2 \left(1 + D_3 + D_1 \log\left(\frac{1}{x}\right)\right)} \left(\left(\frac{1}{x}\right)^{D_1 \log\left(1+\frac{Q^2}{Q_0^2}\right)} \left(1 + \frac{Q^2}{Q_0^2}\right)^{D_3+1} - 1\right) \tag{2.6}$$

which has the power law growth in $\left(\frac{1}{x}\right)$. $\log\left(\frac{1}{x}\right)$ comes only in the denominator. Here

$$e^{D_0} = \sum_{i=1}^{n_f} e_i^2 \left(e^{D_0^i} + e^{\bar{D}_0^i}\right) \tag{2.7}$$

Eq. 2.5 involves both quarks and anti-quarks. As in Ref. [1] we use the same parametrization both for quarks and anti-quarks. Assuming the quark and anti-quark have equal normalization constants, we obtain for a specific flavor

$$e^{D_0} = \sum_{i=1}^{n_f} e_i^2 \left(2e^{D_0^i}\right) \tag{2.8}$$

It shows that the value of D_0 will increase as more and more number of flavors contribute to the structure function.

With $n_f = 3, 4$ and 5 it reads explicitly as

$$n_f = 3 \quad : \quad e^{D_0} = 2\left(\frac{4}{9}e^{D_0{}^u} + \frac{1}{9}e^{D_0{}^d} + \frac{1}{9}e^{D_0{}^s}\right) \tag{2.9}$$

$$n_f = 4 \quad : \quad e^{D_0} = 2\left(\frac{4}{9}e^{D_0{}^u} + \frac{1}{9}e^{D_0{}^d} + \frac{1}{9}e^{D_0{}^s} + \frac{4}{9}e^{D_0{}^c}\right) \tag{2.10}$$

$$n_f = 5 \quad : \quad e^{D_0} = 2\left(\frac{4}{9}e^{D_0{}^u} + \frac{1}{9}e^{D_0{}^d} + \frac{1}{9}e^{D_0{}^s} + \frac{4}{9}e^{D_0{}^c} + \frac{1}{9}e^{D_0{}^b}\right) \tag{2.11}$$

Since each term of right hand sides of Eqs. 2.9, 2.10, and 2.11 is positive definite, it is clear, the measured value of D_0 increases as n_f increases. However, single determined parameter D_0 can not ascertain the individual contribution from various flavors.

From HERA data [57, 58], Eq. 2.6 was fitted in Ref. [1] with

$$\begin{aligned} D_0 &= 0.339 \pm 0.145 \\ D_1 &= 0.073 \pm 0.001 \\ D_2 &= 1.013 \pm 0.01 \\ D_3 &= -1.287 \pm 0.01 \\ Q_0^2 &= 0.062 \pm 0.01 \text{ GeV}^2 \end{aligned} \tag{2.12}$$

in the kinematical region,

$$\begin{aligned} &6.2 \times 10^{-7} \leq x \leq 10^{-2} \\ &0.045 \leq Q^2 \leq 120 \text{ GeV}^2 \end{aligned} \tag{2.13}$$

Table 2.1 Results of the fit of F_2''; Eq.2.14

D_0''	D_1''	D_2''	D_3''	$Q_0''^2(\mathrm{GeV}^2)$	χ^2/ndf
$0.354_{\pm 0.02}$	$0.071_{\pm 0.001}$	$1.032_{\pm 0.004}$	$-1.314_{\pm 0.01}$	$0.064_{\pm 0.0008}$	0.12

2.2.2 Reanalysis of Lastovicka model

Model 2

The defining equations of the model of Ref. [1] (Eqs. 2.1-2.4 above) do not ascertain the numerical values and signs of the parameters D_j s. These are determined from data [57, 58] leading to the set of Eq. 2.12 in the kinematic range (Eq. 2.13). Redefining the structure function as F_2'' and the model parameters as D_j''s i.e. viz

$$F_2''(x,Q^2) = \frac{e^{D_0''}\, Q_0''^2\, \left(\frac{1}{x}\right)^{D_2''-1}}{M^2\left(1+D_3''+D_1''\log\frac{1}{x}\right)} \left(\left(\frac{1}{x}\right)^{D_1''\log\left(1+\frac{Q^2}{Q_0''^2}\right)} \left(1+\frac{Q^2}{Q_0''^2}\right)^{D_3''+1} - 1 \right) \quad (2.14)$$

and refitting Eq. 2.14 by using the compiled HERAPDF1.0 [59] to check the behavior of the model parameters and obtain a new set of it. However, it makes no significance difference whether we use Refs. [57, 58] or Ref. [59] in analyzing the model, as it results a negative D_3 with the best fit of data compared to Eq. 2.12, if we don't impose any extra condition on the model parameters while parametrizing it. The result of the fitting is shown in Table 2.1 with the χ^2 analysis. The total number of F_2'' data points are 257. The phenomenological range of x and Q^2 are obtained within:

$$6.62\times 10^{-6} \leq x \leq 10^{-2}$$
$$0.35 \leq Q^2 \leq 150 \ \mathrm{GeV}^2 \quad (2.15)$$

In Fig. 2.1, we plot F_2'' as a function of x for few representative values of Q^2 (Q^2= 0.35, 0.65, 2, 3.5, 6.5, 15, 22, 35, 45, 90, 120, 150 GeV^2) within the phenomenologically allowed range of x and Q^2. We also show the corresponding available data from Ref. [59].

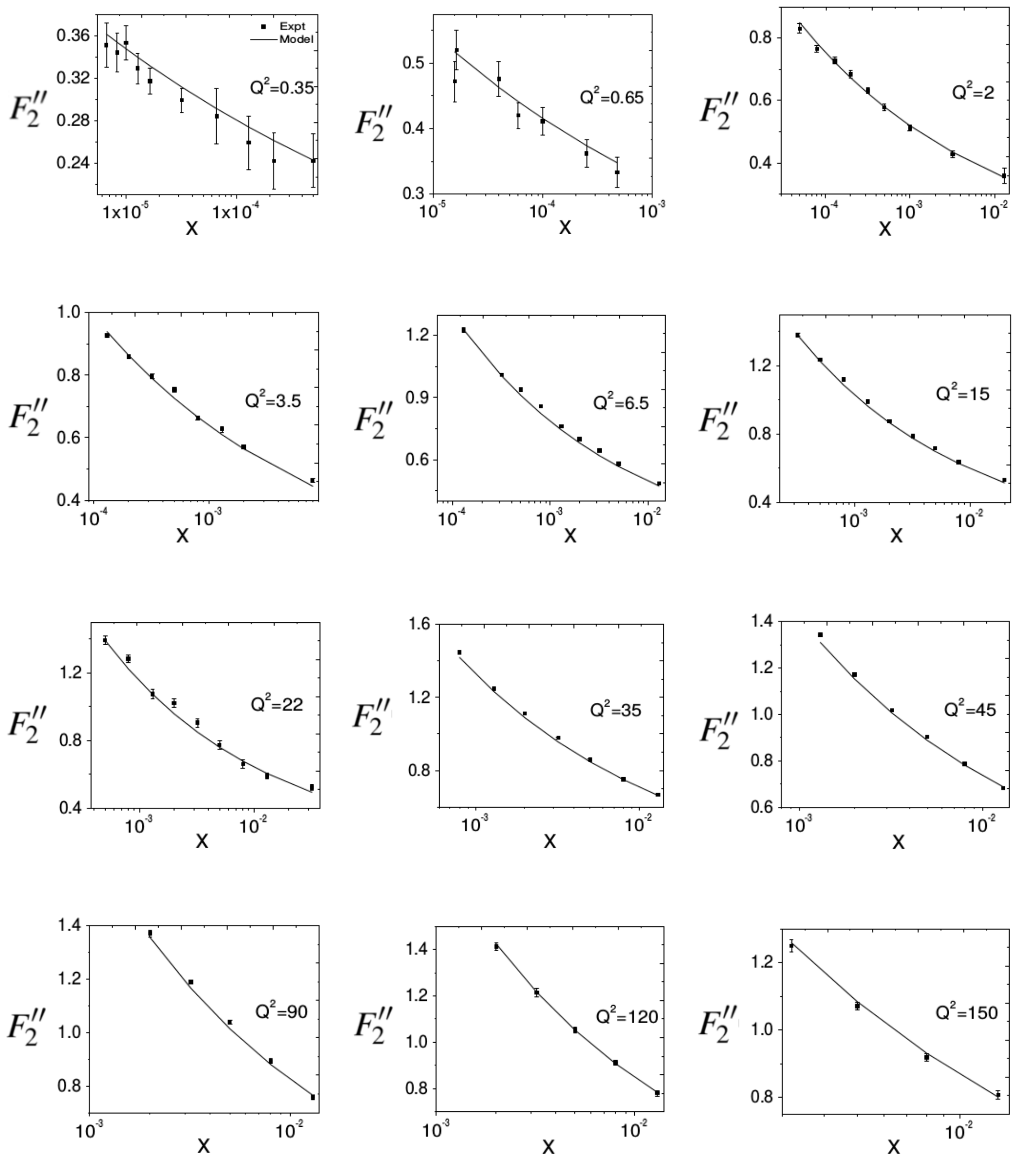

Fig. 2.1 Comparison of the structure function F_2'' (Eq.2.14) as a function of x in bins of Q^2 with measured data of F_2 from HERAPDF1.0[59]

2.3 Summary

In this chapter, we have first made a reanalysis of the self-similarity based model at small x proposed by Lastovicka [1] using more recent HERA data. The analysis does not make any big difference with the previous one except the phenomenological range of validity enhance upto $Q^2 \leq 150$ GeV^2 instead of $Q^2 \leq 120$ GeV^2. The two analyses have singularities at $x_0 \sim 0.019$ and $x_0'' \sim 0.012$ respectively, even though outside each phenomenological range of validity. In the next chapter, we therefore explore the possibility of an alternative model which is singularity free.

3

Singularity free self-similarity based proton structure function at small x

3.1 Introduction

In chapter 2, we noted that the defining equations of the model of Ref. [1] (Eqs.2.1-2.4 of chapter 2) do not ascertain the numerical values and signs of the parameters D_js. These are determined from data [57, 58] leading to the set of Eq. 2.12 in the kinematic range (Eq. 2.13) of chapter 2. However, the phenomenological analyses of models 1 and 2 have one inherent limitation: due to the negative value of D_3, Eq. 2.6 and 2.14 develop singularities at $x_0 \backsim 0.019$ [78, 79] and $x_0'' \sim 0.012$ respectively as it satisfies the condition $1 + D_3 + D_1 \log \frac{1}{x_0} = 0$, contrary to the expectation of a physically viable form of structure function. We therefore explore the possibility of an alternate model which is singularity free in the entire x-range; $0 < x < 1$.

In section 3.2 we outline the essential formalism. We discuss the results in section 3.3. Section 3.4 contains the summary of the present chapter.

3.2 Formalism

Redefining the model parameters D_j s by D'_j s (j=1,2,3) and (PDF) $q_i(x,Q^2)$ by $q'_i(x,Q^2)$ and also structure function $F_2(x,Q^2)$ by $F'_2(x,Q^2)$ in the present analysis, we observe that it can be made singularity free under the following specific conditions:

Case 1

If $D'_1, D'_3 \ll D'_2$ in Eq. 2.1 then the PDF Eq. 2.3 and the Structure Function Eq. 2.6 will be of the form:

$$q'_i(x,Q^2) = \frac{e^{D_0'^i}\, Q^2\, x^{-D'_2}}{M^2} \tag{3.1}$$

$$F'_2(x,Q^2) = \frac{e^{D'_0}\, Q^2\, x^{-D'_2+1}}{M^2} \tag{3.2}$$

Case 2

In this case $D'_1 \ll D'_2, D'_3$ in Eq. 2.1 then the corresponding expressions for the PDF and Structure Function in this limit are respectively:

$$q'_i(x,Q^2) = \frac{e^{D_0'^i}\, Q_0'^2\, x^{-D'_2}}{M^2\left(1+D'_3\right)} \left(\left(1+\frac{Q^2}{Q_0'^2}\right)^{D'_3+1} - 1\right) \tag{3.3}$$

$$F'_2(x,Q^2) = \frac{e^{D'_0}\, Q_0'^2\, x^{-D'_2+1}}{M^2\left(1+D'_3\right)} \left(\left(1+\frac{Q^2}{Q_0'^2}\right)^{D'_3+1} - 1\right) \tag{3.4}$$

Case 3

In this case, $D'_3 \ll D'_1, D'_2$ in Eq. 2.1 then the corresponding PDF and the Structure Function are set in the form:

$$q'_i(x,Q^2) = \frac{e^{D'^i_0}\, Q^2\, x^{-D'_2}}{M^2\left(1+D'_1\log\frac{1}{x}\right)}\left(\left(\frac{1}{x}\right)^{D'_1\log\left(1+\frac{Q^2}{Q'^2_0}\right)}\left(1+\frac{Q^2}{Q'^2_0}\right)-1\right) \tag{3.5}$$

$$F'_2(x,Q^2) = \frac{e^{D'_0}\, Q^2\, x^{-D'_2+1}}{M^2\left(1+D'_1\log\frac{1}{x}\right)}\left(\left(\frac{1}{x}\right)^{D'_1\log\left(1+\frac{Q^2}{Q'^2_0}\right)}\left(1+\frac{Q^2}{Q'^2_0}\right)-1\right) \tag{3.6}$$

respectively.

Case 4

This is the most general case for the singularity free model of Parton Distribution Function (PDF) Eq. 2.3 and Structure Function Eq. 2.6 under the condition that D'_1, D'_2, D'_3 are positive.

$$q'_i(x,Q^2) = \frac{e^{D'^i_0}\, Q'^2_0\, \left(\frac{1}{x}\right)^{D'_2}}{M^2\left(1+D'_3+D'_1\log\frac{1}{x}\right)}\left(\left(\frac{1}{x}\right)^{D'_1\log\left(1+\frac{Q^2}{Q'^2_0}\right)}\left(1+\frac{Q^2}{Q'^2_0}\right)^{D'_3+1}-1\right) \tag{3.7}$$

and

$$F'_2(x,Q^2) = \frac{e^{D'_0}\, Q'^2_0\, \left(\frac{1}{x}\right)^{D'_2-1}}{M^2\left(1+D'_3+D'_1\log\frac{1}{x}\right)}\left(\left(\frac{1}{x}\right)^{D'_1\log\left(1+\frac{Q^2}{Q'^2_0}\right)}\left(1+\frac{Q^2}{Q'^2_0}\right)^{D'_3+1}-1\right) \tag{3.8}$$

which has the power law growth in $\left(\frac{1}{x}\right)$. $\log\left(\frac{1}{x}\right)$ comes only in the denominator.

3.3 Results

To determine the parameters of the model $\left(D'_0,\, D'_1,\, D'_2,\, D'_3,\, Q'^2_0\right)$ we use recently compiled HERA data [59] instead of earlier data [57, 58] used in Ref. [1]. Following this procedure of Ref. [1], we make χ^2-analysis of the data and find the following results.

Case 1

We note that D'_2=1 is ruled out since it will make the Structure Function Eq. 3.2 x-independent. In Table 3.1 we show the results. From the χ^2-analysis, it is obtained that the model in case 1 is confined well with data for $0.35 \le Q^2 \le 70$ GeV^2 and $6.62\times\, 10^{-6} \le x \le 0.08$. D'_3 and D'_1 are taken to be zero in this limit. Here the number of F'_2 data points is 222.

Case 2

The parameters D'_0, D'_2, D'_3 and Q'^2_0 are determined (given in Table 3.2) in the similar manner as in case 1 and the range of validity has been obtained as: $0.35 \le Q^2 \le 27$ GeV^2 and $6.62\times 10^{-6} \le x \le 0.032$. As in case 1, here too $D_2 = 1$ is ruled out since it will make Eq. 3.4 x-independent. The number of F'_2 data points is 174.

Case 3

Here, parameters are best fitted in the range: $0.35 \le Q^2 \le 15$ GeV^2 and $6.62\times\, 10^{-6} \le x \le 0.02$ and given in Table 3.3. The number of F'_2 data points is 146.

Table 3.1 Results of the fit of case 1; Eq. 3.2

D'_0	D'_1	D'_2	D'_3	Q'^2_0(GeV^2)	χ^2/ndf
-4.129$_{\pm 0.332}$	0	1.226$_{\pm 0.01}$	0	-	0.81

Table 3.2 Results of the fit of case 2; Eq. 3.4

D'_0	D'_1	D'_2	D'_3	Q'^2_0(GeV^2)	χ^2/ndf
-6.125$_{\pm 0.444}$	0	1.214$_{\pm 0.01}$	0.531$_{\pm 0.01}$	0.053$_{\pm 0.001}$	0.80

Table 3.3 Results of the fit of case 3; Eq. 3.6

D'_0	D'_1	D'_2	D'_3	Q'^2_0(GeV^2)	χ^2/ndf
-3.533$_{\pm 0.350}$	0.411$_{\pm 0.02}$	0.582$_{\pm 0.003}$	0	0.035$_{\pm 0.0005}$	0.80

Case 4

Parameters D'_0, D'_1, D'_2, D'_3 and Q'^2_0 are determined and given in Table 3.4 and obtained in a more restrictive range: $0.85 \leq Q^2 \leq 10$ GeV^2 and $2\times\ 10^{-5} \leq x \leq 0.02$. The number of F'_2 data points is 95.

In Fig. 3.1, we plot F'_2 (Eq. 3.8) for the case 4 as a function of x for eight representative values of Q^2 (Q^2= 1.5, 2.7, 3.5, 6.5, 8.5, 10 GeV^2) in the phenomenologically allowed range $0.85 \leq Q^2 \leq 10$ GeV^2. We also show the corresponding available data from Ref. [59].

It shows that as the model parameters have additional positivity constraint, the range of validity shrinks from $Q^2 = 120$ GeV^2 to $Q^2 = 10$ GeV^2. Thus our analysis indicates that the phenomenological range of validity of the present version of the model is more restrictive: $0.85 \leq Q^2 \leq 10$ GeV^2 and $2\times 10^{-5} \leq x \leq 0.02$ to be compared with Eq. 2.13 of the previous version of Ref. [1]. Also, the individual χ^2 at $Q^2 = 8.5$ and 10 GeV^2 is minimum to be compared with $Q^2 = 4.5$ and 10 GeV^2 which is quite larger than that of 10 GeV^2. It is same for $Q^2 = 1.5$ GeV^2 too. Basically, our results valid in small area in between Q^2 of 8.5 and 10 GeV^2. But due to the unavailability of the experimental data points, the difference cant be shown explicitly.

Table 3.4 Results of the fit of case 4; Eq. 3.8

D'_0	D'_1	D'_2	D'_3	Q'^2_0(GeV^2)	χ^2/ndf
-2.971$_{\pm 0.409}$	0.065$_{\pm 0.0003}$	1.021$_{\pm 0.004}$	0.0003$_{\pm 0.0001}$	0.20$_{\pm 0.0008}$	0.20

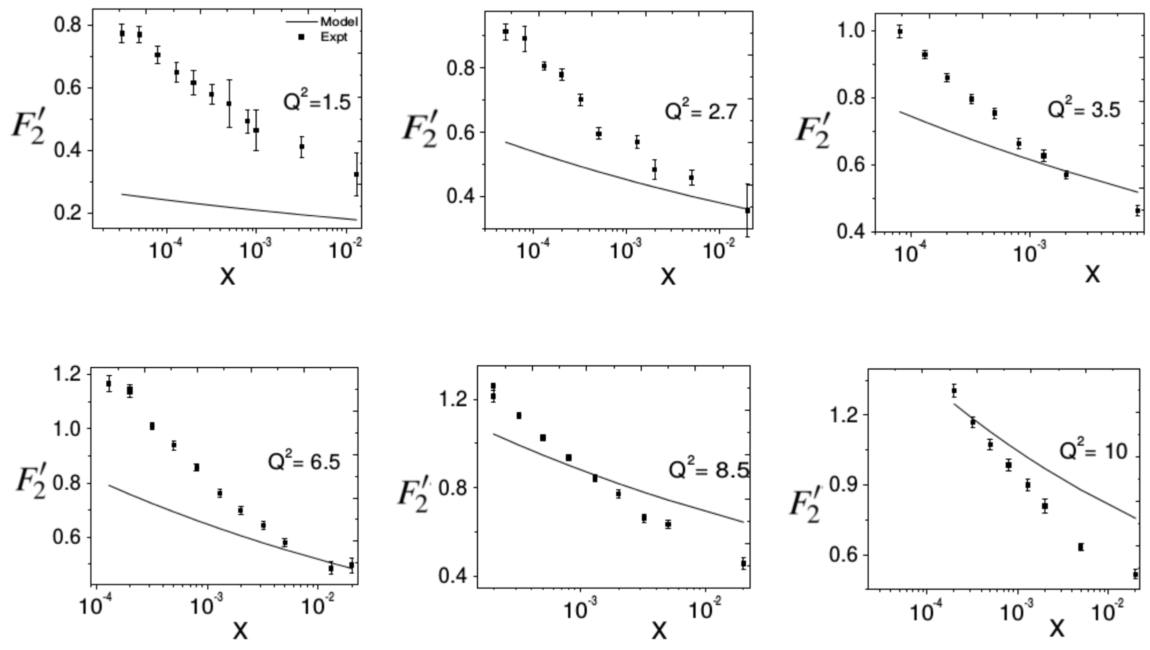

Fig. 3.1 Comparison of the structure function F_2' of Model 2 as a function of x in bins of Q^2 with measured data of F_2 from HERAPDF1.0 [59]

We also observe the following features of the model compared to data: at $Q^2 = 1.5$ GeV^2 data overshoots the theory. But as Q^2 increases, the theoretical curve comes closer to data. At Q^2=10 GeV^2, on the other hand, the theory exceeds data. Main reason of this feature is that the x-slope of the model is less than that of the data. Specifically, due to positive D_3, the growth of the structure function with Q^2 becomes faster than a linear growth as can be seen from Eq. 2.4 i.e.

$$\left(1+\frac{Q^2}{Q_0'^2}\right)^{(1+D_3')} \approx \left(1+\frac{Q^2}{Q_0'^2}\right)^{1.0003}$$

at higher values of $Q^2 > 1$ GeV^2 to be compared with

$$\left(1+\frac{Q^2}{Q_0^2}\right)^{(1+D_3)} \approx \left(1+\frac{Q^2}{Q_0^2}\right)^{-0.287}$$

of Ref. [1] which is faster than data. This is the major limitation of the present singularity free version of the model which calls for further improvement.

3.4 Summary

In this chapter, we have removed the singularities in the models discussed in chapter 2 within the entire x-range: $0 < x < 1$ by putting an extra condition on parameters that it should be positive definite. But an effort to make a model singularity free reduces its phenomenological range of validity drastically. Therefore, in the next chapter, we explore alternative ways of making the model singularity free and not pursue the present singularity free model further.

4

Improved singularity free self-similarity based models of proton structure function at small and large x

4.1 Introduction

Let us discuss a possible way of removing the short coming of the models under discussion. This approach has taken the notion of self-similarity to parametrize Parton Distribution Function (PDF) and eventually the structure function. However, the variables in which the supposed fractal scaling of the quark distributions and $F_2(x,Q^2)$ occur are not known from the underlying theory. In Ref. [1], the choice of $\left(\frac{1}{x}\right)$ is presumably because of the power law form of the quark distributions at small x found in Glück-Reya-Vogt (GRV) [3] distribution. However, this form is not derived theoretically but rather follows from the power law distributions in x assumed for the input quark distributions used by the GRV distribution for the QCD evolution. The choice of $\left(\frac{1}{x}\right)$ as the proper scaling variable is therefore not established from the underlying theory. Same is true for the magnification factor $M_1 = \left(1+\frac{Q^2}{Q_0^2}\right)$ as defined in Eq. 2.1.

4.2 Formalism

4.2.1 Improved version of the self-similarity based models

The magnification factor M_1 can be considered as a special case of more general form :

$$\hat{M}_1 = \sum_{i=-n}^{n} \alpha_i M_1^i \tag{4.1}$$

Only in a specific case, where $\alpha_1 = 1$ and all other coefficients cases vanish lead to the original M_1 as defined in Eq. 2.1. If we take this generalization form of Eq. 4.1 and if all the coefficients $\alpha_i (i = 0,\ 1,\ 2,\ \ldots, n)$ vanish then Eq. 4.1 becomes

$$\hat{M}_1 = \sum_{j=1}^{n} \frac{B_j}{\left(1+\frac{Q^2}{\hat{Q}_0^2}\right)^j} \tag{4.2}$$

where

$$B_j = \alpha_{-j} \tag{4.3}$$

The defining uPDF therefore can be generalized to

$$\log[M^2.\hat{f}_i(x,Q^2)] = \hat{D}_1 \log\frac{1}{x}\log\hat{M}_1 + \hat{D}_2\log\frac{1}{x} + \hat{D}_3\log\hat{M}_1 + \hat{D}_0^i \tag{4.4}$$

instead of Eq. 2.1, such that it will take the form

$$\hat{f}_i(x,Q^2) = \frac{e^{\hat{D}_0^i}}{M^2}\left(\frac{1}{x}\right)^{\hat{D}_2}\left(\hat{M}_1\right)^{\hat{D}_3+\hat{D}_1\log\frac{1}{x}} \tag{4.5}$$

Taking only the two terms of Eq. 4.2, $\hat{M}_1$ can be written as

$$\hat{M}_1 = \frac{B_1}{\left(1+\frac{Q^2}{\hat{Q}_0^2}\right)} + \frac{B_2}{\left(1+\frac{Q^2}{\hat{Q}_0^2}\right)^2} \tag{4.6}$$

and the corresponding uPDF (Eq. 4.5) becomes

$$\hat{f}_i(x,Q^2) = \frac{e^{\hat{D}_0^i}}{M^2}\left(\frac{1}{x}\right)^{\hat{D}_2}\left(\frac{B_1}{\left(1+\frac{Q^2}{\hat{Q}_0^2}\right)}\right)^{\hat{D}_3+\hat{D}_1\log\frac{1}{x}}\left(1+\frac{B_2}{B_1}\frac{1}{\left(1+\frac{Q^2}{\hat{Q}_0^2}\right)}\right)^{\hat{D}_3+\hat{D}_1\log\frac{1}{x}} \tag{4.7}$$

Assuming the convergence of the polynomials as occurred in Eq. 4.7 we obtain :

Model 3

uPDF

$$\hat{f}_i(x,Q^2) = \frac{e^{\hat{D}_0^i}}{M^2}\left(\frac{1}{x}\right)^{\hat{D}_2}\left(\frac{B_1}{\left(1+\frac{Q^2}{\hat{Q}_0^2}\right)}\right)^{\hat{D}_3+\hat{D}_1\log\frac{1}{x}}\left(1+\frac{B_2}{B_1}\frac{\left(\hat{D}_3+\hat{D}_1\log\frac{1}{x}\right)}{\left(1+\frac{Q^2}{\hat{Q}_0^2}\right)}\right) \tag{4.8}$$

After integration over Q^2, it yields the desired PDF

$$\hat{q}_i(x,Q^2) = \frac{e^{\hat{D}_0^i}\hat{Q}_0^2}{M^2}\left(\frac{1}{x}\right)^{\hat{D}_2}(B_1)^{\left(\hat{D}_3+\hat{D}_1\log\frac{1}{x}\right)}\left[\frac{\left(\left(1+\frac{Q^2}{\hat{Q}_0^2}\right)^{\left(1-\hat{D}_3-\hat{D}_1\log\frac{1}{x}\right)}-1\right)}{\left(1-\hat{D}_3-\hat{D}_1\log\frac{1}{x}\right)} - \frac{B_2}{B_1}\left(\left(1+\frac{Q^2}{\hat{Q}_0^2}\right)^{\left(-\hat{D}_3-\hat{D}_1\log\frac{1}{x}\right)}-1\right)\right] \tag{4.9}$$

Using Eq. 4.9 in Eq. 2.5, the usual definition of structure function, it gives

$$\hat{F}_2(x,Q^2) = \frac{e^{\hat{D}_0}\hat{Q}_0^2}{M^2}\left(\frac{1}{x}\right)^{\hat{D}_2-1}(B_1)^{\left(\hat{D}_3+\hat{D}_1\log\frac{1}{x}\right)}\left[\frac{\left(\left(1+\frac{Q^2}{\hat{Q}_0^2}\right)^{\left(1-\hat{D}_3-\hat{D}_1\log\frac{1}{x}\right)}-1\right)}{\left(1-\hat{D}_3-\hat{D}_1\log\frac{1}{x}\right)} - \frac{B_2}{B_1}\left(\left(1+\frac{Q^2}{\hat{Q}_0^2}\right)^{\left(-\hat{D}_3-\hat{D}_1\log\frac{1}{x}\right)}-1\right)\right] \tag{4.10}$$

with the condition that

$$\hat{D}_3+\hat{D}_1\log\frac{1}{x} \neq 1 \tag{4.11}$$

as the equality will yield a undesired singularity.

The above model of structure function (Model 3) has new 7 independent parameters B_1, B_2, $\hat{D}_0$, $\hat{D}_1$, $\hat{D}_2$, $\hat{D}_3$, $\hat{Q}_0^2$ to be fitted from data and compared with the previous models (Models 1 and 2). It has also power law growth in Q^2 as in the models of chapters 2 and 3.

Model 4

If the model parameters $\hat{D}_1$ and $\hat{D}_3$ satisfy the additional condition

$$\hat{D}_3 + \hat{D}_1 \log \frac{1}{\hat{x}_0} = 1 \tag{4.12}$$

then the resultant uPDF becomes :

$$\tilde{f}_i(x,Q^2) = \frac{e^{\tilde{D}_0^i}}{M^2} \left(\frac{1}{x}\right)^{\tilde{D}_2} \left(\frac{\tilde{B}_1}{\left(1+\frac{Q^2}{\tilde{Q}_0^2}\right)}\right) \left(1 + \frac{\tilde{B}_2}{\tilde{B}_1} \frac{1}{\left(1+\frac{Q^2}{\tilde{Q}_0^2}\right)}\right) \tag{4.13}$$

while the integration over Q^2 leads to the PDF

$$\tilde{q}_i(x,Q^2) = \frac{e^{\tilde{D}_0^i}\tilde{Q}_0^2}{M^2} \left(\frac{1}{x}\right)^{\tilde{D}_2} \tilde{B}_1 \left[\log\left(1+\frac{Q^2}{\tilde{Q}_0^2}\right) - \frac{\tilde{B}_2}{\tilde{B}_1} \left(\frac{1}{\left(1+\frac{Q^2}{\tilde{Q}_0^2}\right)} - 1\right)\right] \tag{4.14}$$

And the corresponding structure function is

$$\tilde{F}_2(x,Q^2) = \frac{e^{\tilde{D}_0}\tilde{Q}_0^2}{M^2} \left(\frac{1}{x}\right)^{\tilde{D}_2-1} \tilde{B}_1 \left[\log\left(1+\frac{Q^2}{\tilde{Q}_0^2}\right) - \frac{\tilde{B}_2}{\tilde{B}_1} \left(\frac{1}{\left(1+\frac{Q^2}{\tilde{Q}_0^2}\right)} - 1\right)\right] \tag{4.15}$$

which is completely free from singularity except for $\tilde{D}_2 \geq 1$. It has the power law growth in Q^2 in contrast to the Eq. 4.10 which has also power law rise in Q^2. However, Eq. 4.10 has a non-leading correction of the order of $\left(\frac{1}{Q^2}\right)$. Such singularity is, however, consistent with the usual Regge expectation [85–89]. The model has now got 4 parameters: $\tilde{B}_1,\ \tilde{D}_2,\ \tilde{Q}_0^2,\ \tilde{D}_0^i$.

4.2.2 Extrapolation of the self-similarity based PDF from small x to large x

The models of uPDFs or PDFs discussed above were basically constructed to test it in the small x range. It did not take into account the large x behavior [86–90] of the PDF or structure function

$$\lim_{x\to 1} F_2(x,Q^2) = 0 \tag{4.16}$$

which is not unexpected. The important observation which motivated and justified the use of self-similarity concept was that for $x < 0.01$; the logarithm of the derivative of the unintegrated parton distributions $\log\left(\frac{\partial f_i(x,Q^2)}{\partial Q^2}\right)$ is a linear function of $\log x$ (Fig. 2.8.a of Ref. [1]). The idea of self-similarity is based on the fact that at small x, the behavior of quark density is driven by gluon emissions and splittings such that the parton distribution function at small x and those at still smaller x look similar (upto some magnification factor). In the opposite limit, at large x, there is no physical reason for self-similarity and no phenomenological justification till date. In other words, extending the approach of large x means applying the self-similarity concept where it is not expected to work. On the other hand, as noted in [80], it is not unreasonable to assume that the self-similarity does not terminate abruptly at $x \approx 0.01$, but smoothly vanishes at $x = 1$, the valence quark limit of proton with no trace of self-similarity at all.

Therefore, we take this alternative point of view in structure function. We suggest a simple interpolating model of uPDF/PDF which approaches the self-similar one at $x \to 0$ (Eq. 2.1), and still satisfy Eq. 4.16 at large x, $x \to 1$. A plausible way of achieving it in a parameter-free way is to make a formal replacement of $\left(\frac{1}{x}\right)$ factor to $\left(\frac{1}{x} - 1\right)$ in Eq. 2.1. The former one is identified as one of the magnification factors in the self-similar model, while the later can be so interpreted only for $\frac{1}{x} \gg 1$. In such case, Eq. 2.1 of uPDF will be modified to $\bar{f}_i(x,Q^2)$ defined as

$$\log[M^2.\bar{f}_i(x,Q^2)] = \bar{D}_1.\log\left(\frac{1}{x}-1\right).\log\left(1+\frac{Q^2}{\bar{Q}_0^2}\right)+\bar{D}_2.\log\left(\frac{1}{x}-1\right) + \bar{D}_3.\log\left(1+\frac{Q^2}{\bar{Q}_0^2}\right)+\bar{D}_0^i \quad (4.17)$$

which leads to a PDF

$$\bar{f}_i(x,Q^2) = \frac{e^{\bar{D}_0^i}}{M^2}\left(\frac{1}{x}-1\right)^{\bar{D}_2}\left(1+\frac{Q^2}{\bar{Q}_0^2}\right)^{\bar{D}_3+\bar{D}_1\log\left(\frac{1}{x}-1\right)} \quad (4.18)$$

Generalizing the magnification factor $\hat{M}_1$ as in Eq. 4.6 and taking only the two terms and assuming the convergence of the polynomials occurring in the expression as in Eq. 4.7 we obtain the generalized uPDF as :

Model 5

uPDF

$$\bar{f}_i(x,Q^2) = \frac{e^{\bar{D}_0^i}}{M^2}\left(\frac{1}{x}\right)^{\bar{D}_2}(1-x)^{\bar{D}_2}\left(\frac{\bar{B}_1}{\left(1+\frac{Q^2}{\bar{Q}_0^2}\right)}\right)^{\bar{D}_3+\bar{D}_1\log\frac{1}{x}+\bar{D}_1\log(1-x)} \left(1+\frac{\bar{B}_2}{\bar{B}_1}\frac{\left(\bar{D}_3+\bar{D}_1\log\frac{1}{x}+\bar{D}_1\log(1-x)\right)}{\left(1+\frac{Q^2}{\bar{Q}_0^2}\right)}\right) \quad (4.19)$$

And hence corresponding PDF($\bar{q}_i$) and structure function($\bar{F}_2$) will be

$$\bar{q}_i(x,Q^2) = \frac{e^{\bar{D}_0^i}\bar{Q}_0^2}{M^2}\left(\frac{1}{x}\right)^{\bar{D}_2}(1-x)^{\bar{D}_2}(\bar{B}_1)^{\left(\bar{D}_3+\bar{D}_1\log\frac{1}{x}+\bar{D}_1\log(1-x)\right)}$$
$$\left[\frac{\left(\left(1+\frac{Q^2}{\bar{Q}_0^2}\right)^{\left(1-\bar{D}_3-\bar{D}_1\log\frac{1}{x}-\bar{D}_1\log(1-x)\right)}-1\right)}{\left(1-\bar{D}_3-\bar{D}_1\log\frac{1}{x}-\bar{D}_1\log(1-x)\right)}-\frac{\bar{B}_2}{\bar{B}_1}\left(\left(1+\frac{Q^2}{\bar{Q}_0^2}\right)^{\left(-\bar{D}_3-\bar{D}_1\log\frac{1}{x}-\bar{D}_1\log(1-x)\right)}-1\right)\right] \tag{4.20}$$

and

$$\bar{F}_2(x,Q^2) = \frac{e^{\bar{D}_0}\bar{Q}_0^2}{M^2}\left(\frac{1}{x}\right)^{\bar{D}_2-1}(1-x)^{\bar{D}_2-1}(\bar{B}_1)^{\left(\bar{D}_3+\bar{D}_1\log\frac{1}{x}+\bar{D}_1\log(1-x)\right)}$$
$$\left[\frac{\left(\left(1+\frac{Q^2}{\bar{Q}_0^2}\right)^{\left(1-\bar{D}_3-\bar{D}_1\log\frac{1}{x}-\bar{D}_1\log(1-x)\right)}-1\right)}{\left(1-\bar{D}_3-\bar{D}_1\log\frac{1}{x}-\bar{D}_1\log(1-x)\right)}-\frac{\bar{B}_2}{\bar{B}_1}\left(\left(1+\frac{Q^2}{\bar{Q}_0^2}\right)^{\left(-\bar{D}_3-\bar{D}_1\log\frac{1}{x}-\bar{D}_1\log(1-x)\right)}-1\right)\right] \tag{4.21}$$

which has the power law growth in $\left(\frac{1}{x}\right)$ as well as in Q^2.

Model 6

Imposing the condition

$$\bar{D}_3+\bar{D}_1\log\frac{1}{\bar{x}_0}+\bar{D}_1\log(1-\bar{x}_0) = 1 \tag{4.22}$$

will lead to corresponding uPDF, PDF and structure function as :

uPDF

$$\bar{f}_i'(x,Q^2) = \frac{e^{\bar{D}_0'^i}}{M^2}\left(\frac{1}{x}\right)^{\bar{D}_2'}(1-x)^{\bar{D}_2'}\left(\frac{\bar{B}_1'}{\left(1+\frac{Q^2}{\bar{Q}_0'^2}\right)}\right)\left(1+\frac{\bar{B}_2'}{\bar{B}_1'}\frac{1}{\left(1+\frac{Q^2}{\bar{Q}_0'^2}\right)}\right) \tag{4.23}$$

Corresponding PDF

$$\bar{q}'_i(x,Q^2) = \frac{e^{\bar{D}'^i_0}\bar{Q}'^2_0}{M^2}\left(\frac{1}{x}\right)^{\bar{D}'_2}(1-x)^{\bar{D}'_2}\bar{B}'_1\left[\log\left(1+\frac{Q^2}{\bar{Q}'^2_0}\right)-\frac{\bar{B}'_2}{\bar{B}'_1}\left(\frac{1}{\left(1+\frac{Q^2}{\bar{Q}'^2_0}\right)}-1\right)\right] \tag{4.24}$$

and corresponding structure function

$$\bar{F}'_2(x,Q^2) = \frac{e^{\bar{D}'_0}\bar{Q}'^2_0}{M^2}\left(\frac{1}{x}\right)^{\bar{D}'_2-1}(1-x)^{\bar{D}'_2}\bar{B}'_1\left[\log\left(1+\frac{Q^2}{\bar{Q}'^2_0}\right)-\frac{\bar{B}'_2}{\bar{B}'_1}\left(\frac{1}{\left(1+\frac{Q^2}{\bar{Q}'^2_0}\right)}-1\right)\right] \tag{4.25}$$

which has the power law growth in Q^2 and also a non-leading correction of the order of $\left(\frac{1}{Q^2}\right)$.

4.2.3 Comparison of self-similarity PDFs with standard PDFs

We now compare the parametrization of self-similarity PDFs: Eqs. 2.3, 3.7, 4.9, 4.14, 4.20, and 4.24 with the common behavior of quark and gluon distributions obtained in the standard parametrization like CTEQ [91]. Setting $Q^2 = Q_0^2$ we have from Eqs. 2.3, 3.7, 4.9, 4.14, 4.20, and 4.24

(Model 1)

$$q_i(x,Q_0^2) = A_1^i\left(\frac{1}{x}\right)^{D_2}\left(\left(\frac{1}{x}\right)^{D_1\log 2}2^{D_3+1}-1\right) \tag{4.26}$$

which has the power law growth in $\left(\frac{1}{x}\right)$.

Here

$$A_1^i = \frac{e^{D_0^i}\,Q_0^2}{M^2\,l_1(x)} \tag{4.27}$$

and

$$l_1(x) = 1+D_3+D_1\log\frac{1}{x} \tag{4.28}$$

(Model 2)

$$q'_i(x,Q_0^2) = A_2^i \left(\frac{1}{x}\right)^{D'_2} \left(\left(\frac{1}{x}\right)^{D'_1 \log 2} 2^{D'_3+1} - 1\right) \tag{4.29}$$

which has also the power law growth in $\left(\frac{1}{x}\right)$.

Here

$$A_2^i = \frac{e^{D'^i_0}\, Q'^2_0}{M^2\, l_2(x)} \tag{4.30}$$

and

$$l_2(x) = 1 + D'_3 + D'_1 \log \frac{1}{x} \tag{4.31}$$

(Model 3)

$$\hat{q}_i(x,Q_0^2) = A_3^i \left(\frac{1}{x}\right)^{\hat{D}_2} \left(W_1 \left(\frac{1}{x}\right)^{\hat{D}_1 \log \frac{B_1}{2}} + W_2 \left(\frac{1}{x}\right)^{\hat{D}_1 \log B_1} + W_3 \left(\frac{1}{x}\right)^{\hat{D}_1 \log \frac{B_1}{2}} \log\left(\frac{1}{x}\right) + W_4 \left(\frac{1}{x}\right)^{\hat{D}_1 \log B_1} \log\left(\frac{1}{x}\right)\right) \tag{4.32}$$

which has the power law growth in $\left(\frac{1}{x}\right)$ with $\left(\log \frac{1}{x}\right)$ term.

Here

$$A_3^i = \frac{e^{\hat{D}^i_0}\, \hat{Q}^2_0}{M^2\, l_3(x)} \tag{4.33}$$

and

$$l_3(x) = 1 - \hat{D}_3 - \hat{D}_1 \log \frac{1}{x} \tag{4.34}$$

And

$$W_1 = B_1^{\hat{D}_3} 2^{1-\hat{D}_3} - 2^{-\hat{D}_3} B_1^{\hat{D}_3 - 1} \left(B_2 - B_2 \hat{D}_3\right) \tag{4.35}$$

$$W_2 = (B_2 - B_2 \hat{D}_3) B_1^{\hat{D}_3 - 1} - B_1^{\hat{D}_3} \tag{4.36}$$

$$W_3 = B_2 \hat{D}_1 2^{-\hat{D}_3} B_1^{\hat{D}_3 - 1} \tag{4.37}$$

$$W_4 = -B_2 \hat{D}_1 B_1^{\hat{D}_3 - 1} \tag{4.38}$$

(Model 4)

$$\tilde{q}_i(x,Q_0^2) = A_4^i \left(\frac{1}{x}\right)^{\tilde{D}_2} \left(\tilde{B}_1 \log 2 + \frac{1}{2}\tilde{B}_2\right) \tag{4.39}$$

which has the power law growth in $\left(\frac{1}{x}\right)$ where

$$A_4^i = \frac{e^{\tilde{D}_0^i}\tilde{Q}_0^2}{M^2} \tag{4.40}$$

(Model 5)

$$\begin{aligned}\bar{q}_i(x,Q_0^2) = A_5^i \left(\frac{1}{x}\right)^{\bar{D}_2} (1-x)^{\bar{D}_2} \Bigg(& Z_1 \left(\frac{1}{x}-1\right)^{\bar{D}_1 \log \frac{\bar{B}_1}{2}} + Z_2 \left(\frac{1}{x}-1\right)^{\bar{D}_1 \log \bar{B}_1} \\ & + Z_3 \left(\frac{1}{x}-1\right)^{\bar{D}_1 \log \frac{\bar{B}_1}{2}} \log\left(\frac{1}{x}-1\right) + Z_4 \left(\frac{1}{x}-1\right)^{\bar{D}_1 \log \bar{B}_1} \log\left(\frac{1}{x}-1\right)\Bigg)\end{aligned} \tag{4.41}$$

which has the power law growth in $\left(\frac{1}{x}\right)$ with $\left(\log\frac{1}{x}\right)$ term where

$$A_5^i = \frac{e^{\bar{D}_0^i}\,\bar{Q}_0^2}{M^2\, l_4(x)} \tag{4.42}$$

Here

$$l_4(x) = 1 - \bar{D}_3 - \bar{D}_1 \log\frac{1}{x} - \bar{D}_1 \log(1-x) \tag{4.43}$$

And

$$Z_1 = \bar{B}_1^{\bar{D}_3} 2^{1-\bar{D}_3} - 2^{-\bar{D}_3} \bar{B}_1^{\bar{D}_3 - 1} (\bar{B}_2 - \bar{B}_2\bar{D}_3) \tag{4.44}$$

$$Z_2 = (\bar{B}_2 - \bar{B}_2\bar{D}_3)\bar{B}_1^{\bar{D}_3-1} - \bar{B}_1^{\bar{D}_3} \tag{4.45}$$

$$Z_3 = \bar{B}_2\bar{D}_1 2^{-\bar{D}_3} \bar{B}_1^{\bar{D}_3-1} \tag{4.46}$$

$$Z_4 = -\bar{B}_2\bar{D}_1\bar{B}_1^{\bar{D}_3-1} \tag{4.47}$$

(Model 6)

$$\bar{q}_i'(x,Q_0^2) = A_6^i \left(\frac{1}{x}\right)^{\bar{D}_2'} (1-x)^{\bar{D}_2'} \left(\bar{B}_1' \log 2 + \frac{1}{2}\bar{B}_2'\right) \tag{4.48}$$

Eq. 4.48 has the power law growth in $\left(\frac{1}{x}\right)$ where

$$A_6^i = \frac{e^{\bar{D}_0'^i}\, \bar{Q}_0'^2}{M^2} \tag{4.49}$$

The x-dependence of $l_1(x)$ and $l_2(x)$ defined above are due to the correlation between two magnification factors $M_1 = \left(1+\frac{Q^2}{Q_0^2}\right)$ and $M_2 = \left(\frac{1}{x}\right)$ (Eq. 2.1). Similarly x-dependence of $l_3(x)$ and $l_4(x)$ are due to the correlation between M_2 and $\hat{M}_1$ (Eq. 4.4). In Eqs. 4.39 and 4.48, the extra x-dependence do not occur due to the initial conditions of logarithmic rise (Eqs. 4.12 and 4.22). If the terms occurring in D_1s are assumed to be negligible, then Eq. 4.48 has a form similar to the canonical parametrization [86, 88]

$$q_i(x,Q_0^2) \approx A_0^i\, x^{A_1^i}\, (1-x)^{A_2^i} \tag{4.50}$$

where the superscript i indicates flavor dependence. At small x it reduces to Eq. 4.39.

Let us construct the number of parameters as occurred in standard canonical parametrization and self-similarity parametrization Eqs. 2.3, 3.7, 4.9, 4.14, 4.20, and 4.24. If n_f is the number of flavors for both quarks and anti quarks then the number of parameters in Eq. 4.50 will be $6n_f + 3$. The first factor is due to the quark and anti quark flavors and additional number 3 corresponding to the 3 parameters A_0^q , A_1^q, and A_2^q for gluon distributions. In a self-similar parametrization like Eqs. 4.26-4.48, the exponents of x and B_1s and B_2s all are flavor independent. It implies, each flavor does not distinguish quark and anti quark. Thus the number of parameters in self-similar PDFs for the above models (1-6) are given in Table4.1. The first brackets in Column 2 of Table 4.1 correspond to number of parameters for quarks, while the second one, number of parameters for gluon.

Table 4.1 Number of parameters in self-similar pdf

Models	Parameters
1	$(n_f+4)+(4+1)$
2	$(n_f+4)+(4+1)$
3	$(n_f+6)+(6+1)$
4	$(n_f+4)+(4+1)$
5	$(n_f+6)+(6+1)$
6	$(n_f+4)+(4+1)$

The CTEQ [91], more recent HERAPDF1.0 [59], HERAPDF2.0 [92], and Ref. [89] parametrization have the corresponding forms

$$q_i^1(x,Q_0^2) = A_0^i x^{A_1^i}(1-x)^{A_2^i} L_1(x) \tag{4.51}$$

$$q_i^2(x,Q_0^2) = A^i x^{B^i}(1-x)^{C^i} L_2(x) \tag{4.52}$$

$$q_i^3(x,Q_0^2) = A^i x^{B^i}(1-x)^{C^i} L_3(x) \tag{4.53}$$

$$q_i^4(x,Q_0^2) = A_{f_i} x^{a_{f_i}}(1-x)^{b_{f_i}} L_4(x) \tag{4.54}$$

respectively, where

$$L_1(x) = e^{A_3^i x}\left(1+e^{A_4^i}x\right)^{A_5^i} \tag{4.55}$$

$$L_2(x) = \left(1+\varepsilon\sqrt{x}+Dx+Ex^2\right) \tag{4.56}$$

$$L_3(x) = \left(1+Dx+Ex^2\right) \tag{4.57}$$

$$L_4(x) = \mathscr{F}\left(x,\{c_{f_i}\}\right) \tag{4.58}$$

Here L_4 basically represents an interpolating smooth function which remains finite both $x \to 0$ and $x \to 1$. In the limit D_1s = 0, the terms occurring in D_1s $(D_1, D_1', \hat{D}_1, \bar{D}_1)$ becomes zero and the Eqs. 4.26, 4.29, 4.32, 4.41 have the similar form to the corresponding standard parametrization (Eqs. 4.51-4.54).

4.2.4 Comparison of the structure functions having power law growth in Q^2 and $\log Q^2$ with data and determination of the corresponding PDFs

From the above models of structure function (Models 3-6), one can observe that Models 3 and 5 have power law in Q^2 but Models 4 and 6 has both power law in Q^2 as well as in $\log Q^2$, which are also closer to QCD expectation. Therefore, we choose the Models 4 and 6 for further comparison and study.

Comparison of data of Models 4 and 6 and determination of the model parameters

In this section, we make a comparison of PDF and structure function of Models 4 and 6 since only these two have logarithmic rise in Q^2 rise in PDF and structure function. Model 6 is the large x extrapolation of Model 4.

To determine the parameters of Model 4 and Model 6, we have used the compiled HERA data [59] as used in earlier work (Model 2). We make χ^2-analysis of the data and obtain the phenomenological range of validity of Q^2 and x.

For Model 4 the fitted parameters are given in Table 4.2 . The range of validity is found within

$$
\begin{aligned}
&2\times 10^{-5} \le x \le 0.4 \\
&1.2 \le Q^2 \le 800\ \text{GeV}^2
\end{aligned}
\tag{4.59}
$$

The number of data points of $\tilde{F}_2$ is 284. Similarly for Model 6 the range of validity is

$$
\begin{aligned}
&2\times 10^{-5} \le x \le 0.4 \\
&1.2 \le Q^2 \le 1200\ \text{GeV}^2
\end{aligned}
\tag{4.60}
$$

which is quite large in comparative to earlier works (Models 1 and 2). The fitted parameters for Model 6 are given in Table 4.3. The number of data points of $\bar{F}_2'$ is 302.

Table 4.2 Results of the fit of Model 4; Eq. 4.15

$\tilde{D}_0$	$\tilde{D}_2$	$\tilde{B}_1$	$\tilde{B}_2$	$\tilde{Q}_0^2$ (GeV^2)	χ^2/ndf
$0.294_{\pm 0.009}$	$1.237_{\pm 0.01}$	$0.438_{\pm 0.004}$	$0.687_{\pm 0.02}$	$0.046_{\pm 0.0004}$	0.60

Table 4.3 Results of the fit of Model 6; Eq. 4.25

$\bar{D}'_0$	$\bar{D}'_2$	$\bar{B}'_1$	$\bar{B}'_2$	$\bar{Q}'^2_0$ (GeV^2)	χ^2/ndf
$0.335_{\pm 0.003}$	$1.194_{\pm 0.0009}$	$0.519_{\pm 0.006}$	$0.082_{\pm 0.001}$	$0.056_{\pm 0.001}$	0.24

In Figs. 4.1 and 4.2, we plot $\tilde{F}_2$ and $\bar{F}'_2$ of Models 4 and 6 respectively as a function of x for few representative values of Q^2 (Model 4: $Q^2 = 1.2, 8.5, 15, 27, 45, 60, 90, 150, 300, 400, 650, 800$ GeV^2 and Model 6: $Q^2 = 1.2, 8.5, 15, 27, 60, 90, 150, 200, 500, 650, 800, 1200$ GeV^2).

The above analysis indicates that a singularity free version of a self-similarity based model in Proton is possible if proper choice of magnification factor is made. It has allowed a such wider phenomenological range of validity in Q^2 than that of the model of Ref. [1]. It has also logarithmic rise in virtually Q^2 instead of power law.

Graphical representation of PDFs of Models 4 and 6

The given form of PDFs for Models 4 and 6 are:

$$\text{Model 4}: \quad \tilde{q}_i(x,Q^2) = \frac{e^{\tilde{D}_0^i}\tilde{Q}_0^2}{M^2}\left(\frac{1}{x}\right)^{\tilde{D}_2}\tilde{B}_1\left[\log\left(1+\frac{Q^2}{\tilde{Q}_0^2}\right)-\frac{\tilde{B}_2}{\tilde{B}_1}\left(\frac{1}{\left(1+\frac{Q^2}{\tilde{Q}_0^2}\right)}-1\right)\right] \tag{4.61}$$

$$\text{Model 6}: \quad \bar{q}'_i(x,Q^2) = \frac{e^{\bar{D}'^i_0}\bar{Q}'^2_0}{M^2}\left(\frac{1}{x}\right)^{\bar{D}'_2}(1-x)^{\bar{D}'_2}\bar{B}'_1\left[\log\left(1+\frac{Q^2}{\bar{Q}'^2_0}\right)-\frac{\bar{B}'_2}{\bar{B}'_1}\left(\frac{1}{\left(1+\frac{Q^2}{\bar{Q}'^2_0}\right)}-1\right)\right] \tag{4.62}$$

with $e^{\tilde{D}_0^u} = 0.964 = e^{\tilde{D}_0^d}$ and $e^{\tilde{D}_0^s} = 0.241 = e^{\tilde{D}_0^c}$ for Model 4 and
$e^{\bar{D}'^u_0} = 1.004 = e^{\bar{D}'^d_0}$ and $e^{\bar{D}'^s_0} = 0.251 = e^{\bar{D}'^c_0}$ for Model 6 respectively.

Graphical representation of PDFs of Model 4 and 6 are shown in Figs. 4.3 and 4.4. As expected both the models have $\log Q^2$ rise to be compared with linear rise in Models 1

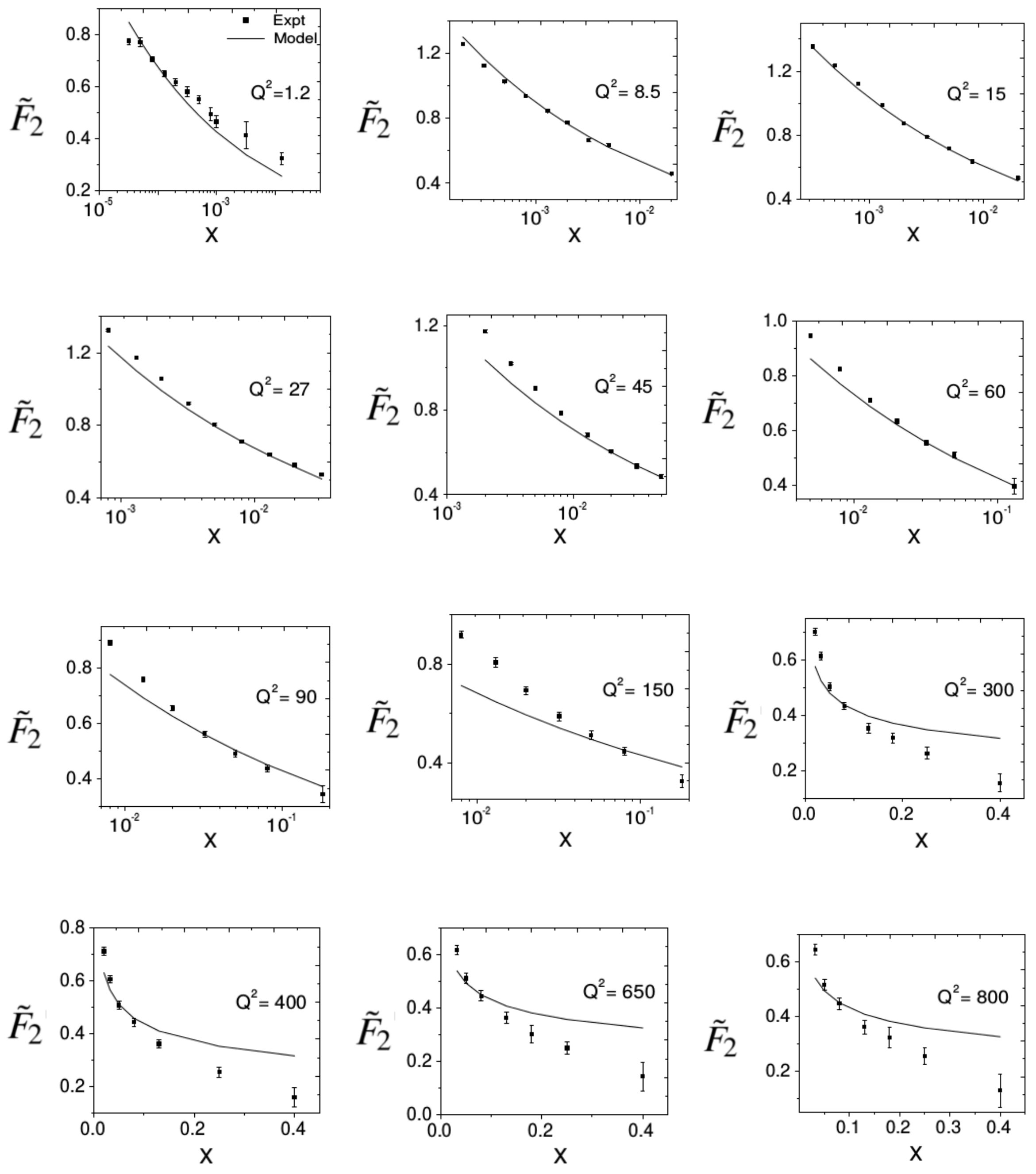

Fig. 4.1 Comparison of the structure function $\tilde{F}_2$ (Model 4; Eq. 4.15) as a function of x in bins of Q^2 with measured data of F_2 from HERAPDF1.0 [59]

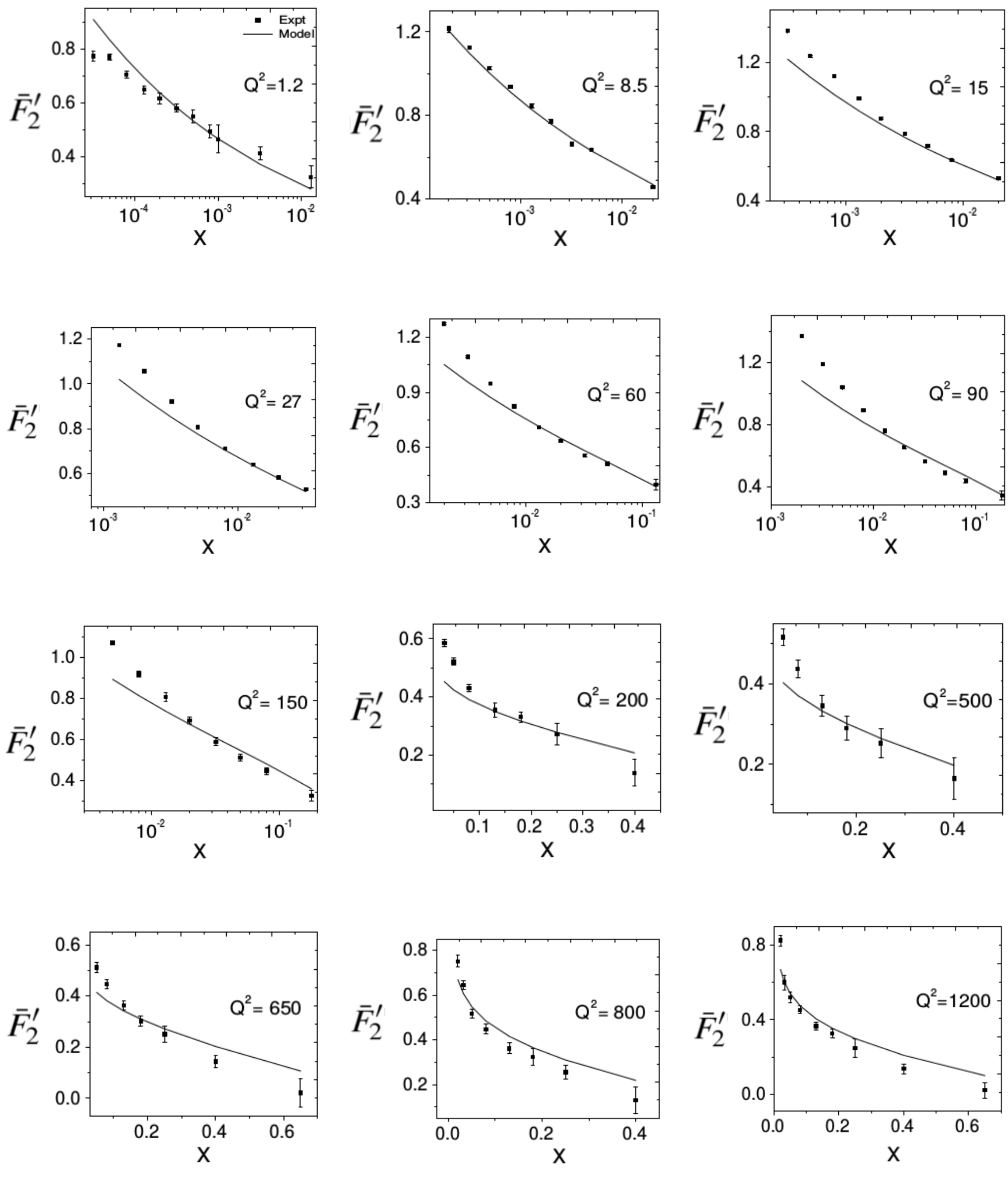

Fig. 4.2 Comparison of structure function $\bar{F}_2'$ (Model 6; Eq. 4.25) as a function of x in bins of Q^2 with measured data of F_2 from HERAPDF1.0 [59]

and 2. It has also power law rise in $\left(\frac{1}{x}\right)$ which is compatible with Regge based models [85, 89, 86–88].

4.3 Summary

In chapter 2, we have obtained singularities in structure function within the x-range; $0 < x < 1$ which is not physically viable. Therefore in chapter 3, we find a singularity free version of the model demanding positivity on the model parameters. However, this version has a very limited Q^2 range in validity; $Q^2 \leq 10\ \mathrm{GeV}^2$. Moreover, all the models of structure functions have linear growth in Q^2. We therefore address, if this approach can yield a singularity free model of proton structure function with better phenomenological range of validity. Furthermore, it will be interesting if the model even yield linear growth in $\log Q^2$ rather than linear Q^2. To that end, in this chapter, we have generalized the definitions of defining magnification factors in uPDF occurred in Eq. 2.1 such that it has expected qualitative features. We have found that in specific case, if the defining parameters satisfy certain conditions among themselves, linear rise in Q^2 with singularity free features unlike in models 1 and 2 emerge (Models 4 and 6).

Assuming that the notion of self-similarity can be smoothly extrapolated into larger x, we have also obtained a model at large and small x (Model 5) for PDF and structure function. As in previous case at small x (Model 4), under specific condition amongst its model parameters, $\log Q^2$ rise in the resulting structure function (Model 6) emerges. The extrapolated model has also been tested with combined HERA data [59] and wider phenomenological range of x and Q^2 has been obtained as expected.

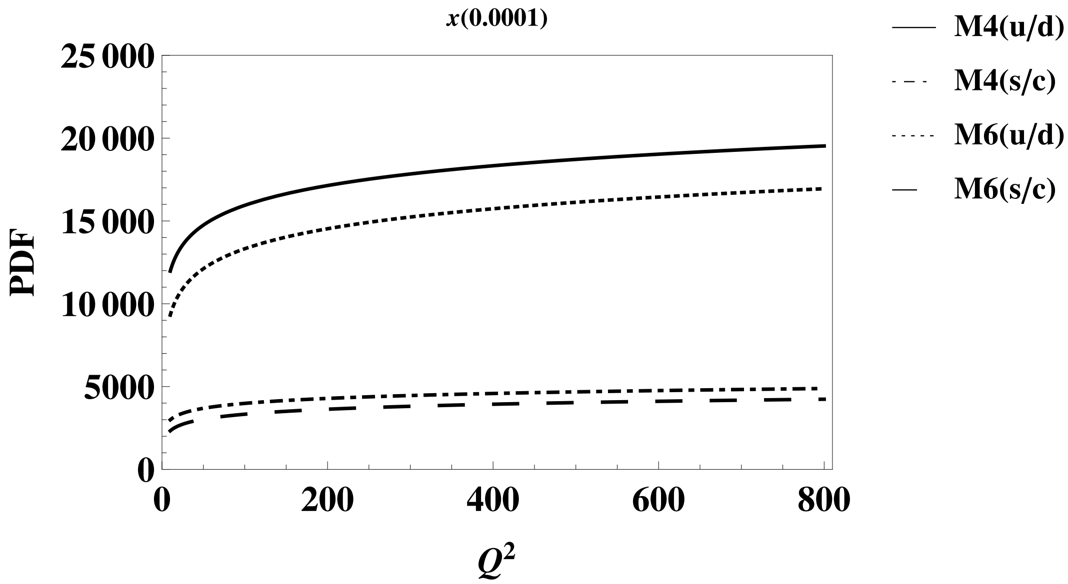

a)

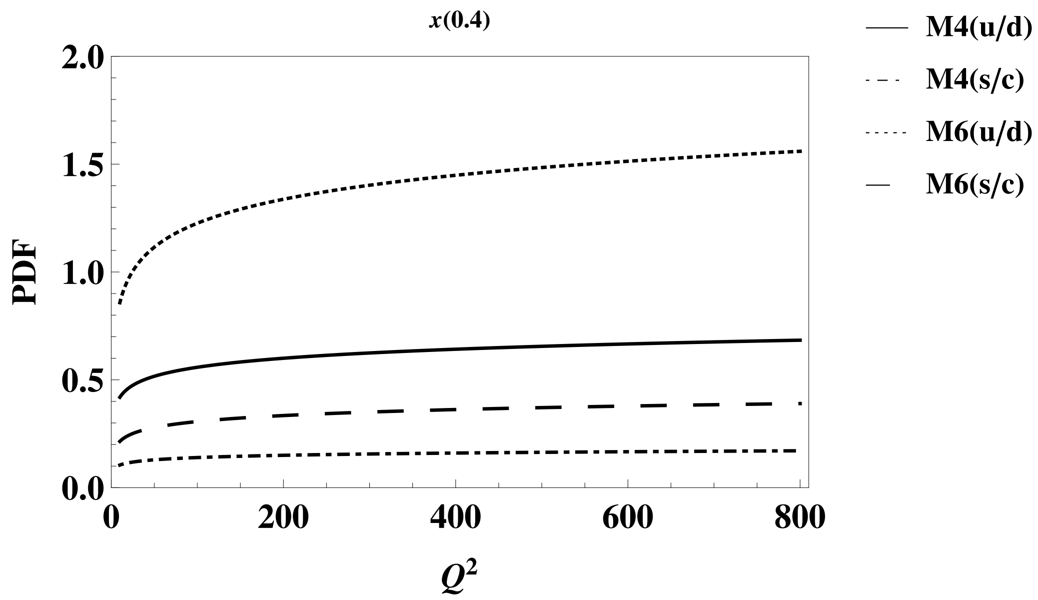

b)

Fig. 4.3 PDF vs Q^2 for two representative values of (a) $x = 10^{-4}$ and (b) $x = 0.4$ for Models 4 and 6. Here, M4(u/d) (line) and M6(u/d) (dotted) represents the PDF for u and d quarks for Models 4 and 6 respectively. Similarly, M4(s/c) (dot-dashed) and M6(s/c) (dashed) represents the PDF for s and c quarks for Models 4 and 6 respectively.

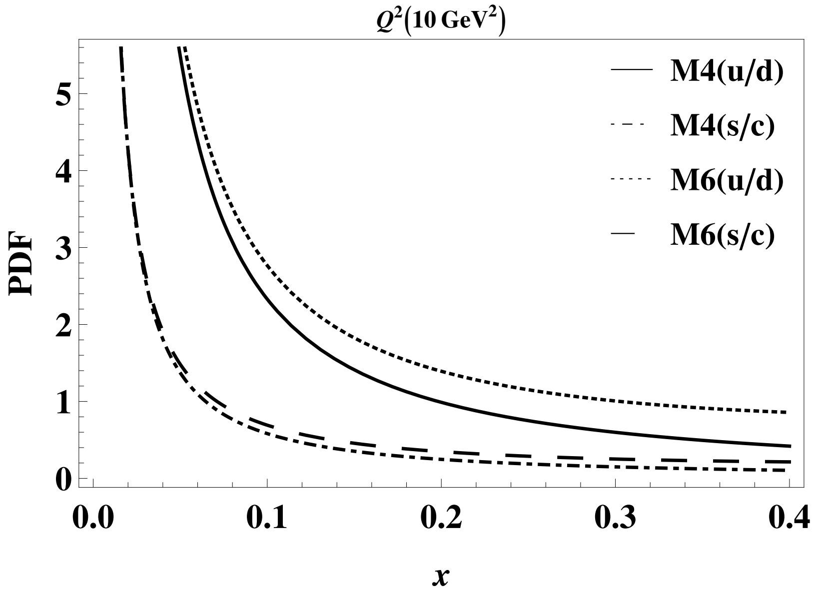

a)

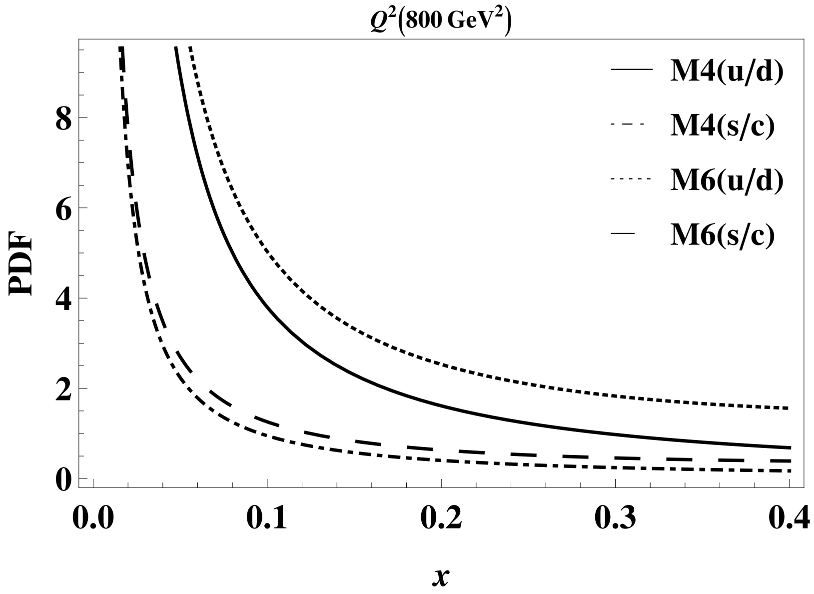

b)

Fig. 4.4 PDF vs x for two representative values of (a) $Q^2 = 10$ GeV^2 and (b) $Q^2 = 800$ GeV^2 for Models 4 and 6. Here, M4(u/d) (line) and M6(u/d) (dotted) represents the PDF for u and d quarks for Models 4 and 6 respectively. Similarly, M4(s/c) (dot-dashed) and M6(s/c) (dashed) represents the PDF for s and c quarks for Models 4 and 6 respectively.

5

Froissart bound in self-similarity based models of proton structure function

5.1 Introduction

The physical significance of Froissart bound has already been discussed in chapter 1. In this chapter, we outline the method of incorporation of this notion in the self-similarity based proton structure functions discussed in chapter 4.

5.2 Formalism

5.2.1 Froissart bound in self-similarity based Proton structure function

The possibility of incorporating Froissart bound in the self-similarity based model of proton structure function was first attempted in Ref. [82]. It was observed that if the magnification factor M_2 is changed to $\left(\log\frac{1}{x}\right)$, then it is possible for structure function. However, we observe that it is true only for PDF but not for structure function.

Below we address this point. Following the method of Ref. [82] for very small x and large Q^2, we can write the PDF as

$$\acute{q}_i(x,Q^2) = \frac{e^{\acute{D}_0^i}\,\acute{Q}_0^2\,\left(\log\frac{1}{x}\right)^{\acute{D}_2+\acute{D}_1\log\left(1+\frac{Q^2}{\acute{Q}_0^2}\right)}}{M^2\left(1+\acute{D}_3+\acute{D}_1\log(\log 1/x)\right)}\left(1+\frac{Q^2}{\acute{Q}_0^2}\right)^{\acute{D}_3+1} \tag{5.1}$$

and the corresponding structure function as

$$\acute{F}_2(x,Q^2) = \frac{e^{\acute{D}_0}\,\acute{Q}_0^2\,x\,\left(\log\frac{1}{x}\right)^{\acute{D}_2+\acute{D}_1\log\left(1+\frac{Q^2}{\acute{Q}_0^2}\right)}}{M^2\left(1+\acute{D}_3+\acute{D}_1\log(\log 1/x)\right)}\left(1+\frac{Q^2}{\acute{Q}_0^2}\right)^{\acute{D}_3+1} \tag{5.2}$$

If an extra condition on the power of $\left(\log\frac{1}{x}\right)$ i.e. $\acute{D}_2+\acute{D}_1\log\left(1+\frac{Q^2}{\acute{Q}_0^2}\right)=2$ is imposed, then PDF of Eq. 5.1 shows Froissart saturation behavior $\sim\left(\log\frac{1}{x}\right)^2$. But it is not so for the structure function of Eq. 5.2 due to the additional multiplicative factor x.

If we recast the multiplicative factor x as

$$x = \left(\log\frac{1}{x}\right)^A \tag{5.3}$$

with

$$A = \frac{-\log\frac{1}{x}}{\log\left(\log\frac{1}{x}\right)} \tag{5.4}$$

then the Froissart condition on the structure function of Eq. 5.2 will be

$$\frac{-\log\frac{1}{x}}{\log\left(\log\frac{1}{x}\right)} + \acute{D}_2 + \acute{D}_1 \log\left(1 + \frac{Q^2}{\acute{Q}_0^2}\right) = 2 \tag{5.5}$$

The first term in LHS of Eq. 5.5 is negative for $0 < x < 1$ and independent of the model parameters. For very small $D_2, D_1 \sim 0$ the condition will be invalid and hence the general Froissart saturation like behavior in structure function is not possible. Therefore we choose an alternative way to get a proper Froissart Bound condition.

5.2.2 Froissart bound compatible self-similarity based Proton structure function with three magnification factors

Case 1

Taking three magnification factors instead of two:

$$\begin{aligned} M_1 &= \left(1 + \frac{Q^2}{Q_0^2}\right) \\ M_2 &= \frac{1}{x} \\ M_3 &= \log\frac{1}{x} \end{aligned} \tag{5.6}$$

one can construct uPDF, PDF and structure function as:

uPDF

$$\begin{aligned} \log[M^2.\grave{f}_i(x,Q^2)] = {}& \grave{D}_1 \log M_1 \log M_2 \log M_3 + \grave{D}_2 \log M_1 \log M_2 + \grave{D}_3 \log M_2 \log M_3 \\ & + \grave{D}_4 \log M_1 \log M_3 + \grave{D}_5 \log M_1 + \grave{D}_6 \log M_2 + \grave{D}_7 \log M_3 + \grave{D}_0{}^i \end{aligned} \tag{5.7}$$

leads to

$$\grave{f}_i(x,Q^2) = e^{\grave{D}_0^i}\left(\frac{1}{x}\right)^{\grave{D}_2\log\left(1+\frac{Q^2}{\grave{Q}_0^2}\right)+\grave{D}_6}$$
$$\times\left(\log\frac{1}{x}\right)^{\grave{D}_1\log\left(1+\frac{Q^2}{\grave{Q}_0^2}\right)\log 1/x+\grave{D}_3\log 1/x+\grave{D}_4\log\left(1+\frac{Q^2}{\grave{Q}_0^2}\right)+\grave{D}_7}\left(1+\frac{Q^2}{\grave{Q}_0^2}\right)^{\grave{D}_5} \tag{5.8}$$

Using the Eq. 2.2 of chapter 2, one can obtain the corresponding PDF becomes

$$\grave{q}_i(x,Q^2) = \frac{e^{\grave{D}_0^i}\,\grave{Q}_0^2\,(1/x)^{\grave{D}_6}\,\left(\log\frac{1}{x}\right)^{\grave{D}_3\log\frac{1}{x}+\grave{D}_7}}{M^2\left(1+\grave{D}_5+\grave{D}_2\log\frac{1}{x}+(\grave{D}_4+\grave{D}_1\log\frac{1}{x})\log\log\frac{1}{x}\right)}$$

$$\times\left((1/x)^{\grave{D}_2\log\left(1+\frac{Q^2}{\grave{Q}_0^2}\right)}(\log 1/x)^{\log\left(1+\frac{Q^2}{\grave{Q}_0^2}\right)\left(\grave{D}_4+\grave{D}_1\log\frac{1}{x}\right)}\left(1+\frac{Q^2}{\grave{Q}_0^2}\right)^{\grave{D}_5+1}-1\right) \tag{5.9}$$

For very small x and large Q^2 , the second term of Eq. (5.9) can be neglected, leading to

$$\grave{q}_i(x,Q^2) = \frac{e^{\grave{D}_0^i}\,\grave{Q}_0^2\,(1/x)^{\grave{D}_2\log\left(1+\frac{Q^2}{\grave{Q}_0^2}\right)+\grave{D}_6}}{M^2\left(1+\grave{D}_5+\grave{D}_2\log\frac{1}{x}+(\grave{D}_4+\grave{D}_1\log\frac{1}{x})\log\log\frac{1}{x}\right)}$$

$$\times\left(\log\frac{1}{x}\right)^{\grave{D}_7+\grave{D}_3\log\frac{1}{x}+\left(\grave{D}_4+\grave{D}_1\log\frac{1}{x}\right)\times\log\left(1+\frac{Q^2}{\grave{Q}_0^2}\right)}\left(1+\frac{Q^2}{\grave{Q}_0^2}\right)^{\grave{D}_5+1} \tag{5.10}$$

from which one can define structure function as:

$$\grave{F}_2(x,Q^2) = \frac{e^{\grave{D}_0}\ \grave{Q}_0^2\ (1/x)^{\grave{D}_2 \log\left(1+\frac{Q^2}{\grave{Q}_0^2}\right)+\grave{D}_6-1}}{M^2\left(1+\grave{D}_5+\grave{D}_2\log\frac{1}{x}+(\grave{D}_4+\grave{D}_1\log\frac{1}{x})\log\log\frac{1}{x}\right)}$$

$$\times\left(\log\frac{1}{x}\right)^{\grave{D}_7+\grave{D}_3\log\frac{1}{x}+\left(\grave{D}_4+\grave{D}_1\log\frac{1}{x}\right)\times\log\left(1+\frac{Q^2}{\grave{Q}_0^2}\right)}\left(1+\frac{Q^2}{\grave{Q}_0^2}\right)^{\grave{D}_5+1} \tag{5.11}$$

which has total 9 parameters: $\grave{Q}_0^2$ and $\grave{D}_i$s with $i = 0$ to 7.

Eq. 5.11 can show the proper Froissart saturation behavior in the structure function under the following conditions:

$$\begin{aligned}
&(1)\quad \grave{D}_2\log\left(1+\frac{Q^2}{\grave{Q}_0^2}\right)+\grave{D}_6 = 1\\
&(2)\quad \grave{D}_7+\grave{D}_3\log\frac{1}{x}+\left(\grave{D}_4+\grave{D}_1\log\frac{1}{x}\right)\times\log\left(1+\frac{Q^2}{\grave{Q}_0^2}\right) = 2
\end{aligned} \tag{5.12}$$

Further if $\grave{D}_7,\ \grave{D}_3,\ \grave{D}_1 \ll \grave{D}_4$, then $\grave{D}_4 = \dfrac{2-\grave{D}_7}{\log\left(1+\frac{Q^2}{\grave{Q}_0^2}\right)}$, the Froissart compatible structure function will be

$$\grave{F}_2(x,Q^2) = \frac{e^{\grave{D}_0}\ \grave{Q}_0^2\ \left(\log\frac{1}{x}\right)^2\left(1+\frac{Q^2}{\grave{Q}_0^2}\right)^{\grave{D}_5+1}}{M^2\left(1+\grave{D}_5+\grave{D}_2\log\frac{1}{x}+(\grave{D}_4+\grave{D}_1\log\frac{1}{x})\log\log\frac{1}{x}\right)} \tag{5.13}$$

which reduces the number parameters by 3.

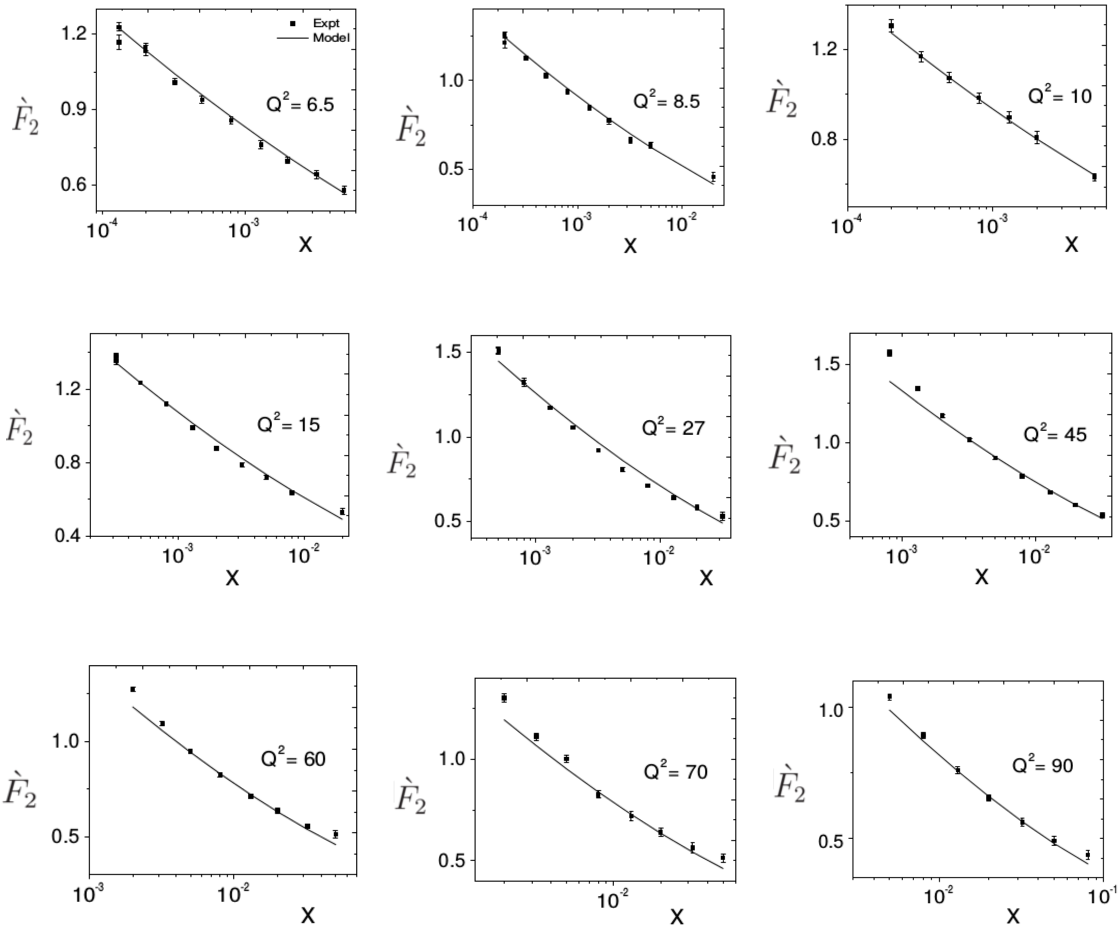

Fig. 5.1 Comparison of the structure function $\grave{F}_2$ (Eq 5.13; case 1) as a function of x in bins of Q^2 with measured data of F_2 from HERAPDF1.0 [59]

Using HERAPDF1.0 [59], Eq. 5.13 is fitted and found its phenomenological ranges of validity: $1.3 \times 10^{-4} \leq x \leq 0.02$ and $6.5 \leq Q^2 \leq 90$ GeV^2 with the fitted parameters listed in Table 5.1. The no. of $\grave{F}_2$ data points is 155.

In Fig. 5.1, we have shown the graphical representation of $\grave{F}_2$ with data for a few representative values of Q^2.

Table 5.1 Results of the fit of $\grave{F}_2$, Eq.5.13; case 1

$\grave{D}_0$	$\grave{D}_1$	$\grave{D}_2$	$\grave{D}_4$	$\grave{D}_5$	$\grave{Q}_0^2$(GeV^2)	χ^2/ndf
$0.1006_{\pm 0.003}$	$0.028_{\pm 0.0008}$	$-0.036_{\pm 0.0001}$	$3.585_{\pm 0.05}$	$-0.857_{\pm 0.01}$	$0.060_{\pm 0.001}$	0.11

Case 2

The above observation thus generalized to improved self-similarity based models suggested in chapter 4. Thus we can construct another new set of magnification factors:

$$\begin{aligned} \hat{M}_1 &= \sum_{j=1}^{n} \frac{B_j}{\left(1+\frac{Q^2}{\hat{Q}_0^2}\right)^j} \qquad j = 1,2 \\ M_2 &= \frac{1}{x} \\ M_3 &= \log\frac{1}{x} \end{aligned} \tag{5.14}$$

from which we can define uPDF, PDF and structure function as follows:

The defining equation of uPDF is

$$\begin{aligned} \log[M^2.\ddot{f}_i(x,Q^2)] = {} & \ddot{D}_1 \log\hat{M}_1 \log M_2 \log M_3 + \ddot{D}_2 \log\hat{M}_1 \log M_2 + \ddot{D}_3 \log M_2 \log M_3 \\ & + \ddot{D}_4 \log\hat{M}_1 \log M_3 + \ddot{D}_5 \log\hat{M}_1 + \ddot{D}_6 \log M_2 + \ddot{D}_7 \log M_3 + \ddot{D}_0{}^i \end{aligned} \tag{5.15}$$

leads to

$$\ddot{f}_i(x,Q^2) = e^{\ddot{D}_0^i}\, \ddot{Q}_0^2 \left(\frac{1}{x}\right)^{\ddot{D}_6} \left(\log\frac{1}{x}\right)^{\ddot{D}_3 \log\frac{1}{x} + \ddot{D}_7} \ddot{B}_1 \left[\frac{1}{\left(1+\frac{Q^2}{\ddot{Q}_0^2}\right)} + \frac{\ddot{B}_2}{\ddot{B}_1} \frac{1}{\left(1+\frac{Q^2}{\ddot{Q}_0^2}\right)^2}\right] \tag{5.16}$$

and therefore corresponding PDF

$$\ddot{q}_i(x,Q^2) = e^{\ddot{D}_0^i}\, \ddot{Q}_0^2\, (1/x)^{\ddot{D}_6} \left(\log\frac{1}{x}\right)^{\ddot{D}_3 \log\frac{1}{x} + \ddot{D}_7} \ddot{B}_1 \left[\log\left(1+\frac{Q^2}{\ddot{Q}_0^2}\right) - \frac{\ddot{B}_2}{\ddot{B}_1} \left(\frac{1}{\left(1+\frac{Q^2}{\ddot{Q}_0^2}\right)} - 1\right)\right] \tag{5.17}$$

So the structure function will be

$$\ddot{F}_2(x,Q^2) = e^{\ddot{D}_0}\,\ddot{Q}_0^2\,(1/x)^{\ddot{D}_6-1}\left(\log\frac{1}{x}\right)^{\ddot{D}_3\log\frac{1}{x}+\ddot{D}_7} \times \ddot{B}_1\left[\log\left(1+\frac{Q^2}{\ddot{Q}_0^2}\right)-\frac{\ddot{B}_2}{\ddot{B}_1}\left(\frac{1}{\left(1+\frac{Q^2}{\ddot{Q}_0^2}\right)}-1\right)\right] \tag{5.18}$$

Putting the extra conditions

$$\begin{aligned} &(1)\quad \ddot{D}_6-1=0\\ &(2)\quad \ddot{D}_3\log\frac{1}{x}+\ddot{D}_7=2 \end{aligned} \tag{5.19}$$

will give the Froissart like behavior in structure function of Eq. 5.18 a new form :

$$\ddot{F}_2(x,Q^2) = e^{\ddot{D}_0}\,\ddot{Q}_0^2\,\log^2(1/x)\,\ddot{B}_1\left[\log\left(1+\frac{Q^2}{\ddot{Q}_0^2}\right)-\frac{\ddot{B}_2}{\ddot{B}_1}\left(\frac{1}{\left(1+\frac{Q^2}{\ddot{Q}_0^2}\right)}-1\right)\right] \tag{5.20}$$

Now using the HERAPDF1.0 [59], Eq.5.20 is fitted and obtained its phenomenological ranges of validity within: $1.3\times10^{-4}\leq x\leq 0.02$ and $6.5\leq Q^2\leq 60$ GeV^2 and also obtained the model parameters which are given in Table 5.2. The no. of $\ddot{F}_2$ data points is 153.

In Fig 5.2, we have shown the graphical representation of $\ddot{F}_2$ with data for a few representative values of Q^2.

Table 5.2 Results of the fit of $\ddot{F}_2$, Eq.5.20; case 2

$\ddot{D}_0$	$\ddot{B}_1$	$\ddot{B}_2$	$\ddot{Q}_0^2$(GeV^2)	χ^2/ndf
$0.00047_{\pm0.0003}$	$0.056_{\pm0.002}$	$0.672_{\pm0.02}$	$0.022_{\pm0.001}$	0.17

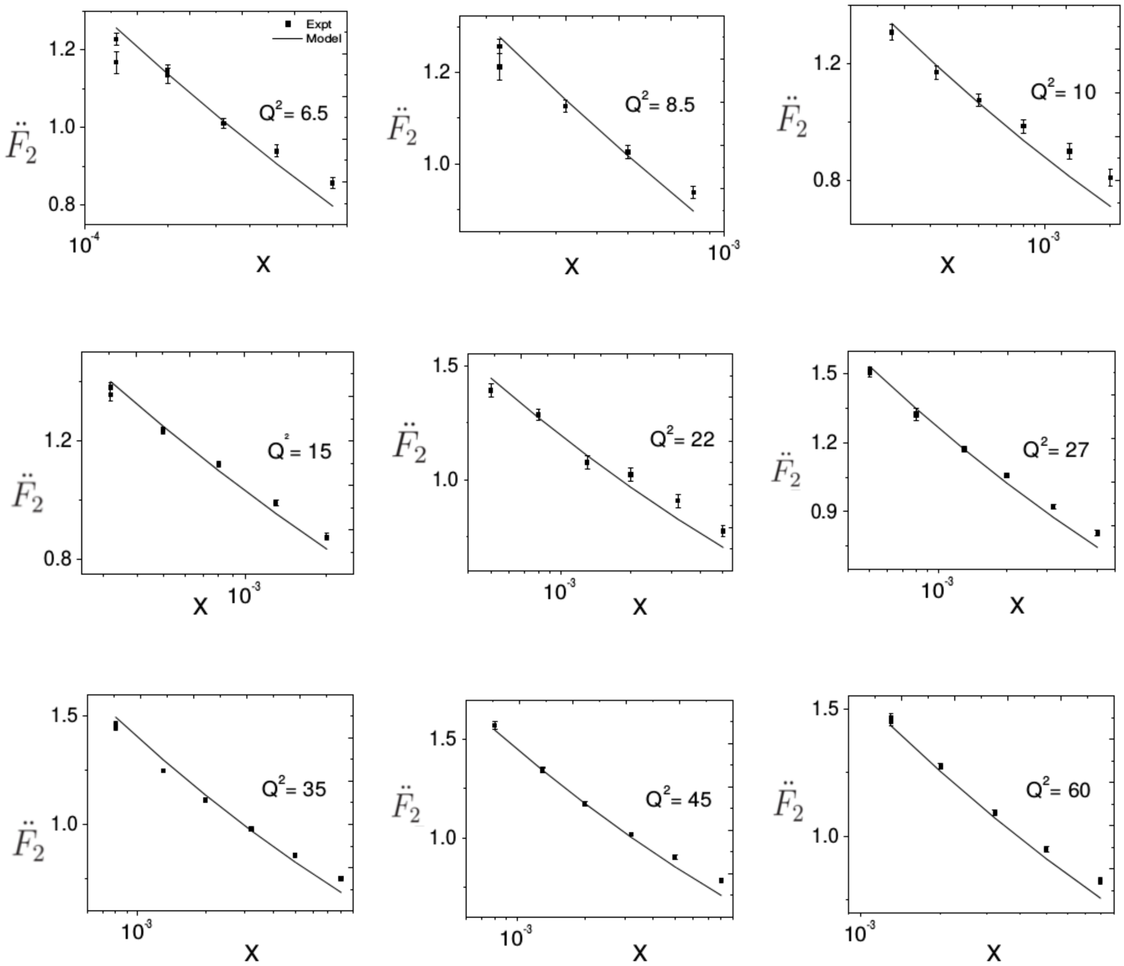

Fig. 5.2 Comparison of the structure function $\ddot{F}_2$ (Eq 5.20; case 2) as a function of x in bins of Q^2 with measured data of F_2 from HERAPDF1.0 [59]

Case 3

We now study how far the analytical structure of the model can come closer to the QCD based model of Block et.al. of Ref. [53]. If the magnification factor M_2 is extrapolated to large x in a parameter free way $\frac{1}{x} \rightarrow \left(\frac{1}{x} - 1\right)$, one obtains a set of magnification factors

$$
\begin{aligned}
\hat{M}_1 &= \sum_{j=1}^{n} \frac{B_j}{\left(1+\frac{Q^2}{\hat{Q}_0^2}\right)^j} \qquad j=1,2 \\
M_2 &= \frac{1}{x}-1 \\
M_3 &= \ln\frac{1}{x} \qquad (5.21)
\end{aligned}
$$

One obtains the following uPDF, PDF and structure function:

uPDF

$$
\breve{f}_i(x,Q^2) = \frac{e^{\breve{D}_0^i}}{M^2}\,(1/x)^{\breve{D}_6}\,(1-x)^{\breve{D}_6}\left(\log\frac{1}{x}\right)^{\breve{D}_3\log\frac{1}{x}+\breve{D}_7} \times \breve{B}_1\left[\frac{1}{\left(1+\frac{Q^2}{\breve{Q}_0^2}\right)}+\frac{\breve{B}_2}{\breve{B}_1}\frac{1}{\left(1+\frac{Q^2}{\breve{Q}_0^2}\right)^2}\right] \qquad (5.22)
$$

Corresponding PDF

$$
\breve{q}_i(x,Q^2) = e^{\breve{D}_0^i}\,\breve{Q}_0^2\,(1/x)^{\breve{D}_6}(1-x)^{\breve{D}_6}\left(\log\frac{1}{x}\right)^{\breve{D}_3\log\left(\frac{1}{x}-1\right)+\breve{D}_7} \times \breve{B}_1\left[\log\left(1+\frac{Q^2}{\breve{Q}_0^2}\right)-\frac{\breve{B}_2}{\breve{B}_1}\left(\frac{1}{\left(1+\frac{Q^2}{\breve{Q}_0^2}\right)}-1\right)\right] \qquad (5.23)
$$

and the structure function

$$
\breve{F}_2(x,Q^2) = e^{\breve{D}_0}\,\breve{Q}_0^2\,(1/x)^{\breve{D}_6-1}(1-x)^{\breve{D}_6}\left(\log\frac{1}{x}\right)^{\breve{D}_3\log\left(\frac{1}{x}-1\right)+\breve{D}_7} \times \breve{B}_1\left[\log\left(1+\frac{Q^2}{\breve{Q}_0^2}\right)-\frac{\breve{B}_2}{\breve{B}_1}\left(\frac{1}{\left(1+\frac{Q^2}{\breve{Q}_0^2}\right)}-1\right)\right] \qquad (5.24)
$$

Putting the extra conditions

$$\begin{aligned} &(1) \quad \breve{D}_6 - 1 = 0 \\ &(2) \quad \breve{D}_3 \log\left(\frac{1}{x} - 1\right) + \breve{D}_7 = 2 \end{aligned} \tag{5.25}$$

will give the Froissart like behavior in structure function as:

$$\breve{F}_2(x,Q^2) = e^{\breve{D}_0}\, \breve{Q}_0^2\, (1-x) \log^2 1/x \times \breve{B}_1 \left[\log\left(1 + \frac{Q^2}{\breve{Q}_0^2}\right) - \frac{\breve{B}_2}{\breve{B}_1} \left(\frac{1}{\left(1 + \frac{Q^2}{\breve{Q}_0^2}\right)} - 1 \right) \right] \tag{5.26}$$

Using the HERAPDF1.0 [59], Eq.5.26 is fitted and obtained its phenomenological ranges of validity within: $1.3 \times 10^{-4} \leq x \leq 0.02$ and $6.5 \leq Q^2 \leq 120$ GeV^2 and also obtained the model parameters which are given in Table 5.3. The no. of $\breve{F}_2$ data points is 215.

In Fig. 5.3, we have shown the graphical representation of $\breve{F}_2$ with data for a few representative values of Q^2.

Table 5.3 Results of the fit of $\breve{F}_2$, Eq.5.26; case 3

$\breve{D}_0$	$\breve{B}_1$	$\breve{B}_2$	$\breve{Q}_0^2$(GeV^2)	χ^2/ndf
$0.006_{\pm 0.0005}$	$0.032_{\pm 0.0005}$	$0.309_{\pm 0.009}$	$0.048_{\pm 0.001}$	0.25

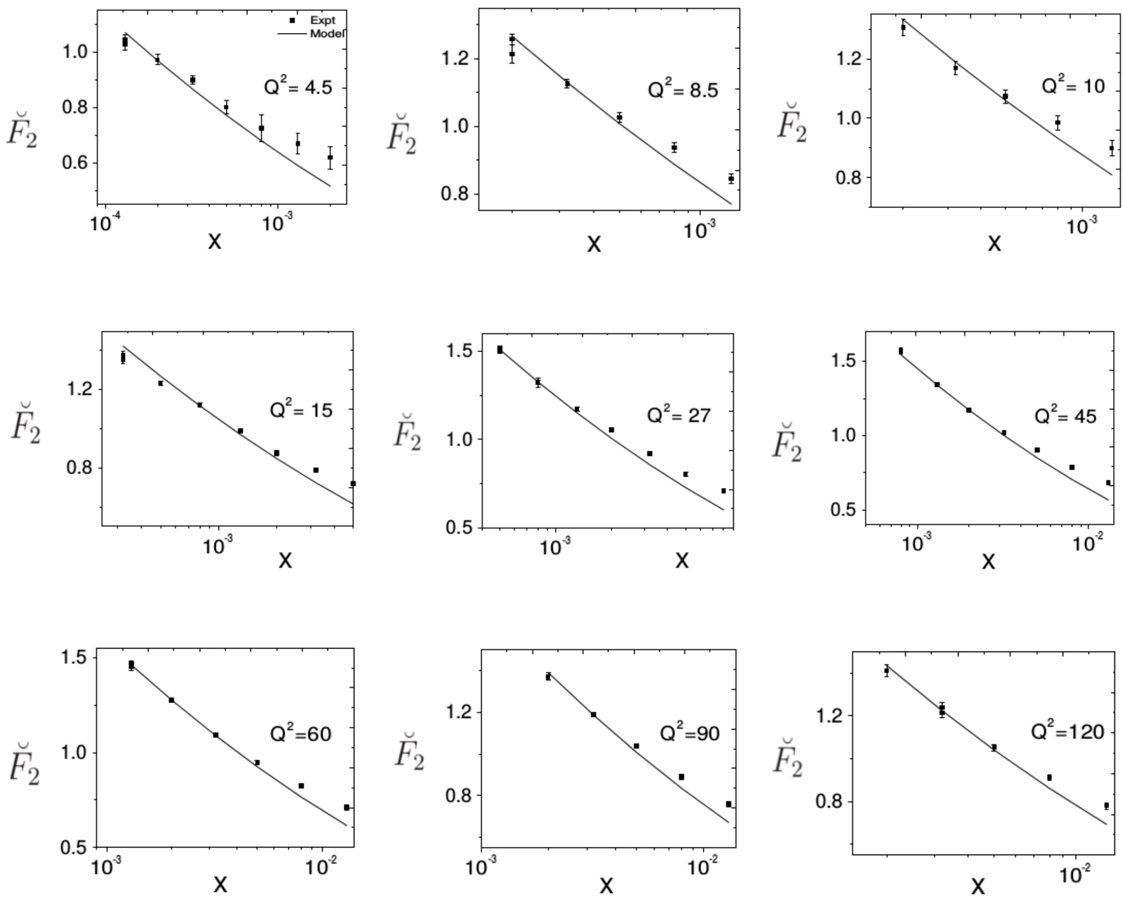

Fig. 5.3 Comparison of the structure function $\breve{F}_2$ (Eq 5.26; case 3) as a function of x in bins of Q^2 with measured data of F_2 from HERAPDF1.0 [59]

Case 4

If the third magnification factor is also large-x extrapolated: $\log\frac{1}{x} \to \log\left(\frac{1}{x}-1\right)$ i.e

$$
\begin{aligned}
\hat{M}_1 &= \sum_{j=1}^{n} \frac{B_j}{\left(1+\frac{Q^2}{\hat{Q}_0^2}\right)^j} \qquad j=1,2 \\
M_2 &= \frac{1}{x}-1 \\
M_3 &= \log\left(\frac{1}{x}-1\right)
\end{aligned}
\tag{5.27}
$$

the corresponding uPDF PDF and structure function becomes:

uPDF

$$\breve{f}_i'(x,Q^2) = \frac{e^{\breve{D}_0'^i}}{M^2}\,(1/x)^{\breve{D}_6'}\,(1-x)^{\breve{D}_6'}\left(\log\frac{1-x}{x}\right)^{\breve{D}_3'\log\left(\frac{1}{x}-1\right)+\breve{D}_7'} \times \breve{B}_1'\left[\frac{1}{\left(1+\frac{Q^2}{\breve{Q}_0'^2}\right)}+\frac{\breve{B}_2'}{\breve{B}_1'}\frac{1}{\left(1+\frac{Q^2}{\breve{Q}_0'^2}\right)^2}\right] \quad (5.28)$$

Corresponding PDF

$$\breve{q}_i'(x,Q^2) = e^{\breve{D}_0'^i}\,\breve{Q}_0'^2\,(1/x)^{\breve{D}_6'}(1-x)^{\breve{D}_6'}\left(\log\frac{1-x}{x}\right)^{\breve{D}_3'\log\left(\frac{1}{x}-1\right)+\breve{D}_7'} \times \breve{B}_1'\left[\log\left(1+\frac{Q^2}{\breve{Q}_0'^2}\right)-\frac{\breve{B}_2'}{\breve{B}_1'}\left(\frac{1}{\left(1+\frac{Q^2}{\breve{Q}_0'^2}\right)}-1\right)\right] \quad (5.29)$$

and the structure function

$$\breve{F}_2'(x,Q^2) = e^{\breve{D}_0'}\,\breve{Q}_0'^2\,(1/x)^{\breve{D}_6'-1}(1-x)^{\breve{D}_6'}\left(\log\frac{1-x}{x}\right)^{\breve{D}_3'\log\left(\frac{1}{x}-1\right)+\breve{D}_7'} \times \breve{B}_1'\left[\log\left(1+\frac{Q^2}{\breve{Q}_0'^2}\right)-\frac{\breve{B}_2'}{\breve{B}_1'}\left(\frac{1}{\left(1+\frac{Q^2}{\breve{Q}_0'^2}\right)}-1\right)\right] \quad (5.30)$$

Putting the extra conditions

$$\begin{aligned}&(1)\quad \breve{D}_6'-1=0\\ &(2)\quad \breve{D}_3'\log\left(\frac{1}{x}-1\right)+\breve{D}_7'=2\end{aligned} \quad (5.31)$$

can show the Froissart like behavior in structure as:

$$\breve{F}_2'(x,Q^2) = e^{\breve{D}_0'}\ \breve{Q}_0'^2\ (1-x)\ \log^2 \frac{1-x}{x}\ \breve{B}_1' \left[\log\left(1+\frac{Q^2}{\breve{Q}_0'^2}\right) - \frac{\breve{B}_2'}{\breve{B}_1'} \left(\frac{1}{\left(1+\frac{Q^2}{\breve{Q}_0'^2}\right)} - 1 \right) \right] \tag{5.32}$$

to be compared with a more recent phenomenologically successful model suggested by Block, Durand, Ha and McKay [53]. The model has wide range of phenomenological validity in Q^2: $0.11 \leq Q^2 \leq 1200$ GeV^2 for small $x \leq x_p = 0.11$ [84] which has Froissart Saturation like behavior [33].

The expression for $F_2^p(x,Q^2)$ [53] is:

$$F_2^p(x,Q^2) = (1-x)\left\{ \frac{F_p}{1-x_p} + A(Q^2)\ln\frac{x_p(1-x)}{x(1-x_p)} + B(Q^2)\ln^2\frac{x_p(1-x)}{x(1-x_p)} \right\} \tag{5.33}$$

Where,

$$\begin{aligned} A(Q^2) &= a_0 + a_1 \ln Q^2 + a_2 \ln^2 Q^2 \\ B(Q^2) &= b_0 + b_1 \ln Q^2 + b_2 \ln^2 Q^2 \end{aligned} \tag{5.34}$$

and the parameters fitted from deep inelastic scattering data [53] are

$$x \leqslant x_p = 0.11 \ \text{ and } \ F_p = 0.413 \pm 0.003\ , \tag{5.35}$$

$$
\begin{aligned}
a_0 &= -8.471\times10^{-2}\pm2.62\times10^{-3}\ , \\
a_1 &= 4.190\times10^{-2}\pm1.56\times10^{-3}\ , \\
a_2 &= -3.976\times10^{-3}\pm2.13\times10^{-4}\ , \\
b_0 &= 1.292\times10^{-2}\pm3.62\times10^{-4}\ , \\
b_1 &= 2.473\times10^{-4}\pm2.46\times10^{-4}\ , \\
b_2 &= 1.642\times10^{-3}\pm5.52\times10^{-5}\ .
\end{aligned}
\tag{5.36}
$$

More recently, expression of Eq. 5.33 was used as an input at $Q^2 = 4.5$ GeV^2 in DGLAP evolution equations in LO and obtained a phenomenological Q^2-range upto $Q^2 \leq 3000$ GeV^2 using more recent HERA data [59].

One can write the Eq. 5.33 in a more simplified version:

$$
\begin{aligned}
F_2^{\mathrm{p}} \sim (1-x)\Bigg[\, & C + a_0' \ln\frac{1-x}{x} + a_1' \ln Q^2 \ln\frac{1-x}{x} + a_2' \ln^2 Q^2 \ln\frac{1-x}{x} \\
& + b_0' \ln^2\frac{1-x}{x} + b_1' \ln Q^2 \ln^2\frac{1-x}{x} + b_2' \ln^2 Q^2 \ln^2\frac{1-x}{x}\Bigg]
\end{aligned}
\tag{5.37}
$$

where

$$C = \frac{F_p}{1-x_p}\ ,\ a_0' = a_0\frac{x_p}{1-x_p}\ ,\ a_1' = a_1\frac{x_p}{1-x_p}\ ,\ a_2' = a_2\frac{x_p}{1-x_p}\ ,$$

$$b_0' = b_0\frac{x_p}{1-x_p}\ ,\ b_1' = b_1\frac{x_p}{1-x_p}\ ,\ b_2' = b_2\frac{x_p}{1-x_p}$$

A comparison of Eq. 5.32 and 5.37 shows that terms like $\ln\dfrac{1-x}{x}$, $\ln^2 Q^2$, and $\ln^2 Q^2 \ln^2\dfrac{1-x}{x}$ are absent in Eq. 5.32 which makes the prediction different.

Table 5.4 Results of the fit of $\breve{F}_2'$, Eq.5.32; case 4

$\breve{D}_0'$	$\breve{B}_1'$	$\breve{B}_2'$	$\breve{Q}_0'^2$(GeV^2)	χ^2/ndf
$0.008_{\pm0.001}$	$0.034_{\pm0.0008}$	$0.251_{\pm0.01}$	$0.057_{\pm0.005}$	0.26

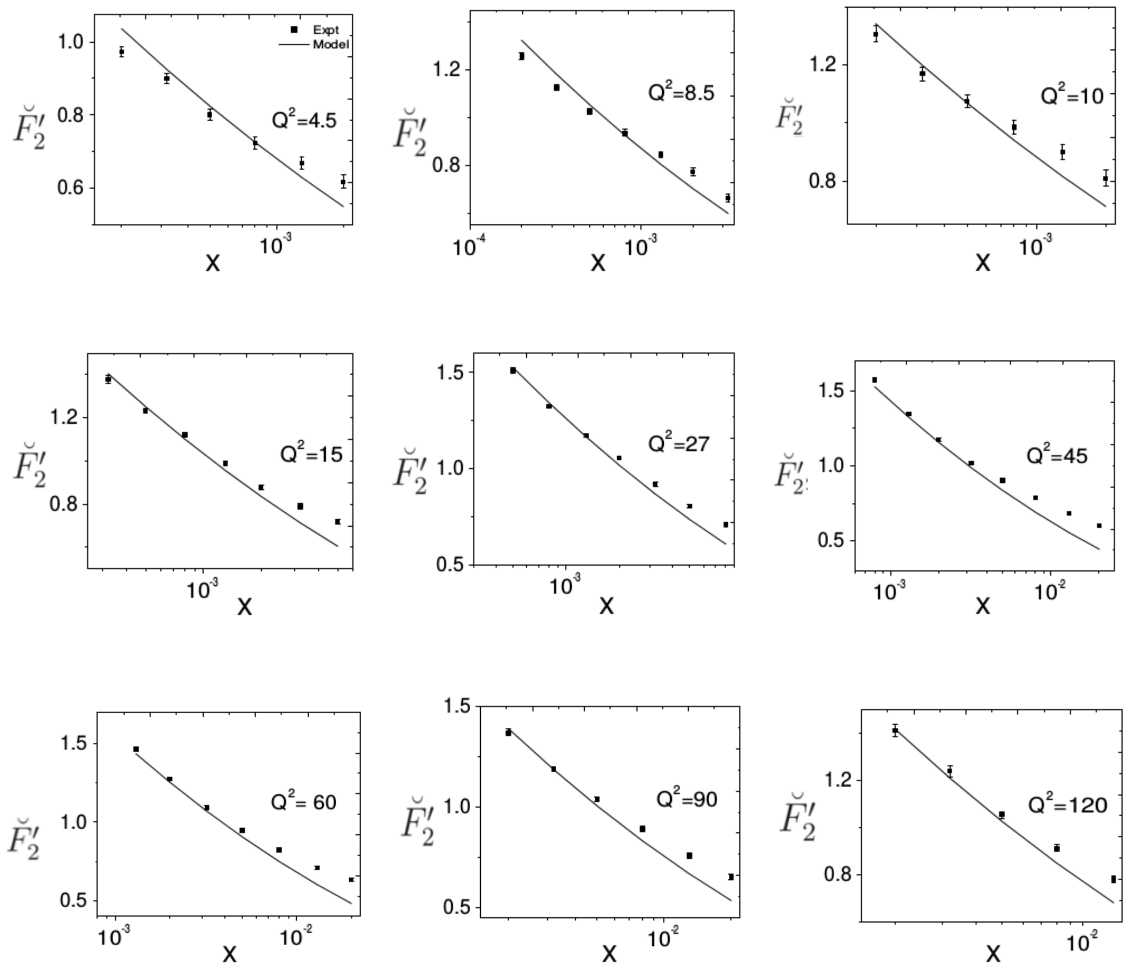

Fig. 5.4 Comparison of the structure function $\breve{F}_2'$ (Eq. 5.32; case 4) as a function of x in bins of Q^2 with measured data of F_2 from HERAPDF1.0 [59]

Using the HERAPDF1.0 [59], Eq. 5.32 is fitted and obtained its phenomenological ranges of validity within: $1.3 \times 10^{-4} \leq x \leq 0.02$ and $6.5 \leq Q^2 \leq 120$ GeV^2 with the obtained model parameters which are given in Table 5.4. The no. of $\breve{F}_2'$ data points is 195.

In Fig. 5.4, we have shown the graphical representation of $\breve{F}_2'$ with data for a few representative values of Q^2.

5.3 Summary

In this chapter, we have found the Froissart saturated form of structure functions based on self-similarity with the power law rise in Q^2 as well as in $\log Q^2$. It needs at least three magnification factors not two as compared to earlier work in Ref. [82]. The ranges of validity for four different cases with three magnification factors are:

$$\begin{aligned}
\text{Eq.5.13} &: \quad 1.3\times 10^{-4} \le x \le 0.02\ ;\ 6.5 \le Q^2 \le 90\ \text{GeV}^2 \\
\text{Eq.5.20} &: \quad 1.3\times 10^{-4} \le x \le 0.02\ ;\ 6.5 \le Q^2 \le 60\ \text{GeV}^2 \\
\text{Eq.5.26} &: \quad 1.3\times 10^{-4} \le x \le 0.02\ ;\ 6.5 \le Q^2 \le 120\ \text{GeV}^2 \\
\text{Eq.5.32} &: \quad 1.3\times 10^{-4} \le x \le 0.02\ ;\ 6.5 \le Q^2 \le 120\ \text{GeV}^2
\end{aligned}$$

to be compared with

$$\begin{aligned}
\text{Eq.4.15} &: \quad 2\times 10^{-5} \le x \le 0.4\ ;\ 1.2 \le Q^2 \le 800\ \text{GeV}^2 \\
\text{Eq.4.25} &: \quad 2\times 10^{-5} \le x \le 0.4\ ;\ 1.2 \le Q^2 \le 1200\ \text{GeV}^2
\end{aligned}$$

of chapter 4 which shows the Froissart saturated structure function has smaller validity ranges as compared to that of structure function having power law growth in Q^2 and $\log Q^2$.

So our inference is that perhaps the present HERA data has not reached its asymptotic regime to have a Froissart saturation like behavior if self-similarity is assumed to be a symmetry of the structure function.

6

Momentum Fractions carried by quarks and gluons in models of proton structure functions

6.1 Introduction

How the quarks and gluons share their longitudinal momentum in proton is an important topic of study by itself. It has been studied in [94–96, 52, 97, 98] within perturbative QCD and Lattice QCD [99]. It is equally interesting to study the corresponding pattern of such momentum fractions in other phenomenological models of proton [100–105], available in current literature. Since the physics at small x has not yet been understood completely, it is an worthwhile topic to study phenomenologically.

In chapters 2-5, we have discussed some of such models based on self-similarity. In this chapter, we will consider self-similarity based models (models 1-4, 7), one QCD based and Froissart bound compatible model (model 5), one with DGLAP approach (model 6) and one with Froissart bound compatible based on self-similarity (model 8). Each of the model has its own phenomenological range of validity, while models 1-3 have power law growth in Q^2, the other model has a logarithmic growth in Q^2.

The aim of the present chapter is to calculate the partial momentum fractions of small x quarks ($\langle \hat{x} \rangle_q$) and the corresponding upper bound for small x gluons ($\langle \hat{x} \rangle_g$). We will then compare the predictions of all the models with perturbative QCD, Lattice QCD and Ads/QCD models.

Since each of the models has phenomenological range of validity only for a limited small x range, its role in calculating the second moments of parton distributions might be minor. Still it will be instructive to calculate quantitatively how much it contributes to the total momentum fractions.

Another aim of this chapter is therefore to compare the models predictions of $\langle \hat{x} \rangle_q$ at fixed Q^2 considering a common x-range and compare with theory and experimental data. We will also study if by any specific model can be preferred over others from this analysis.

Finally, possible role of high x quarks and ultra small x gluons are also discussed to realize the expected QCD behavior, not included in the small x models under study.

In section 6.2, we outline the models and essential formalism. In section 6.3, we report the results and discussion. Section 6.4 contains the conclusion.

6.2 Models

The method of construction of self-similarity based models has been already discussed in chapters 2, 3, 4 and 5. For completeness we will outline six models for the calculation of momentum fractions carried by quarks and gluons:

Model 1: Proton structure function based on self-similarity:

We will consider Eq. 2.6 as model 1 from chapter 2:

$$F_2(x,Q^2) = \frac{e^{D_0}\, Q_0^2\, \left(\frac{1}{x}\right)^{D_2-1}}{M^2\left(1+D_3+D_1\log\left(\frac{1}{x}\right)\right)} \left(\left(\frac{1}{x}\right)^{D_1\log\left(1+\frac{Q^2}{Q_0^2}\right)} \left(1+\frac{Q^2}{Q_0^2}\right)^{D_3+1} - 1 \right) \tag{6.1}$$

with the validity range :

$$6.2\times10^{-7} \leq x \leq 10^{-2}$$
$$0.045 \leq Q^2 \leq 120 \text{ GeV}^2$$

Model 2: Phenomenological analysis of model 1 with more recent data

From the same chapter i.e chapter 2, we take Eq. 2.14 is for model 2.

$$F_2''(x,Q^2) = \frac{e^{D_0''}\, Q_0''^2\, \left(\frac{1}{x}\right)^{D_2''-1}}{M^2\left(1+D_3''+D_1''\log\frac{1}{x}\right)} \left(\left(\frac{1}{x}\right)^{D_1''\log\left(1+\frac{Q^2}{Q_0''^2}\right)} \left(1+\frac{Q^2}{Q_0''^2}\right)^{D_3''+1} - 1 \right) \tag{6.2}$$

with the validity range :

$$6.62\times10^{-6} \leq x \leq 10^{-2}$$
$$0.35 \leq Q^2 \leq 150 \text{ GeV}^2$$

Model 3: Singularity free self-similarity based structure function at small *x*

Model 3 represents Eq. 3.8 of chapter 3.

$$F_2'(x,Q^2) = \frac{e^{D_0'}\, Q_0'^2\, \left(\frac{1}{x}\right)^{D_2'-1}}{M^2\left(1+D_3'+D_1'\log\frac{1}{x}\right)} \left(\left(\frac{1}{x}\right)^{D_1'\log\left(1+\frac{Q^2}{Q_0'^2}\right)} \left(1+\frac{Q^2}{Q_0'^2}\right)^{D_3'+1} - 1 \right) \tag{6.3}$$

with the validity range :

$$2 \times 10^{-5} \leq x \leq 0.02$$
$$0.85 \leq Q^2 \leq 10 \text{ GeV}^2$$

Model 4: An improved singularity free self-similarity based model of proton structure function at small *x*

Eq. 4.15 is taken from chapter 4 as model 4.

$$\tilde{F}_2(x,Q^2) = \frac{e^{\tilde{D}_0}\tilde{Q}_0^2}{M^2}\left(\frac{1}{x}\right)^{\tilde{D}_2-1}\tilde{B}_1\left[\log\left(1+\frac{Q^2}{\tilde{Q}_0^2}\right) - \frac{\tilde{B}_2}{\tilde{B}_1}\left(\frac{1}{\left(1+\frac{Q^2}{\tilde{Q}_0^2}\right)}-1\right)\right] \tag{6.4}$$

with the validity range :

$$2 \times 10^{-5} \leq x \leq 0.4$$
$$1.2 \leq Q^2 \leq 800 \text{ GeV}^2$$

Model 5: Froissart bound compatible model of Block, Durand, Ha and McKay

For model 5, we choose Block et. al model as described in chapter 5; Eq. 5.33

$$F_2^p(x,Q^2) = (1-x)\left\{\frac{F_p}{1-x_p} + A(Q^2)\ln\frac{x_p(1-x)}{x(1-x_p)} + B(Q^2)\ln^2\frac{x_p(1-x)}{x(1-x_p)}\right\} \tag{6.5}$$

Where,

$$\begin{aligned} A(Q^2) &= a_0 + a_1 \ln Q^2 + a_2 \ln^2 Q^2 \\ B(Q^2) &= b_0 + b_1 \ln Q^2 + b_2 \ln^2 Q^2 \end{aligned} \tag{6.6}$$

with the validity range

$$x \le 0.11$$
$$0.11 \le Q^2 \le 1200 \text{ GeV}^2$$

The numerical values of the model parameters are already given in chapter 5 of Eq. 5.36.

Model 6: The model of structure function based on approximate solution of DGLAP equation of small x

Model 6 represents the model of structure function based on approximate solution of DGLAP equation of small x. Here, we will consider the t-evolution of singlet structure function [107]

$$F_2^S(x,t) = F_2^S(x,t_0)\left(\frac{t}{t_0}\right) \tag{6.7}$$

where, $t = \log\frac{Q^2}{\Lambda^2}$ and $t_0 = \log\frac{Q_0^2}{\Lambda^2}$ and $\Lambda = 0.22$ GeV.

The above Eq. 6.7 is based on small x approximation of DGLAP equation [108] and obtained their solution with Lagrange method [109].

Using the inputs provided by HERAPDF2.0 [92] at $Q^2 = Q_0^2 = 1.9$ GeV^2 in the definition of

$$F_2^S = \sum_i x(q_i + \bar{q}_i) \tag{6.8}$$

we can get the form of $F_2^S(x,t_0)$ as:

$$\begin{aligned} F_2^S(x,t_0) = 4.07x^{0.714}(1-x)^{4.84}(1+13.4x^2) + 3.15x^{0.806}(1-x)^{4.08} \\ + 0.105x^{-0.172}(1-x)^{8.06}(1+11.9x) + 0.1056x^{-0.172}(1-x)^{4.88} \end{aligned} \tag{6.9}$$

and use this in Eq. 6.7 for further calculation.

Model 7: An improved singularity free self-similarity based model of proton structure function extrapolated to large x

Eq. 4.25 is the model 7, taken from chapter 4.

$$\bar{F}_2'(x,Q^2) = \frac{e^{\bar{D}_0'}\bar{Q}_0'^2}{M^2}\left(\frac{1}{x}\right)^{\bar{D}_2'-1}(1-x)^{\bar{D}_2'}\bar{B}_1'\left[\log\left(1+\frac{Q^2}{\bar{Q}_0'^2}\right)-\frac{\bar{B}_2'}{\bar{B}_1'}\left(\frac{1}{\left(1+\frac{Q^2}{\bar{Q}_0'^2}\right)}-1\right)\right] \tag{6.10}$$

with the validity range :

$$2\times 10^{-5} \le x \le 0.4$$
$$1.2 \le Q^2 \le 1200\ \text{GeV}^2$$

Model 8 : Froissart Saturated structure function of proton based on self-similarity

Model 8 is Eq. 5.32 taken from chapter 5, which is more closer to the model of [53].

$$\breve{F}_2'(x,Q^2) = e^{\breve{D}_0'}\,\breve{Q}_0'^2\,(1-x)\,\ln^2\frac{1-x}{x}\,\breve{B}_1'\left[\log\left(1+\frac{Q^2}{\breve{Q}_0'^2}\right)-\frac{\breve{B}_2'}{\breve{B}_1'}\left(\frac{1}{\left(1+\frac{Q^2}{\breve{Q}_0'^2}\right)}-1\right)\right] \tag{6.11}$$

with the validity range:

$$1.3\times 10^{-4} \le x \le 0.02$$
$$6.5 \le Q^2 \le 120\ \text{GeV}^2$$

6.2.1 Momentum Sum Rule and partial momentum fractions

The momentum sum rule is given as [78, 79, 110]

$$\int_0^1 x\sum\left(q_i(x,Q^2)+\bar{q}_i(x,Q^2)\right)dx+\int_0^1 G(x,Q^2)\,dx = 1 \tag{6.12}$$

where

$$G(x,Q^2) = xg(x,Q^2) \tag{6.13}$$

$g(x,Q^2)$ is the gluon number density. It can be converted [79] into an inequality if the information about quarks and gluons is available only in a limited range of x, say $x_a \leq x \leq x_b$ i.e.

$$\int_{x_a}^{x_b} x \sum \left(q_i(x,Q^2) + \bar{q}_i(x,Q^2)\right) dx + \int_{x_a}^{x_b} G(x,Q^2)\ dx\ < 1 \tag{6.14}$$

We have omitted the equality sign in Eq. 6.14 because it will correspond to a nucleon, populated by small quarks and gluons (parton) only within the range $x_a < x < x_b$, which makes no sense physically. This yields the respective information when the momentum fractions carried by small x quarks and gluons in $x_a < x < x_b$ to be

$$\langle \hat{x} \rangle_q = \int_{x_a}^{x_b} x \sum \left(q_i(x,Q^2) + \bar{q}_i(x,Q^2)\right) dx \tag{6.15}$$

Using Eq. 2.5, we can write

$$\langle \hat{x} \rangle_q = \left(\sum_{i=1}^{N_f} e_i^2 \right)^{-1} \int_{x_a}^{x_b} F_2(x,Q^2) dx \tag{6.16}$$

e_i is the fractional electric charges of quarks and anti quarks. If we assume their flavored dependence and take number of flavors $N_f = 4$, we obtain

$$\sum_{i=1}^{4} e_i^2 = \frac{10}{9} \tag{6.17}$$

for u, d, s and c quarks leading to

$$\langle \hat{x} \rangle_q = \frac{9}{10} \int_{x_a}^{x_b} F_2(x,Q^2) dx \tag{6.18}$$

Similarly, for $N_f = 5$ i.e. for u, d, s, c and b quarks, we will have

$$\sum_{i=1}^{5} e_i^2 = \frac{11}{9} \tag{6.19}$$

and

$$\langle \hat{x} \rangle_q = \frac{9}{11} \int_{x_a}^{x_b} F_2(x, Q^2) dx \tag{6.20}$$

and

$$\langle \hat{x} \rangle_g < \int_{x_a}^{x_b} G(x, Q^2)\ dx\ < 1 - \langle \hat{x} \rangle_q \tag{6.21}$$

Note that Eq. 2.5 yields only the upper limit of the fractional momentum carried by the gluons in the regime $x_a < x < x_b$.

In terms of structure function, the momentum sum rule inequality is

$$\int_{x_a}^{x_b} \left\{ aF_2(x, Q^2) + G(x, Q^2) \right\} dx\ < 1 \tag{6.22}$$

where $a = \frac{e^{\tilde{D}_0}}{e^{D_0}}$ is Q^2-independent parameter, determined from data [111], $a = 3.1418$ [78], using the fractionally charged quarks.

We note that the structure function defined in Eq. 2.5 and used subsequently in our calculation is only a singlet nature, the valence-quark being assumed to be negligible at small x.

6.3 Results and Discussion

6.3.1 Numerical results of self-similarity based models with linear rise in Q^2: Models 1, 2, 3

We take recourse to numerical method i.e. we evaluate $\langle \hat{x} \rangle_q$ numerically by using Eq. 6.16 for a few representative values of Q^2 (GeV^2). For comparison we choose a particular range of x: $x_a \leqslant x \leqslant x_b$ i.e. $6.2 \times 10^{-7} \leq x \leq 10^{-2}$ as in Ref. [1]. The choice is made because it will be suitable for all the models (models 1-4).

Table 6.1 Results of $\langle\hat{x}\rangle_q$ for $N_f = 4$ of Model 1, 2 and 3 for different Q^2

Q^2 (GeV^2)	$\langle\hat{x}\rangle_q$ (Model 1)	$\langle\hat{x}\rangle_q$ (Model 2)	$\langle\hat{x}\rangle_q$ (Model 3)
$Q^2 = Q_0^2$	6.063×10^{-4}	2.008×10^{-3}	1.232×10^{-3}
2	3.740×10^{-3}	4.021×10^{-3}	3.539×10^{-3}
6	5.328×10^{-3}	5.593×10^{-3}	1.455×10^{-2}
10	6.179×10^{-3}	6.377×10^{-3}	2.833×10^{-2}
60	9.791×10^{-3}	9.714×10^{-3}	-
80	1.050×10^{-2}	1.033×10^{-2}	-
120	1.152×10^{-2}	1.123×10^{-2}	-
150	-	1.172×10^{-2}	-

In Table 6.1, column 2, 3 and 4 represents the numerical values of $\langle\hat{x}\rangle_q$ for models 1, 2 and 3 taking $N_f = 4$. Here, $\langle\hat{x}\rangle_q$ is recorded up to 150 GeV^2, the maximum phenomenological limit for model 2. From the same Table, we observe that the $\langle\hat{x}\rangle_q$ in model 3 is much more than that of model 1 and 2 within its valid range $Q^2 \leqslant 10$ GeV^2. However, the models 1 and 2 have nearly equal $\langle\hat{x}\rangle_q$.

6.3.2 Numerical results of self-similarity based model with linear rise in $\log Q^2$: Model 4

In Table 6.2, we have recorded the numerical results of $\langle\hat{x}\rangle_q$ of model 4 in column 2 upto its valid range: $Q^2 = 800$ GeV^2, considering number of flavor $N_f = 4$ within the same range of x as that of used in earlier calculation (Table 6.1). One can see the pattern of $\langle\hat{x}\rangle_q$ is increasing with increasing Q^2 as that of models 1, 2 and 3 above. In column 3, we have put the corresponding results of upper limit of $\langle\hat{x}\rangle_g$ and this is decreasing with increasing Q^2. As an illustration for model 4, the ratio of $\langle\hat{x}\rangle_g$ vs $\langle\hat{x}\rangle_q$ are nearly equal to 120, 100 and 91 for Q^2= 60, 300 and 800 GeV^2 respectively, far above unity. It indicates that the $\langle\hat{x}\rangle_q$ will never exceed the corresponding upper bound of $\langle\hat{x}\rangle_g$ within their phenomenological ranges of validity where the models make sense.

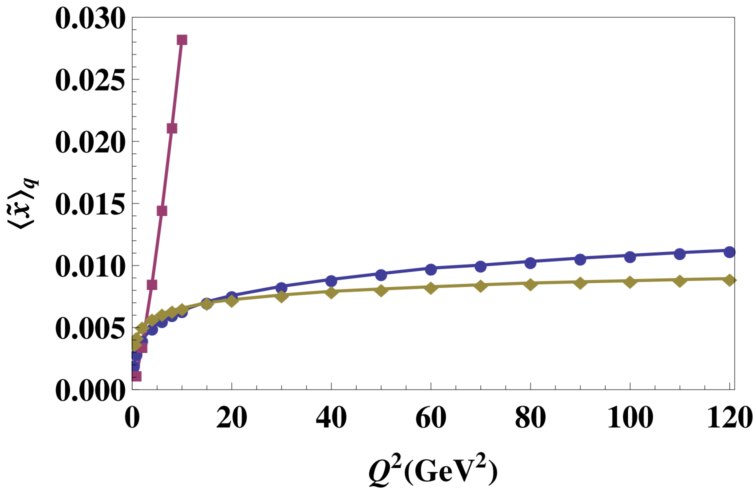

Fig. 6.1 $\langle\hat{x}\rangle_q$ vs Q^2 (GeV^2) for $n_f = 4$ of Model 2 (dots), Model 3 (squares) and Model 4 (diamonds) respectively.

6.3.3 Comparison of models 2, 3 and 4:

In Fig. 6.1, we have shown the pattern of $\langle\hat{x}\rangle_q$ for the models 2, 3 and 4 graphically. The faster linear growth in model 3 can be prominently seen from Fig. 6.1.

6.3.4 Numerical results of models 5 and 6

In Table 6.3, we have recorded the numerical values of $\langle\hat{x}\rangle_q$ as well as the upper limit of $\langle\hat{x}\rangle_g$ (using Eq. 6.21) for Q^2 upto 1200 GeV^2 for models 5 and 6. For comparison, the Q^2-range is taken as that of Ref. [53] : $0.85 \leq Q^2 \leq 1200$ GeV^2 for both the models and also the x-range

Table 6.2 Results of $\langle\hat{x}\rangle_q$ and upper limit of $\langle\hat{x}\rangle_g$ for $N_f = 4$ of Model 4 for different Q^2

Q^2 (GeV^2)	$\langle\hat{x}\rangle_q$	$\langle\hat{x}\rangle_g$
$Q^2 = Q_0^2$	4.563×10^{-3}	9.954×10^{-1}
10	6.574×10^{-3}	9.934×10^{-1}
60	8.288×10^{-3}	9.917×10^{-1}
80	8.591×10^{-3}	9.914×10^{-1}
150	9.161×10^{-3}	9.908×10^{-1}
300	9.812×10^{-3}	9.901×10^{-1}
500	1.031×10^{-2}	9.896×10^{-1}
800	1.076×10^{-2}	9.892×10^{-1}

Table 6.3 Results of $\langle\hat{x}\rangle_q$ and upper limit of $\langle\hat{x}\rangle_g$ for $N_f = 4$ of Model 5 and 6 for different Q^2

Q^2 (GeV^2)	$\langle\hat{x}\rangle_q$ (Model 5)	$\langle\hat{x}\rangle_g$ (Model 5)	$\langle\hat{x}\rangle_q$ (Model 6)	$\langle\hat{x}\rangle_g$ (Model 6)
0.85	2.051×10^{-3}	9.979×10^{-1}	1.553×10^{-2}	9.844×10^{-1}
10	5.882×10^{-3}	9.941×10^{-1}	4.873×10^{-2}	9.512×10^{-1}
80	9.114×10^{-3}	9.908×10^{-1}	7.673×10^{-2}	9.232×10^{-1}
150	1.009×10^{-2}	9.899×10^{-1}	8.520×10^{-2}	9.148×10^{-1}
500	1.196×10^{-2}	9.880×10^{-1}	1.014×10^{-1}	8.986×10^{-1}
1200	1.367×10^{-2}	9.863×10^{-1}	1.162×10^{-1}	8.838×10^{-1}

is $x_a \leqslant x \leqslant x_b$, where x_a= 6.2×10^{-7}, the lower limit of x taken from Ref. [1] and $x_b = 0.11$, the extreme limit of x from Ref. [53]. The calculation is done for $N_f = 4$. Column 2 and 4 represents the numerical values of $\langle\hat{x}\rangle_q$ while column 3 and 5 is for the upper limit of $\langle\hat{x}\rangle_g$ of models 5 and 6 respectively. From Table 6.3, at Q^2= 500 GeV^2 the ratio of $\langle\hat{x}\rangle_g$ vs $\langle\hat{x}\rangle_q$ of model 5 is 82 and that of for 1200 GeV^2 of model 6 is 72 which are again far above unity. A comparison of models 5 and 6 indicates that at any Q^2 under study, $\langle\hat{x}\rangle_q$ of model 5 remains around $\left(\frac{1}{10}\right)^{th}$ of model 6.

It indicates that within the experimental range of validity of each model, upper limit of $\langle\hat{x}\rangle_g$ allowed by the momentum sum rule far exceeds the corresponding value of $\langle\hat{x}\rangle_q$. As noted earlier that the possibility of $\langle\hat{x}\rangle_q$ exceeding the upper bound of $\langle\hat{x}\rangle_g$ cannot be realized in the phenomenological ranges of validity of these two models as well.

6.3.5 Comparison of models having linear growth in $\log Q^2$: Models 4, 5 and 6

In Fig. 6.2, we compare the pattern of $\langle\hat{x}\rangle_q$ for models 4, 5 and 6 by taking Q^2 upto 800 GeV^2. We observe, all the three pattern of $\langle\hat{x}\rangle_q$ increase on increasing Q^2. But the growth for model 6 is larger than that of models 4 and 5. However, the growth can be made closer to models 4 and 5 by decreasing the exponent of $\left(\dfrac{t}{t_0}\right)$ of Eq. 6.7) as has been noted in Refs. [107, 112] by obtaining more generalized solution of small x DGLAP equation [108] using

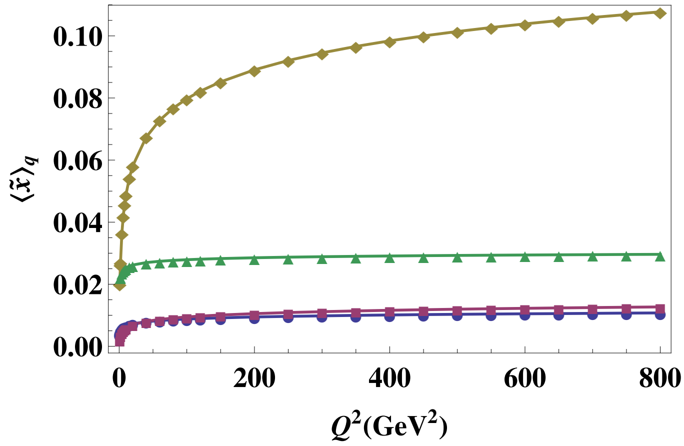

Fig. 6.2 $\langle\hat{x}\rangle_q$ vs Q^2 (GeV^2) for $n_f = 4$ of Model 4 (dots), Model 5 (squares) and Model 6 with $\left(\frac{t}{t_0}\right)$ (diamonds) and Model 6$'$ with $\left(\frac{t}{t_0}\right)^{0.2}$ (triangles) respectively.

the Lagrange method [109]. An evolution of the form of $\sim \left(\frac{t}{t_0}\right)^{0.2}$ which makes the model closer to models 4 and 5 is shown in the same Fig. 6.2. Here after this will be defined as model 6$'$.

A common feature of all the models (1-8) is that the $\langle\hat{x}\rangle_q$ increases with Q^2 while $\langle\hat{x}\rangle_g$ decreases. However, the upper bound of $\langle\hat{x}\rangle_g$ is always far above the corresponding value of $\langle\hat{x}\rangle_q$ within the phenomenological range of validity of each model as noted earlier. In models 1-3, the rise is faster than that of models 4, 5 and 6 as due to the power law growth in structure function with Q^2 of the three models.

6.3.6 Momentum fraction calculation in Froissart bound compatible Proton structure function (model 8) and its comparison with models 5 and 7

Here, we will compare the models 5, 7 and 8 within the Q^2-range taken as $4.5 \leqslant Q^2 \leqslant 120$ GeV^2 which is common for the three models to obtain the values of $\langle\hat{x}\rangle_q$ within the x-range:

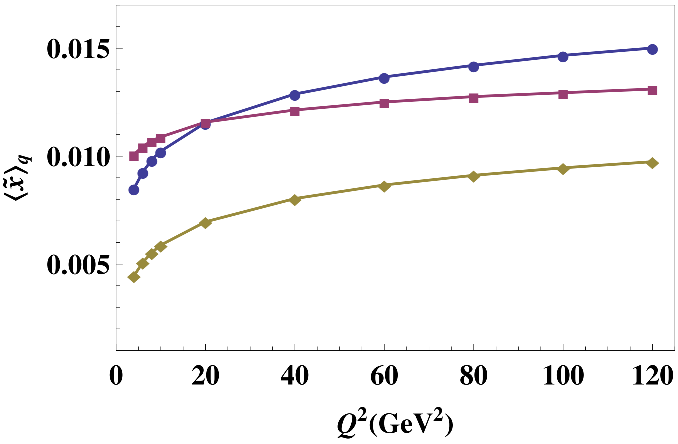

Fig. 6.3 $\langle\hat{x}\rangle_q$ vs Q^2 (GeV^2) for $n_f = 4$ of model 7 (dots), model 8 (squares) and model 5 (diamonds) respectively.

$6.62 \times 10^{-7} \leqslant x \leqslant 0.02$. Note that while the model 7 has got power law growth in $\frac{1}{x}$, models 5 and 8 have slower growth of $\log^2 \frac{1}{x}$.

In Table 6.4, we have listed the values of $\langle\hat{x}\rangle_q$ for the models 7 and 8 and shown their pattern w.r.t Q^2 in Fig. 6.3. From the Fig. 6.3, we can observe that model 7 and 8 has the faster rise than the model 5. Results of model 5 are taken from Table 6.3 column 2.

So from the above analysis, we can conclude that in all the models of small x partons, partial momentum fraction carried by quarks $\langle\hat{x}\rangle_q$ rises with Q^2 in various degrees. However, invariably fall short of allow upper limit of corresponding upper bound partial momentum fractions of gluons $\langle\hat{x}\rangle_g$.

Table 6.4 Results of $\langle\hat{x}\rangle_q$ for $N_f = 4$ of models 7 and 8 for different Q^2

Q^2 (GeV^2)	$\langle\hat{x}\rangle_q$ (model 7)	$\langle\hat{x}\rangle_q$ (model 8)
4	8.500×10^{-3}	1.008×10^{-2}
6	9.270×10^{-3}	1.045×10^{-2}
10	1.023×10^{-2}	1.089×10^{-2}
60	1.367×10^{-2}	1.251×10^{-2}
80	1.050×10^{-2}	1.276×10^{-2}
100	1.467×10^{-2}	1.294×10^{-2}
120	1.501×10^{-2}	1.311×10^{-2}

The above feature of the analysis appears to be in apparent conflict with the QCD expectation that the total momentum fractions of quarks in a Proton should decrease with Q^2 while that of gluons should increase. However, in a subsequence subsection 6.3.8, we will indicate this feature is not incompatible with QCD, by considering the dominance of sea quarks at small x and valence quarks at large x together with a faster rise of gluon at ultra small x compared with sea quarks.

6.3.7 Comparison with perturbative QCD, Lattice QCD and Ads/QCD models

The predictions of perturbative QCD are:

$$\lim_{Q^2\to\infty} \langle x\rangle_q = \frac{3N_f}{2N_g+3N_f}, \tag{6.23}$$

$$\lim_{Q^2\to\infty} \langle x\rangle_g = \frac{2N_g}{2N_g+3N_f}, \tag{6.24}$$

Here, N_f and N_g represent the number of active flavors and number of gluons respectively. For SU(3)$_c$, $N_g = 8$. For N_f = 5, Eqs. 6.23 and 6.24 yield $\langle x\rangle_g = \frac{1}{2}\left(\langle x\rangle_q + \langle x\rangle_g\right)$: 50 % of the momentum of proton is carried by gluons, as noted in [95] and claimed to be experimentally tested in [111].

In Ref. [97], it has alternative asymptotic prediction:

$$\lim_{Q^2\to\infty} \langle x\rangle_q = \frac{6N_f}{N_g+6N_f}, \tag{6.25}$$

$$\lim_{Q^2\to\infty} \langle x\rangle_g = \frac{N_g}{N_g+6N_f}, \tag{6.26}$$

Where Eqs. 6.23 and 6.24 imply that except for $N_f = 6$, $\langle x\rangle_q < \langle x\rangle_g$. Specifically, for N_f=5, Eqs. 6.23-6.24 yield $\langle x\rangle_g = \frac{1}{2}\left(\langle x\rangle_q + \langle x\rangle_g\right)$ and Eqs. 6.25-6.26 give $\langle x\rangle_g = \frac{1}{5}\left(\langle x\rangle_q + \langle x\rangle_g\right)$.

In the above equations, $\langle x \rangle_q$ and $\langle x \rangle_g$ denote the momentum fractions carried by quarks and gluons respectively for the entire x-range .

The difference between Eqs. 6.23-6.24 and Eqs. 6.25-6.26 is attributed in Ref. [97] to the proper gauge invariant definition of gluon momentum density; its definition in earlier works [94–96, 52] includes a quark - gluon interaction term and hence resulted in an inflated value of gluon momentum fraction in proton.

However, later Ji [98] refutes the claim of Chen *et al* [97], underlying the correctness of the QCD prediction, Eqs. 6.23-6.24 [94–96, 52].

However, none of the Refs. [94–96, 52, 97, 98] specifically states about the behavior of partial momentum fractions $\langle \hat{x} \rangle_q$ and $\langle \hat{x} \rangle_g$, relevant for phenomenological study in limited small x regimes and finite Q^2, as in the present analysis.

This is also true for Lattice QCD and Ads/QCD models. With this limitation in mind, we outline the prediction of Lattice QCD [99] as well as Ads/QCD [114] models.

In Lattice QCD, its predictions for total momentum fractions for individual flavor are $\langle x \rangle_u$ = 34%, $\langle x \rangle_d$ = 16%, $\langle x \rangle_s$ = 4% leading to total $\langle x \rangle_q$ = 54%. The lattice analysis also yields $\langle x \rangle_g$ = 36%, while remaining 10% proton momentum fraction remained unaccounted. The analysis was carried out at momentum scale $\mu^2 = 4$ GeV^2. Thus, the analysis does not yet rule out the possibility of $\langle x \rangle_q$ that exceeds $\langle x \rangle_g$ at low momentum scale of lattice QCD, where perturbative QCD is not applicable.

Ads/QCD [114–116] based models of proton structure function on the other hand predicts that the proton momentum fraction carried by valence quarks decreases with Q^2 consistence with perturbative QCD [112, 107] and is reported in Table 6.5.

Table 6.5 Proton momentum fraction carried by valence quarks $\langle \hat{x} \rangle_{qv}$ with Q^2. Table is taken from Ref. [114] for the Ads/QCD model

Q^2 GeV^2	0.2	0.6	1.0	7.0	10	20
$\langle x \rangle_{qv}$	0.60	0.48	0.45	0.38[0.55]	0.37	0.35

Table 6.6 $\langle \hat{x} \rangle_q$ of various models at a fixed Q^2 (= 7 GeV^2) and the same x-range

Models	2	5	6	7	8
$\langle \hat{x} \rangle_q$	5.826×10^{-3}	5.328×10^{-3}	2.671×10^{-3}	5.487×10^{-3}	6.830×10^{-3}

Table 6.7 $\langle x \rangle_q$ of Lattice QCD (= 4 GeV^2) and Ads/QCD, ZEUS data (= 7 GeV^2)

Models	Lattice QCD	Ads/QCD	ZEUS data
$\langle x \rangle_q$	0.54	0.38	0.55

For comparison, we note that the recent ZEUS data [117] yields the momentum fraction due to valence quarks at $Q^2 = 7$ GeV^2 to be $\langle x \rangle_q \approx 0.55$, which is also included in Table 6.5.

We therefore finally compare our predictions of partial momentum fractions of quarks $\langle \hat{x} \rangle_q$ of models 2, 5, 7 and 8 with the predictions of total momentum fractions carried by quarks $\langle x \rangle_q$ in Lattice QCD and Ads/QCD at $Q^2 = 7$ GeV^2 and x-range: $6.62 \times 10^{-6} \leq x \leq 10^{-2}$ within which each model has got its validity. In Table 6.6 results are given for $\langle \hat{x} \rangle_q$. We note that the model predictions of Lattice QCD is at 4 GeV^2 and not at 7 GeV^2. In Table 6.7 we show the results of Lattice QCD and Ads/QCD together with ZEUS data.

A comparison of Table 6.6 with that of 6.7 indicates that the partial momentum fractions of small x quarks calculated in all the models are only a very small fraction of the predicted total momentum fraction in Lattice QCD, Ads/QCD or data which is however not unexpected. The range of small x is merely $6.62 \times 10^{-6} \leq x \leq 10^{-2}$ to be compared with $0 < x < 1$. Therefore it is not possible to infer which model is closer to theory. However, in general a phenomenological model with a larger applicability range should be preferred, unless that comes at the price of making unjustified assumption of the model itself. In this sense, model 5 ($x \leq 0.11$ and $0.11 \leq Q^2 \leq 1200$ GeV^2) should be preferred followed by model 7 ($2 \times 10^{-5} \leq x \leq 0.4$ and $1.2 \leq Q^2 \leq 1200$ GeV^2). For the models 5 and 7, the momentum fractions carried by the small x quarks at $Q^2 = 7$ GeV^2 carries merely 0.2% of the total momentum of proton and 0.1% of the experimentally determined valence quarks momentum fraction.

6.3.8 Possible role of ultra small x gluons and large x partons

As noted above, the partial momentum fraction of quarks discussed above is a very small fractions of the total momentum fractions of proton.

For completeness, we therefore discuss the plausible role of valence quarks and ultra small x gluons to account for the remaining part of momentum fraction of proton.

It is to be noted that the rise of partial momentum fraction of small x quarks with Q^2 (specifically, the logarithmic rise with Q^2 in models 4, 5 and 6) can be accommodated within the overall predictions of total momentum fractions as predicted in perturbative QCD [94–96, 52]. At large x ($x \geqslant 0.2$), valence quarks dominate with the fall of structure function as $F_2^p(x,Q^2) \sim \frac{1}{t^n}$ where $n > 0$ [112, 107] while at small x, ($x \leqslant 0.2$) sea quarks dominate and the rise is power law in $F_2^p(x,Q^2) \sim t^m$, where $m > 0$ [112, 107]. As a result, the parton momentum fraction carried by dominantly sea quarks at small x is expected to rise while the corresponding momentum fraction carried by dominantly valence quarks at large x is expected to fall. However, as the corresponding rise in Q^2 for the gluons is faster [118, 81]

$$xG(x) = k(t)^{\sigma} F_2^s(x,Q^2); \quad k \geq 0, \sigma \geq 0 \tag{6.27}$$

than the quarks, the total gluon momentum will rise faster than the quarks.

We also recall the well known result that the behavior of quarks and gluons at very small and large x limit are [89] :
when $x \to 0$, for small x [85]

$$xf_i(x,Q^2) \longrightarrow x^{a_{f_i}(Q^2)} \tag{6.28}$$

for gluon

$$xf_g(x,Q^2) \longrightarrow x^{a_{f_g}(Q^2)} \tag{6.29}$$

and for large x, when $x \to 1$ [90]

$$xf_i(x,Q^2) \longrightarrow (1-x)^{b_{f_i}(Q^2)} \tag{6.30}$$

also for gluon

$$xf_g(x,Q^2) \longrightarrow (1-x)^{b_{f_g}(Q^2)} \tag{6.31}$$

Here a_{f_g} is -ve and others are +ve.

At intermediate x scale, one generally uses an interpolating function as polynomial [92] in $x \sim \sum_{j=0}^{n} A_j x_j$.

Taking into account all these aspects, it is therefore reasonable to realize the expected QCD behavior. The analysis, done in the present chapter only yields a phenomenological evidence that the partial momentum fractions carried by sea quarks increase with Q^2 but the rise is not inconsistent with QCD expectation that the total momentum fraction carried by quarks (valence quarks) will fall while that of gluons will rise.

6.4 Summary

In this chapter, we have made analysis of small x partial momentum fraction carried by quark $\langle\hat{x}\rangle_q$ and gluon $\langle\hat{x}\rangle_g$ in nine alternative phenomenological models of proton structure function valid in limited small x regions: $x_a \leqslant x \leqslant x_b$; the limits being determined by phenomenological range of validity in each model. Since the physics of small x is not completely understood at this point, we have considered both self-similarity based as well as QCD based models. We find that while the self-similarity based models with linear rise in Q^2 has limited phenomenological ranges of validity, an improved version with liner rise in $\log Q^2$ has an wider phenomenological range. We have also considered phenomenological models with Froissart saturation as well. We then compare the partial momentum fractions in all the small x models and compare with perturbative QCD, Lattice QCD and Ads/QCD.

Our analysis shows that small x quarks under study contribute merely 0.2% of the total momentum fractions of the proton and plays a minor role in accounting for the predicted and experimentally observed feature of second moments quark distributions. Therefore it is not possible to find which of the models is closest to the theory. However, if the range of phenomenological validity is taken as the only criteria for choice of a phenomenological model, the model 5 with leading $\log^2 Q^2$ and $\log^2 \frac{1}{x}$ behavior is the most favorable one followed by the model 7 with $\log Q^2$ and power law growth in $\left(\frac{1}{x}\right)$

7

Self-similarity based Transverse Momentum Dependent Parton Distribution Functions

7.1 Introduction

The physical significance of Transverse Momentum Dependent Parton Distribution Functions (TMD) is outlined in chapter 1 of this thesis. In this chapter, we discuss how this aspects of the proton structure function can be introduced in the self-similarity based models of proton structure functions discussed in chapter 4.

7.2 Formalism

7.2.1 Ansatz of TMD in the self-similarity based models and theoretical limitations

The simplest way to introduce TMD in the self-similarity based model is suggested in Refs. [80, 82] by redefining the magnification factor $\left(1+\frac{Q^2}{Q_0^2}\right)$ by $\left(1+\frac{k_t^2}{k_0^2}\right)$ and is given as

$$\log f_i(x,k_t^2) = D_1.\log\frac{1}{x}.\log\left(1+\frac{k_t^2}{k_0^2}\right) + D_2.\log\frac{1}{x} + D_3.\log\left(1+\frac{k_t^2}{k_0^2}\right) + D_0^i - \log M^2 \quad (7.1)$$

instead of Eq. 2.1 of chapter 2. Here, k_t^2 is the square of the intrinsic transverse momentum of the parton which has corresponding x as the longitudinal fraction. The parameters D_1, D_2, D_3 are determined from Deep Inelastic HERA data as earlier. Redefining the PDF of Eq. 2.2 of chapter 2 to be

$$q_i(x,Q^2) = \int_0^{|k_t|^2<Q^2} dk_t^2\ f_i(x,k_t^2) \quad (7.2)$$

with the cut off $|k_t|^2 < Q^2$, one can obtain the identical expression for integrated PDF and structure function (Eqs. 2.3-2.5). The unintegrated Parton Distribution Function (uPDF) $f_i(x,Q^2)$ is now redefined as TMD: $f_i(x,k_t^2)$. Thus this minimal extension of the approach to transverse structure of Proton keeps the results of the previous form of parton distribution and structure function unchanged.

Clearly, this can be done only in a model frame as in Refs. [120–123]. But it could be of interest to explore this approach to study k_t dependence TMD $f_i(x,k_t^2)$ only in the specific x region where the approach works and where the parameters have been fitted. However, Eq. 7.1 has deep theoretical limitation at the level of quantum field theory as noted by Collins [12].

Further, it has been found in recent years that the DIS experiment is not sufficient to obtain full transverse structure of the nucleon. Additional information is obtained from Semi Inclusive DIS (SIDIS) [123] where one observes a hadron in the final stage. In this case, the hadron, which results from the fragmentation of a scattered quark, remembers the original motion of the quark, including its transverse motion and offers such new information through parton fragmentation process. Such process is described by a fragmentation function $D_i(z_h, P_{ht}; Q^2)$, which is analogous to the uPDF $f_i(x, k_t; Q^2)$ discussed earlier. Here, z_h and P_{ht} are the longitudinal momentum fraction and transverse momentum of the final hadron h with respect to the fragmenting parton. The present model, however, has not accommodated the fragmentation function.

With this theoretical limitation, let us now discuss the graphical representation of TMDs in the model. First, we take the k_t-dependent version of the Lastovicka model using the previous and new data and compare their relative pattern with x and k_t^2.

Using Eq. 2.1, the TMD of the two versions of Lastovicka Model are:

$$\text{Model 1}: \qquad f_i(x, k_t^2) = \frac{e^{D_0^i}}{M^2}\left(\frac{1}{x}\right)^{D_2 + D_1 \log\left(1+\frac{k_t^2}{k_0^2}\right)}\left(1+\frac{k_t^2}{k_0^2}\right)^{D_3} \tag{7.3}$$

$$\text{Model 2}: \qquad f_i''(x, k_t^2) = \frac{e^{D_0''^i}}{M^2}\left(\frac{1}{x}\right)^{D_2'' + D_1'' \log\left(1+\frac{k_t^2}{k_0''^2}\right)}\left(1+\frac{k_t^2}{k_0''^2}\right)^{D_3''} \tag{7.4}$$

We take the mean value of the parameters D_1, D_2, D_3 from Eq. 2.12 and that of D_1'', D_2'', D_3'' from Table 2.1 respectively. Here, for simplicity, Q_0^2 values represent k_0^2s-values. Tables 7.1 and 7.2 give the mean values of the parameters for the models 1 and 2 respectively.

Table 7.1 Mean values taken from Eq. 2.12 for the parameters of model 1

D_0	D_1	D_2	D_3	k_0^2(GeV^2)
0.339	0.073	1.013	-1.287	0.062

Table 7.2 Mean values taken from Table 2.1 for the parameters of model 2

D_0''	D_1''	D_2''	D_3''	$k_0''^2(\mathrm{GeV}^2)$
0.354	0.071	1.032	-1.314	0.064

As an illustration, we use Eq. 2.8 with $N_f = 4$ and assume u, d, s and c are in the ratio

$$e^{D_0^u} : e^{D_0^d} : e^{D_0^s} : e^{D_0^c}$$

$$4:4:1:1 \tag{7.5}$$

for definiteness. This gives $e^{D_0{}^u} = 1.008 = e^{D_0{}^d}$ and $e^{D_0{}^s} = 0.252 = e^{D_0{}^c}$. Similarly $e^{D_0''^u} = 1.024 = e^{D_0''^d}$ and $e^{D_0''^s} = 0.256 = e^{D_0''^c}$.

In Fig. 7.1, TMD vs k_t^2 is shown using Eqs.7.3 and 7.4 for representative values of

(i) $x = 10^{-4}$ and (ii) $x = 0.01$ setting $M^2 = 1$ GeV^2 and

(i) $k_t^2 = 0.01$ GeV^2 and (ii) $k_t^2 = 0.25$ GeV^2

considering the x-range: $10^{-4} \leqslant x \leqslant 0.01$ and k_t^2-range: $0.01 \leqslant k_t^2 \leqslant 0.25$ GeV^2 for convenient.

The present graphical analysis of TMDs (Figs. 7.1-7.2) is a comparison of both the versions of self-similar models of proton structure function. The steep rise of TMD at small x is due to their growth as power law in $\left(\frac{1}{x}\right)$ as evidence from Eqs. 7.3 and 7.4. From Fig. 7.1, it can be seen, both the TMDs decrease in both the versions with increasing k_t^2.

In several TMD models [125–127], x and k_t^2 are parameters in factorisable form:

$$f_i(x,k_t^2;Q^2) = q_i(x,Q^2)h(k_t^2) \tag{7.6}$$

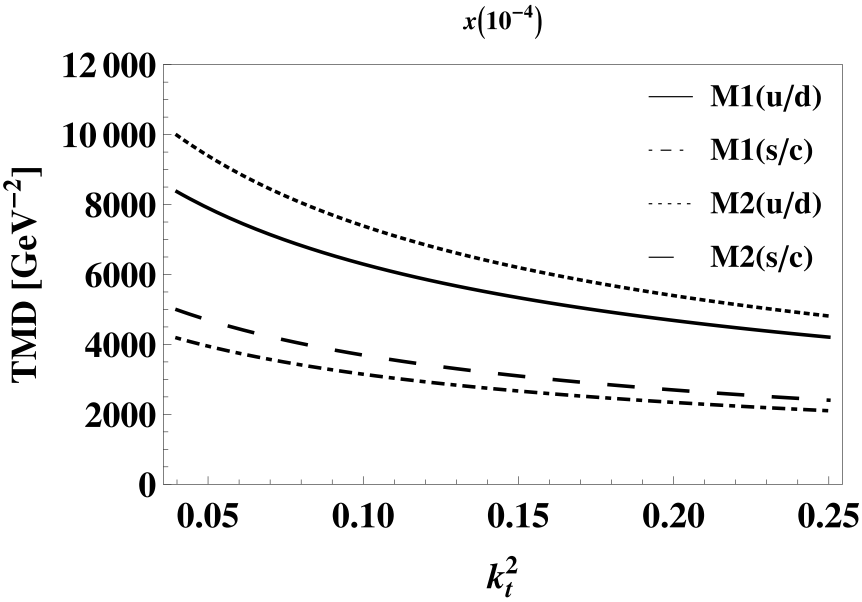

a)

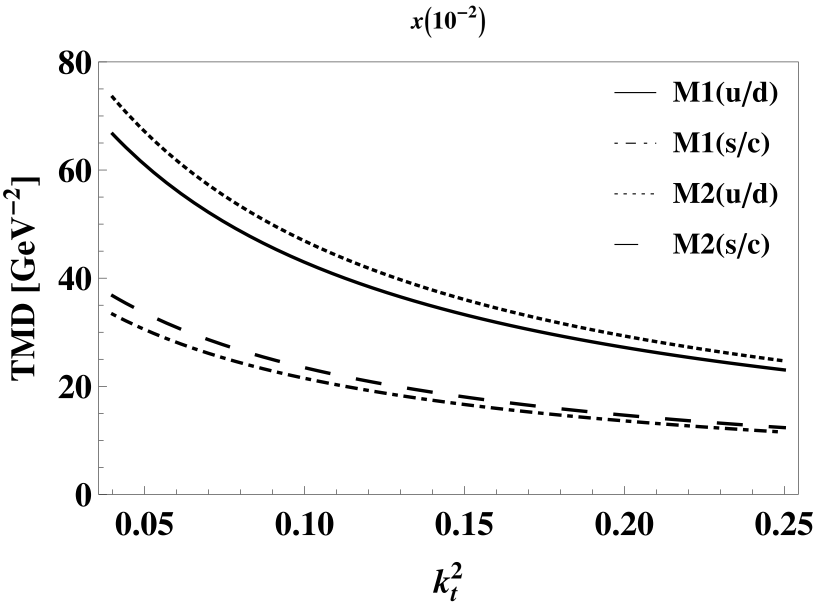

b)

Fig. 7.1 TMD vs k_t^2 for two representative values of (a) $x = 10^{-4}$ and (b) $x = 0.01$ for Models 1 and 2. Here, M1(u/d) (line) and M2(u/d) (dotted) represents the TMD for u and d quarks for Models 1 and 2 respectively. Similarly, M1(s/c) (dot-dashed) and M2(s/c) (dashed) represents the TMD for s and c quarks for Models 1 and 2 respectively.

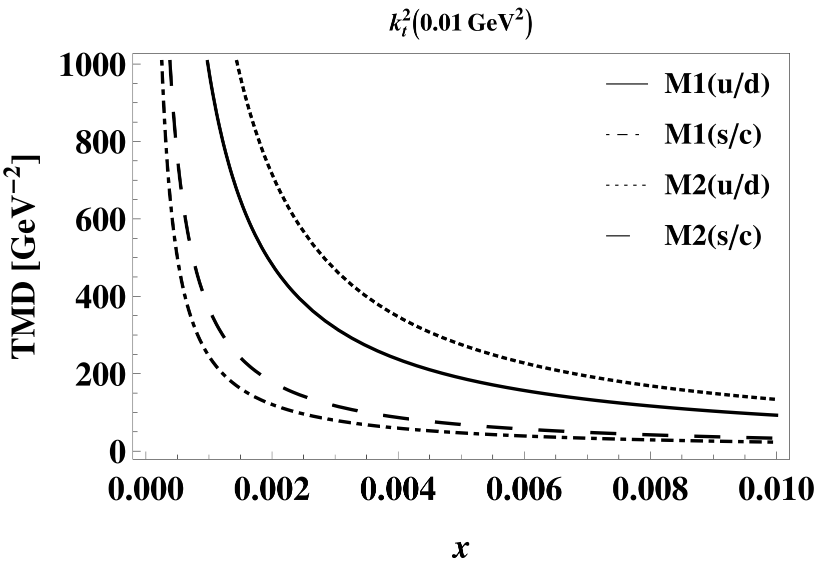

a)

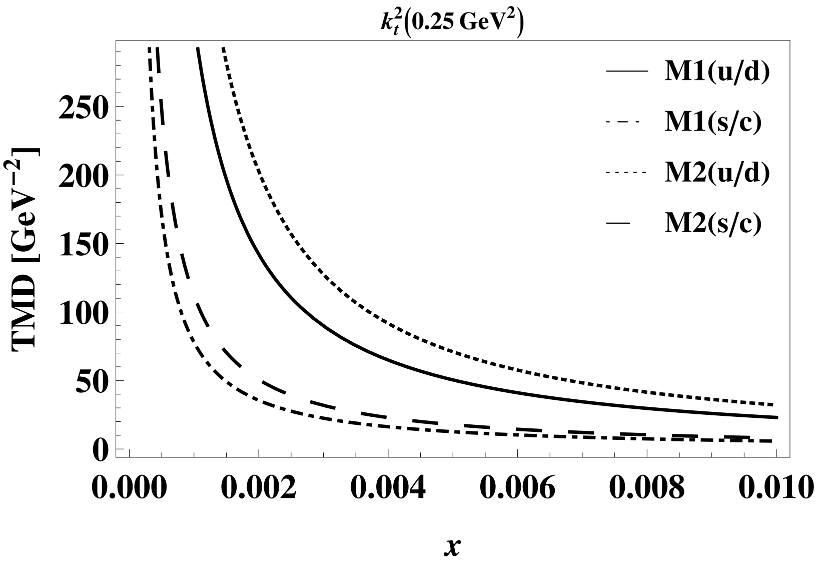

b)

Fig. 7.2 TMD vs x for two representative values of (a) $k_t^2 = 0.01$ GeV^2 and (b) $k_t^2 = 0.25$ GeV^2 for Models 1 and 2. Here, M1(u/d) (line) and M2(u/d) (dotted) represents the TMD for u and d quarks for Models 1 and 2 respectively. Similarly, M1(s/c) (dot-dashed) and M2(s/c) (dashed) represents the TMD for s and c quarks for Models 1 and 2 respectively.

where $h(k_t^2)$ is the Gaussian of the form of

$$h(k_t^2) = \frac{1}{\langle k_t^2 \rangle} e^{-\frac{k_t^2}{\langle k_t^2 \rangle}} \tag{7.7}$$

with normalization constant

$$\int h(k_t^2) dk_t^2 = 1 \tag{7.8}$$

We note, the assumed factorisable parametrization of TMD in x and k_t^2 does not correspond to the k_t^2-factorization theorem [16–18, 128–130, 30, 21, 131, 132] which implies integration over k_t^2 of the product of the Gaussian function and $f_i(x, k_t^2; Q^2)$. In this case, the result of the integration does not depend on k_t^2 but depends on both $< k_t^2 >$ and Q^2. Eq. 7.6 is only a convenient form of parametrization of TMDs and doesn't contradict the form of k_t^2 factorization theorem.

Such factorization property of TMD is not present in the Models 1 and 2 (Eqs. 7.3-7.4) nor the Gaussian form (Eq. 7.7) [123]. In this sense, the present models are close to the corresponding non-factorisable models of Refs. [122, 133–136]. Only in the absence of correlation term D_1 (Eq. 2.1) such factorization property emerges. Specifically, in a model of Ref. [122], it has been shown that this factorization assumption breaks down if one imposes the correct Lorentz structure in the parton model. In this factorisable limit, the k_t^2 dependent functional form of TMD (Eqs. 7.3-7.4) are given by

$$h_i(k_t^2) = \frac{1}{M^2} \left(1 + \frac{k_t^2}{k_0^2}\right)^{D_3} \tag{7.9}$$

and

$$h_i''(k_t^2) = \frac{1}{M^2} \left(1 + \frac{k_t^2}{k_0''^2}\right)^{D_3''} \tag{7.10}$$

respectively (which are not Gaussian) in contrast to a Gaussian function (Eq. 7.7).

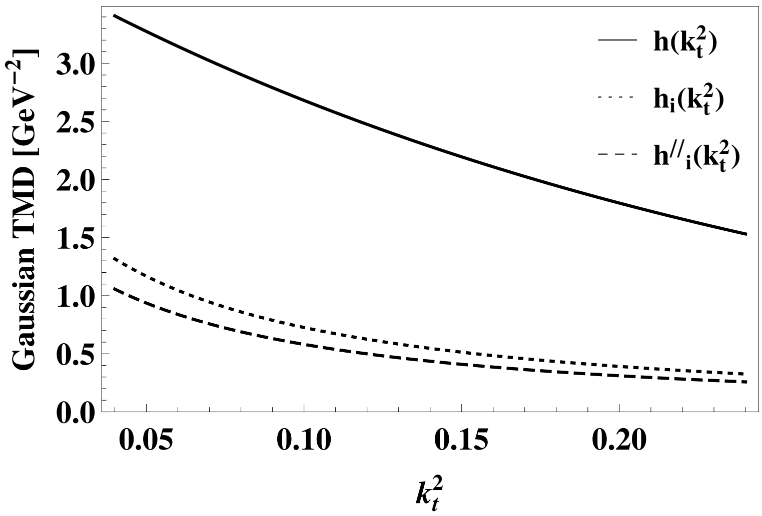

Fig. 7.3 Gaussian TMD vs k_t^2 for $h(k_t^2)$ (line) Eq. 7.7, $h_i(k_t^2)$ (dotted) (Model 1), and $h_i''(k_t^2)$ (dashed) (Model 2) respectively.

In Fig. 7.3, we compare the Gaussian TMD Eq. 7.7 with the model TMDs (Eqs. 7.9-7.10) in the absence of the correlation term, taking $\langle k_t^2 \rangle = 0.25$ GeV^2 from the Ref. [123] which is used in Eq. 7.7. We note that here the k_t^2-dependence is flavor independent. The qualitative feature of Fig. 7.3 is identical to that of Fig. 7.1.

7.2.2 TMD ansatz for models having power law growth in logQ^2

Let us now discuss the TMDs corresponding to models 4 and 6 of chapter 4. The TMD ansatz for the PDFs of Model 4 and 6 will be:

Model 4

TMD

$$\log \hat{f}_i(x,k_t^2) = \hat{D}_1 \log\frac{1}{x}\log\hat{M}_1 + \hat{D}_2 \log\frac{1}{x} + \hat{D}_3 \log\hat{M}_1 + \hat{D}_0^i - \log M^2 \tag{7.11}$$

with

$$\hat{M}_1 = \frac{B_1}{\left(1+\frac{k_t^2}{\hat{k}_0^2}\right)} + \frac{B_2}{\left(1+\frac{k_t^2}{\hat{k}_0^2}\right)^2} \tag{7.12}$$

leads to

$$\hat{f}_i(x,k_t^2) = \frac{e^{\hat{D}_0^i}}{M^2}\left(\frac{1}{x}\right)^{\hat{D}_2}\left(\frac{B_1}{\left(1+\frac{k_t^2}{\hat{k}_0^2}\right)}\right)^{\hat{D}_3+\hat{D}_1\log\frac{1}{x}}\left(1+\frac{B_2}{B_1}\frac{1}{\left(1+\frac{k_t^2}{\hat{k}_0^2}\right)}\right)^{\hat{D}_3+\hat{D}_1\log\frac{1}{x}} \tag{7.13}$$

Assuming the convergence of the polynomials as occurred in Eq. 7.13 we obtain

$$\hat{f}_i(x,k_t^2) = \frac{e^{\hat{D}_0^i}}{M^2}\left(\frac{1}{x}\right)^{\hat{D}_2}\left(\frac{B_1}{\left(1+\frac{k_t^2}{\hat{k}_0^2}\right)}\right)^{\hat{D}_3+\hat{D}_1\log\frac{1}{x}}\left(1+\frac{B_2}{B_1}\frac{\left(\hat{D}_3+\hat{D}_1\log\frac{1}{x}\right)}{\left(1+\frac{k_t^2}{\hat{k}_0^2}\right)}\right) \tag{7.14}$$

If the parameters $\hat{D}_3$ and $\hat{D}_1$ satisfy the additional condition at

$$\hat{D}_3+\hat{D}_1\log\frac{1}{\hat{x}_0} = 1 \tag{7.15}$$

then the resultant TMD will be

$$\tilde{f}_i(x,k_t^2) = \frac{e^{\tilde{D}_0^i}}{M^2}\left(\frac{1}{x}\right)^{\tilde{D}_2}\left(\frac{\tilde{B}_1}{\left(1+\frac{k_t^2}{\tilde{k}_0^2}\right)}\right)\left(1+\frac{\tilde{B}_2}{\tilde{B}_1}\frac{1}{\left(1+\frac{k_t^2}{\tilde{k}_0^2}\right)}\right) \tag{7.16}$$

Model 6

To get the larger x behavior in PDF as well as structure function, magnification factor $\left(\frac{1}{x}\right)$ is changed to $\rightarrow \left(\frac{1}{x}-1\right)$ and so the TMD becomes

$$\log\bar{f}_i(x,k_t^2) = \bar{D}_1.\log\left(\frac{1}{x}-1\right).\log\left(1+\frac{k_t^2}{\bar{k}_0^2}\right)+\bar{D}_2.\log\left(\frac{1}{x}-1\right) + \bar{D}_3.\log\left(1+\frac{k_t^2}{\bar{k}_0^2}\right)+\bar{D}_0^i-\log M^2 \tag{7.17}$$

Table 7.3 Mean values taken from Table 4.2 for the parameters of model 4

$\tilde{D}_0$	$\tilde{D}_2$	$\tilde{B}_1$	$\tilde{B}_2$	$\tilde{k}_0^2$ (GeV^2)
0.294	1.237	0.438	0.687	0.046

and hence

$$\bar{f}_i(x,k_t^2) = \frac{e^{\bar{D}_0^i}}{M^2}\left(\frac{1}{x}\right)^{\bar{D}_2}(1-x)^{\bar{D}_2}\left(\frac{\bar{B}_1}{\left(1+\frac{k_t^2}{\bar{k}_0^2}\right)}\right)^{\bar{D}_3+\bar{D}_1\log\frac{1}{x}+\bar{D}_1\log(1-x)} \left(1+\frac{\bar{B}_2}{\bar{B}_1}\frac{\left(\bar{D}_3+\bar{D}_1\log\frac{1}{x}+\bar{D}_1\log(1-x)\right)}{\left(1+\frac{k_t^2}{\bar{k}_0^2}\right)}\right) \quad (7.18)$$

Imposing the condition

$$\bar{D}_3+\bar{D}_1\log\frac{1}{\bar{x}_0}+\bar{D}_1\log(1-\bar{x}_0)=1 \quad (7.19)$$

will lead to corresponding TMD

$$\bar{f}_i'(x,k_t^2) = \frac{e^{\bar{D}_0'^i}}{M^2}\left(\frac{1}{x}\right)^{\bar{D}_2'}(1-x)^{\bar{D}_2'}\left(\frac{\bar{B}_1'}{\left(1+\frac{k_t^2}{k_0'^2}\right)}\right)\left(1+\frac{\bar{B}_2'}{\bar{B}_1'}\frac{1}{\left(1+\frac{k_t^2}{\bar{k}_0'^2}\right)}\right) \quad (7.20)$$

7.2.3 Graphical representation of TMDs for models having power law growth in $\log Q^2$

To compare the TMDs for Models 4 and 6, we will use Eq. 7.16 for Model 4 with $e^{\tilde{D}_0^u} = 0.964 = e^{\tilde{D}_0^d}$ and Eq. 7.20 for model 6 with $e^{\tilde{D}_0^s} = 0.241 = e^{\tilde{D}_0^c}$ with $e^{\bar{D}_0'^u} = 1.004 = e^{\bar{D}_0'^d}$ and $e^{\bar{D}_0'^s} = 0.251 = e^{\bar{D}_0'^c}$.

The mean values of the parameters for their respective models can be taken from Tables 4.2 and 4.3 and given in Tables 7.3 and 7.4.

Table 7.4 Mean values taken from Table 4.3 for the parameters of model 6

$\bar{D}'_0$	$\bar{D}'_2$	$\bar{B}'_1$	$\bar{B}'_2$	$\bar{k}'^2_0$ (GeV^2)
0.335	1.194	0.519	0.082	0.056

Graphical representation of TMDs of Model 4 and 6 are given in Figs. 7.4 and 7.5 within the ranges of x: $10^{-4} \leqslant x \leqslant 0.01$ and k_t^2: 0.01$\leqslant k_t^2 \leqslant 0.25$ GeV^2 for convenient. It shows both the form of TMDs have got desired k_t^2 fall without the burden of singularities as expected. The steep rise of TMDs at small x is due to their growth as power law in $\left(\frac{1}{x}\right)$ as evidence from Eqs. 7.16 and 7.20

In this case, the models 4 and 6 have got inbuilt factorization in x and k_t^2 unlike in the previous case (Models 1 and 2) where TMDs are not factorisable in x and k_t^2. The k_t^2-dependent functional form of TMD (Eqs. 7.16-7.20) are given by :

$$\tilde{h}_i = \frac{1}{M^2}\left(\frac{\tilde{B}_1}{\left(1+\frac{k_t^2}{\tilde{k}_0^2}\right)}\right)\left(1+\frac{\tilde{B}_2}{\tilde{B}_1}\frac{1}{\left(1+\frac{k_t^2}{\tilde{k}_0^2}\right)}\right) \tag{7.21}$$

and

$$\bar{h}_i = \frac{1}{M^2}\left(\frac{\bar{B}'_1}{\left(1+\frac{k_t^2}{\bar{k}'^2_0}\right)}\right)\left(1+\frac{\bar{B}'_2}{\bar{B}'_1}\frac{1}{\left(1+\frac{k_t^2}{\bar{k}'^2_0}\right)}\right) \tag{7.22}$$

which will be compared with the standard Gaussian $h(k_t^2)$ (Eq. 7.7) in Fig. 7.6.

The above analysis shows whereas the self-similarity based TMDs are in general not factorisable in x and k_t^2, the additional constraints resulting in models 4 and 6 indicate such factorization property.

7.3 Summary

In this chapter, the self-similarity based model of proton structure function as suggested in Ref. [1] and introduced in chapter 2, is then extended to take into account the transverse structure of the proton by making simple plausible assumptions about defining Transverse

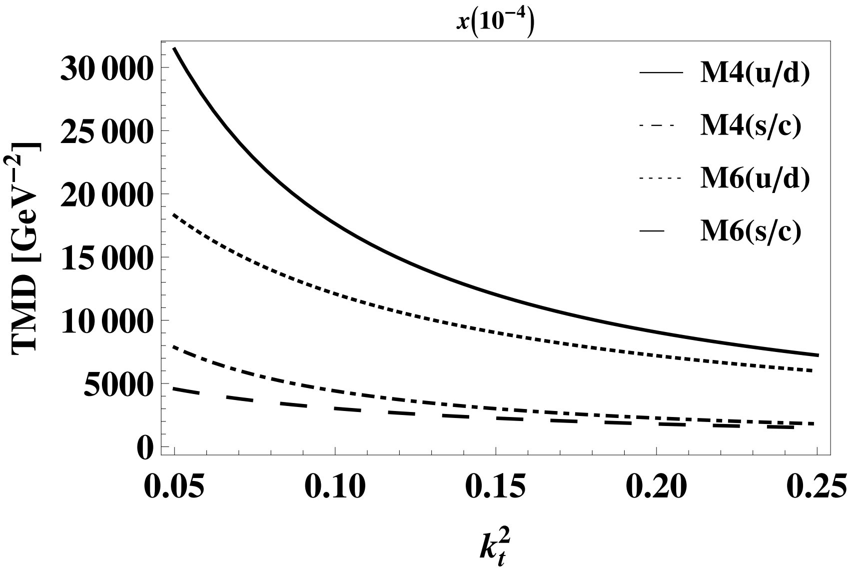

a)

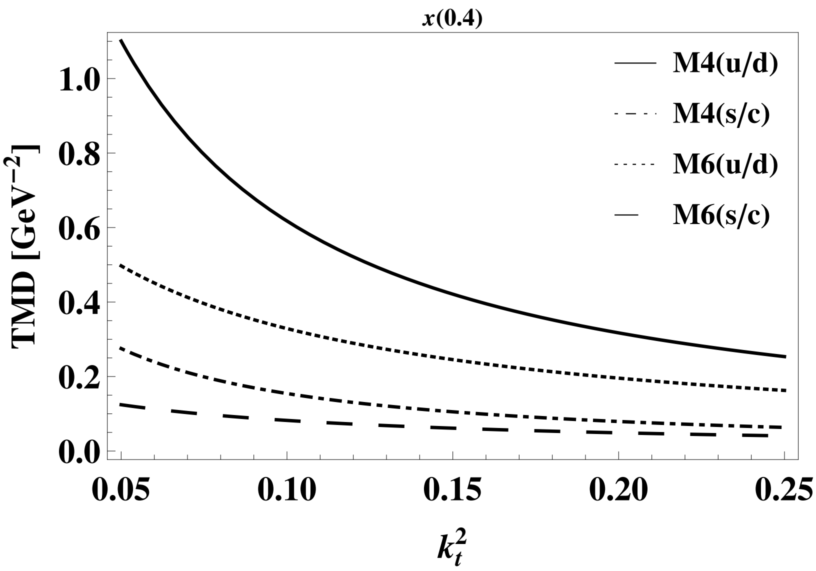

b)

Fig. 7.4 TMD vs k_t^2 for two representative values of (a) $x = 10^{-4}$ and (b) $x = 0.4$ for Models 4 and 6. Here, M4(u/d) (line) and M6(u/d) (dotted) represents the TMD for u and d quarks for Models 4 and 6 respectively. Similarly, M4(s/c) (dot-dashed) and M6(s/c) (dashed) represents the TMD for s and c quarks for Models 4 and 6 respectively.

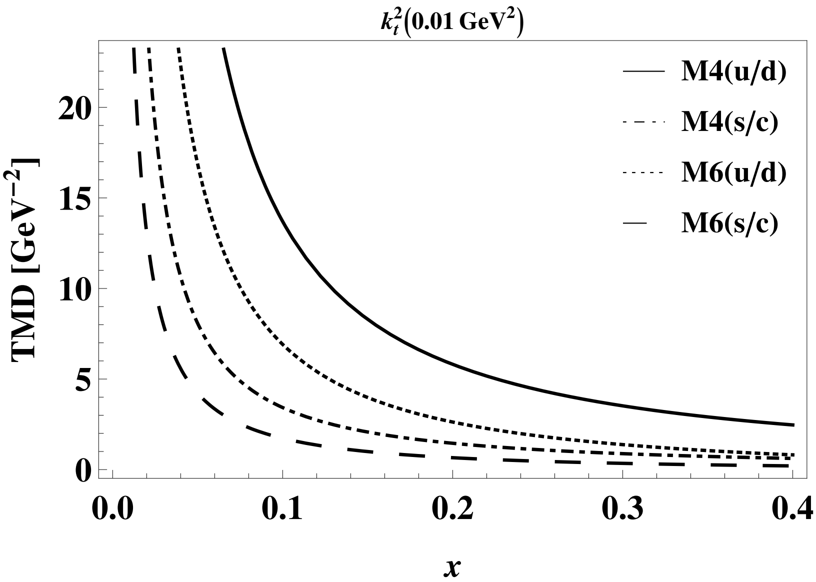

a)

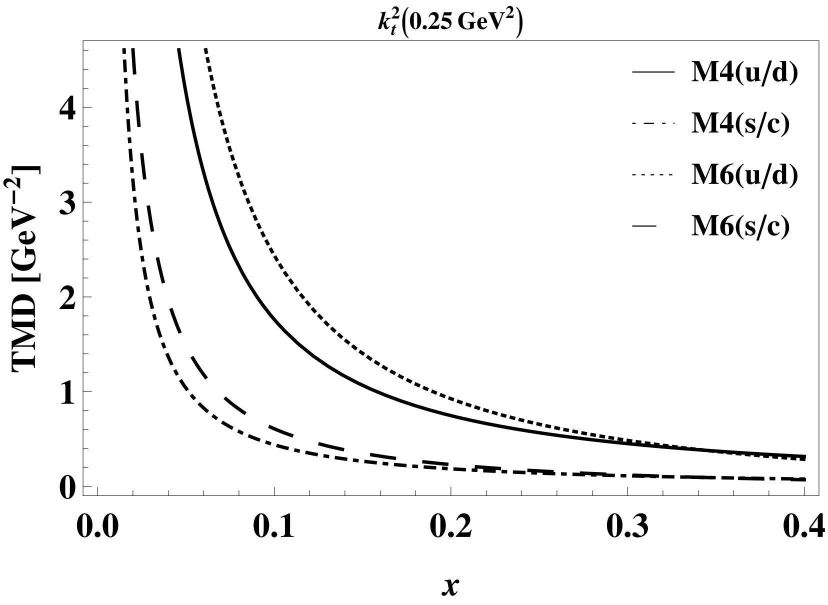

b)

Fig. 7.5 TMD vs x for two representative values of (a) $k_t^2 = 0.01$ GeV^2 and (b) $k_t^2 = 0.25$ GeV^2 for Models 4 and 6. Here, M4(u/d) (line) and M6(u/d) (dotted) represents the TMD for u and d quarks for Models 4 and 6 respectively. Similarly, M4(s/c) (dot-dashed) and M6(s/c) (dashed) represents the TMD for s and b quarks for Models 4 and 6 respectively.

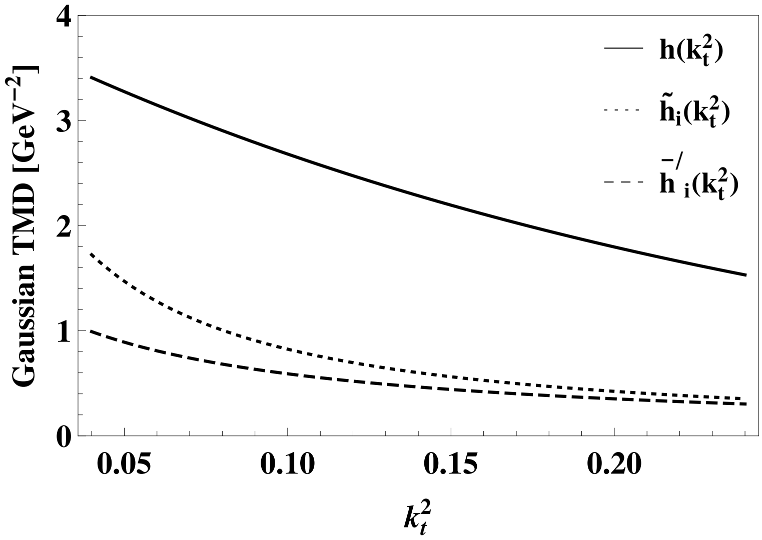

Fig. 7.6 Gaussian TMD vs k_t^2 for $h(k_t^2)$ (line) Eq. 7.7, $\tilde{h}_i(k_t^2)$ (dotted) (Model 4), and $\bar{h}'_i(k_t^2)$ (dashed) (Model 6) respectively.

Momentum Dependent Parton Distribution (TMD). The model ansatzs for TMD however, have general theoretical limitations which are explicitly discussed. Similarities of such model ansatzs for TMD are also compared with several phenomenological models available in current literature. We then obtain graphical representation of TMDs w.r.t. x and k_t^2 which have expected k_t-behavior. The TMDs are in general non-factorisable in x and k_t^2. However, in the models having power law rise in $\log Q^2$ have factorisable property which are similar to a few models, available in the literature.

In this chapter, we however cannot study the TMDs in the entire x-range as the model parameters have phenomenological validity only in the limited ranges of x as discussed in chapters from 2 to 4.

8

Froissart bound and Transverse Momentum Dependent Parton Distribution Functions

8.1 Introduction

The Froissart bound is an interesting aspects of strong interaction and has recently being discussed in the context of the proton structure function by various authors. Self-similarity with Froissart compatibility is also reported in Ref. [82].

In this chapter, we outline the change of the structure of the TMDs discussed in chapter 7 if Froissart compatibility is also additionally introduced. We discuss the difference between the two in this chapter.

8.2 Formalism

8.2.1 Ansatz of TMD in the models with three magnification factors

Let us now discuss the TMDs corresponding to the cases (case 1-4) with three magnification factors discussed in chapter 5.

Case 1

Taking three magnification factors instead of two:

$$\begin{aligned} M_1 &= \left(1+\frac{k_t^2}{k_0^2}\right) \\ M_2 &= \frac{1}{x} \\ M_3 &= \log\frac{1}{x} \end{aligned} \tag{8.1}$$

one can construct the TMD as

$$\begin{aligned} \log[M^2.\grave{f}_i(x,k_t^2)] = {} & \grave{D}_1 \log M_1 \log M_2 \log M_3 + \grave{D}_2 \log M_1 \log M_2 + \grave{D}_3 \log M_2 \log M_3 \\ & + \grave{D}_4 \log M_1 \log M_3 + \grave{D}_5 \log M_1 + \grave{D}_6 \log M_2 + \grave{D}_7 \log M_3 + \grave{D}_0{}^i \end{aligned} \tag{8.2}$$

or

$$\begin{aligned} \grave{f}_i(x,k_t^2) = {} & \frac{e^{\grave{D}_0^i}}{M^2} \left(\frac{1}{x}\right)^{\grave{D}_2 \log\left(1+\frac{k_t^2}{\grave{k}_0^2}\right)+\grave{D}_6} \\ & \times \left(\log\frac{1}{x}\right)^{\grave{D}_1 \log\left(1+\frac{k_t^2}{\grave{k}_0^2}\right)\log\frac{1}{x}+\grave{D}_3 \log 1/x+\grave{D}_4 \log\left(1+\frac{k_t^2}{\grave{k}_0^2}\right)+\grave{D}_7} \left(1+\frac{k_t^2}{\grave{k}_0^2}\right)^{\grave{D}_5} \end{aligned} \tag{8.3}$$

Eq. 8.3 can show the proper Froissart bound like behavior in TMD under the following conditions:

$$
\begin{aligned}
&(1) \quad \grave{D}_2 \log\left(1+\frac{k_t^2}{\grave{k}_0^2}\right)+\grave{D}_6=0 \\
&(2) \quad \grave{D}_7+\grave{D}_3 \log\frac{1}{x}+\left(\grave{D}_4+\grave{D}_1 \log\frac{1}{x}\right)\times\log\left(1+\frac{k_t^2}{\grave{k}_0^2}\right)=2
\end{aligned}
\tag{8.4}
$$

Further, if $\grave{D}_7,\ \grave{D}_3,\ \grave{D}_1 \ll \grave{D}_4$, then $\grave{D}_4 = \dfrac{2-\grave{D}_7}{\log\left(1+\frac{k_t^2}{\grave{k}_0^2}\right)}$, the Froissart Bound compatible TMD will be

$$
\grave{f}_i(x,k_t^2)=\frac{e^{\grave{D}^i_0}}{M^2}\left(\log\frac{1}{x}\right)^2\left(1+\frac{k_t^2}{\grave{k}_0^2}\right)^{\grave{D}_5}
\tag{8.5}
$$

Case 2

The above observation is thus generalized to improved self-similarity based models suggested in chapter 5. Therefore, we can construct another new set of magnification factors:

$$
\begin{aligned}
\hat{M}_1 &= \sum_{j=1}^{n}\frac{B_j}{\left(1+\frac{k_t^2}{\hat{k}_0^2}\right)^j} \qquad j=1,2 \\
M_2 &= \frac{1}{x} \\
M_3 &= \log\frac{1}{x}
\end{aligned}
\tag{8.6}
$$

which can define TMD as follows:

$$
\begin{aligned}
\log[M^2.\ddot{f}_i(x,k_t^2)] = {} & \ddot{D}_1\log\hat{M}_1\log M_2\log M_3+\ddot{D}_2\log\hat{M}_1\log M_2+\ddot{D}_3\log M_2\log M_3 \\
& +\ddot{D}_4\log\hat{M}_1\log M_3+\ddot{D}_5\log\hat{M}_1+\ddot{D}_6\log M_2+\ddot{D}_7\log M_3+\ddot{D}_0{}^i
\end{aligned}
\tag{8.7}
$$

Or

$$\ddot{f}_i(x,k_t^2) = \frac{e^{\ddot{D}_0^i}}{M^2}\left(\frac{1}{x}\right)^{\ddot{D}_6}\left(\log\frac{1}{x}\right)^{\ddot{D}_3\log\frac{1}{x}+\ddot{D}_7}\ddot{B}_1\left[\frac{1}{\left(1+\frac{k_t^2}{\ddot{k}_0^2}\right)}+\frac{\ddot{B}_2}{\ddot{B}_1}\frac{1}{\left(1+\frac{k_t^2}{\ddot{k}_0^2}\right)^2}\right] \tag{8.8}$$

Putting the extra conditions

$$\begin{aligned}
&(1)\quad \ddot{D}_6 = 0\\
&(2)\quad \ddot{D}_3\log\frac{1}{x}+\ddot{D}_7 = 2
\end{aligned} \tag{8.9}$$

will give the Froissart like behavior in TMD as:

$$\ddot{f}_i(x,k_t^2) = \frac{e^{\ddot{D}_0^i}}{M^2}\left(\log\frac{1}{x}\right)^2\ddot{B}_1\left[\frac{1}{\left(1+\frac{k_t^2}{\ddot{k}_0^2}\right)}+\frac{\ddot{B}_2}{\ddot{B}_1}\frac{1}{\left(1+\frac{k_t^2}{\ddot{k}_0^2}\right)^2}\right] \tag{8.10}$$

Case 3

If the magnification factor M_2 is extrapolated to large x in a parameter free way $\frac{1}{x}\to\left(\frac{1}{x}-1\right)$, one obtains a set of magnification factors

$$\begin{aligned}
\hat{M}_1 &= \sum_{j=1}^{n}\frac{B_j}{\left(1+\frac{k_t^2}{\hat{k}_0^2}\right)^j} \qquad j=1,2\\
M_2 &= \left(\frac{1}{x}-1\right)\\
M_3 &= \log\frac{1}{x}
\end{aligned} \tag{8.11}$$

Therefore TMD will be:

$$\breve{f}_i(x,k_t^2) = \frac{e^{\breve{D}_0^i}}{M^2}\left(\frac{1}{x}\right)^{\breve{D}_6}(1-x)^{\breve{D}_6}\left(\log\frac{1}{x}\right)^{\breve{D}_3\log\frac{1}{x}+\breve{D}_7} \times \breve{B}_1\left[\frac{1}{\left(1+\frac{k_t^2}{\breve{k}_0^2}\right)}+\frac{\breve{B}_2}{\breve{B}_1}\frac{1}{\left(1+\frac{k_t^2}{\breve{k}_0^2}\right)^2}\right] \tag{8.12}$$

Putting the extra conditions

$$\begin{aligned} &(1)\quad \breve{D}_6 = 0 \\ &(2)\quad \breve{D}_3\log\left(\frac{1}{x}-1\right)+\breve{D}_7 = 2 \end{aligned} \tag{8.13}$$

will give the Froissart like behavior in TMD as:

$$\breve{f}_i(x,k_t^2) = \frac{e^{\breve{D}_0^i}}{M^2}\left(\log\frac{1}{x}\right)^2\breve{B}_1\left[\frac{1}{\left(1+\frac{k_t^2}{\breve{k}_0^2}\right)}+\frac{\breve{B}_2}{\breve{B}_1}\frac{1}{\left(1+\frac{k_t^2}{\breve{k}_0^2}\right)^2}\right] \tag{8.14}$$

Case 4

If the third magnification factor is also extrapolated to large-x: $\log\frac{1}{x} \to \log\left(\frac{1}{x}-1\right)$ i.e

$$\begin{aligned} \hat{M}_1 &= \sum_{j=1}^{n}\frac{B_j}{\left(1+\frac{k_t^2}{\hat{k}_0^2}\right)^j} \qquad j=1,2 \\ M_2 &= \left(\frac{1}{x}-1\right) \\ M_3 &= \log\left(\frac{1}{x}-1\right) \end{aligned} \tag{8.15}$$

then TMD will be of the form :

$$\breve{f}_i'(x,k_t^2) = \frac{e^{\breve{D}_0'^i}}{M^2}\left(\frac{1}{x}\right)^{\breve{D}_6'}(1-x)^{\breve{D}_6'}\left(\log\frac{1-x}{x}\right)^{\breve{D}_3'\log\left(\frac{1}{x}-1\right)+\breve{D}_7'} \times \breve{B}_1'\left[\frac{1}{\left(1+\frac{k_t^2}{k_0'^2}\right)}+\frac{\breve{B}_2'}{\breve{B}_1'}\frac{1}{\left(1+\frac{k_t^2}{\breve{k}_0'^2}\right)^2}\right] \tag{8.16}$$

Putting the extra conditions

$$\begin{aligned} &(1)\quad \breve{D}_6' = 0 \\ &(2)\quad \breve{D}_3'\log\left(\frac{1}{x}-1\right)+\breve{D}_7' = 2 \end{aligned} \tag{8.17}$$

can show the Froissart like behavior in TMD as:

$$\breve{f}_i'(x,k_t^2) = \frac{e^{\breve{D}_0'^i}}{M^2}\left(\log\frac{1-x}{x}\right)^2 \breve{B}_1'\left[\frac{1}{\left(1+\frac{k_t^2}{\breve{k}_0'^2}\right)}+\frac{\breve{B}_2'}{\breve{B}_1'}\frac{1}{\left(1+\frac{k_t^2}{\breve{k}_0'^2}\right)^2}\right] \tag{8.18}$$

8.3 Results

8.3.1 Graphical representation of TMDs for models having three magnification factors

Here, we will consider the Eqs. 8.5 , 8.10, 8.14 and 8.18 for the graphical analysis of TMDs w.r.t x and k_t^2. For definiteness, we have calculated $e^{D_0^i}$s for each case in the similar way as done in chapter 7. This gives for

case 1: $e^{\grave{D}_0^u} = 0.904 = e^{\grave{D}_0^d}$ and $e^{\grave{D}_0^s} = 0.226 = e^{\grave{D}_0^c}$
case 2: $e^{\ddot{D}_0^u} = 0.818 = e^{\ddot{D}_0^d}$ and $e^{\ddot{D}_0^s} = 0.204 = e^{\ddot{D}_0^c}$
case 3: $e^{\breve{D}_0^u} = 1.008 = e^{\breve{D}_0^d}$ and $e^{\breve{D}_0^s} = 0.252 = e^{\breve{D}_0^c}$

Table 8.1 Mean values of the parameters of $\grave{f}_i$, Eq. 8.5; case 1

$\grave{D}_0$	$\grave{D}_1$	$\grave{D}_2$	$\grave{D}_4$	$\grave{D}_5$	$\grave{k}_0^2(\mathrm{GeV}^2)$
0.1006	0.028	-0.036	3.585	-0.857	0.060

Table 8.2 Mean values of the parameters of $\ddot{f}_i$, Eq. 8.10; case 2

$\ddot{D}_0$	$\ddot{B}_1$	$\ddot{B}_2$	$\ddot{k}_0^2(\mathrm{GeV}^2)$
0.00047	0.056	0.672	0.022

case 4: $e^{\breve{D}_0'^u} = 1.008 = e^{\breve{D}_0'^d}$ and $e^{\breve{D}_0'^s} = 0.252 = e^{\breve{D}_0'^c}$

Also we have taken the mean values of the parameters of Eq. 8.5 i.e $\grave{D}_5$ and $\grave{k}_0^2$ from Table 5.1; parameters $\ddot{B}_1$, $\ddot{B}_2$ and $\ddot{k}_0^2$ of Eq. 8.10 from Table 5.2 ; parameters $\breve{B}_1$, $\breve{B}_2$ and $\breve{k}_0^2$ of Eq. 8.14 from Table 5.3 and parameters $\breve{B}'_1$, $\breve{B}'_2$ and $\breve{k}_0'^2$ of Eq. 8.18 from Table 5.4. Mean values for the respective cases are given in Tables 8.1-8.4.

In Figs. 8.1 and 8.2, we have shown TMDs vs x and TMDs vs k_t^2 respectively. From both the figures, we can see: TMDs have got the desired k_t^2 fall. Also the present graphical analysis of TMDs indicates that TMDs at small x is smaller than that of Figs. 7.1-7.2 and 7.4 and 7.5 of chapter 7, due to the absence of the factor having power law growth in $\left(\frac{1}{x}\right)$.

The k_t^2 dependent functional form of TMDs (Eqs. 8.5, 8.10 and 8.18) are given by :

$$\grave{h}_i = \frac{1}{M^2}\left(1+\frac{k_t^2}{\grave{k}_0^2}\right)^{\grave{D}_5} \tag{8.19}$$

Table 8.3 Mean values of the parameters of $\breve{f}_i$, Eq. 8.14; case 3

$\breve{D}_0$	$\breve{B}_1$	$\breve{B}_2$	$\breve{k}_0^2(\mathrm{GeV}^2)$
0.006	0.032	0.309	0.048

Table 8.4 Mean values of the parameters of $\breve{f}_i'$, Eq. 8.18; case 4

$\breve{D}_0'$	$\breve{B}_1'$	$\breve{B}_2'$	$\breve{k}_0'^2(\text{GeV}^2)$
0.008	0.034	0.251	0.057

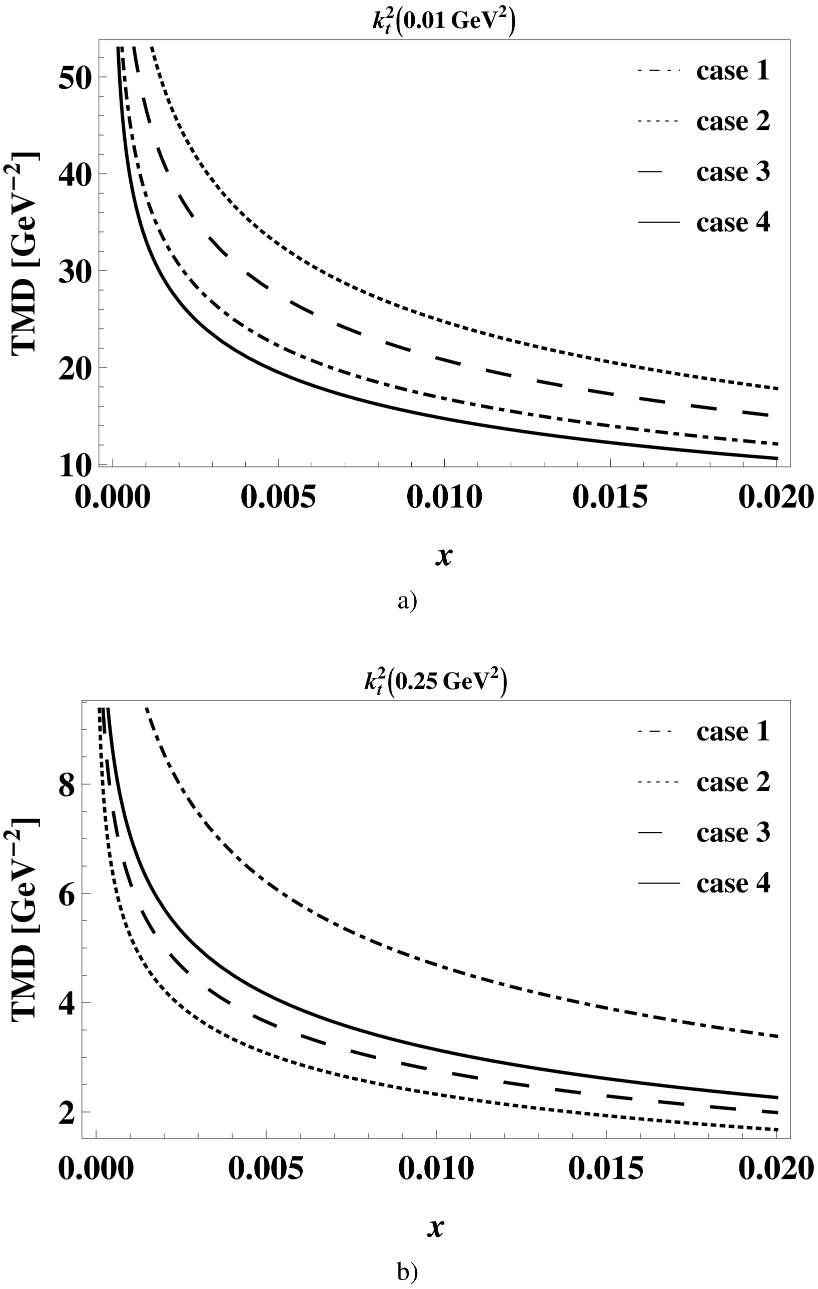

Fig. 8.1 TMD vs x for two representative values of (a) $k_t^2 = 0.01$ GeV^2 and (b) $k_t^2 = 0.25$ GeV^2 for cases 1-4 taking only u and d quarks contributions.

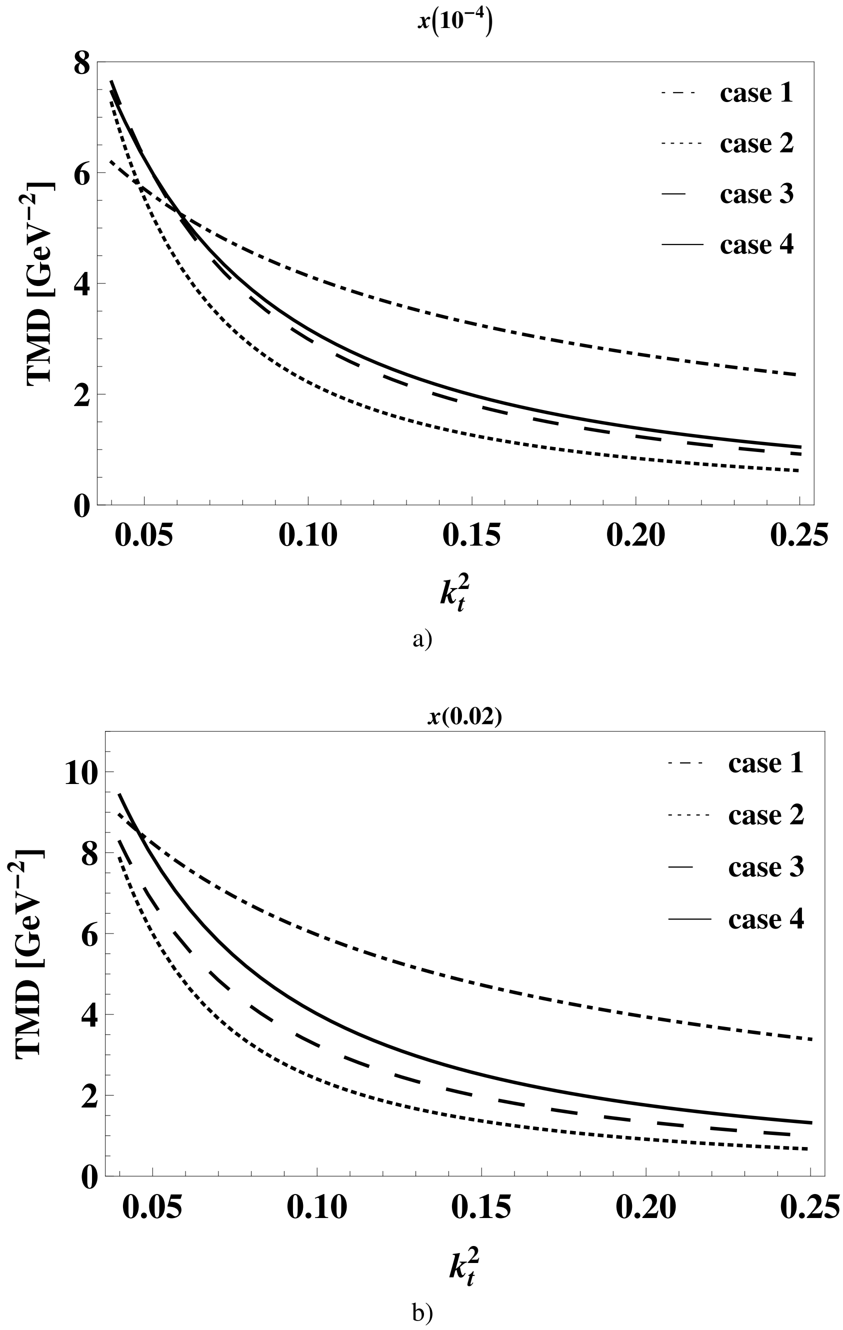

Fig. 8.2 TMD vs k_t^2 for two representative values of (a) $x = 10^{-4}$ and (b) $x = 0.01$ for cases 1-4 taking only u and d quarks contributions.

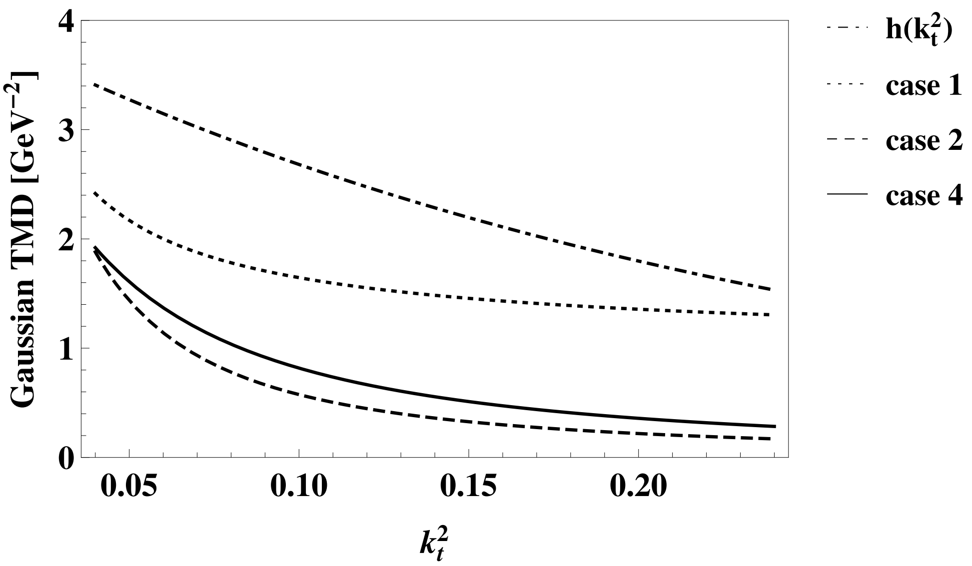

Fig. 8.3 Gaussian TMD vs k_t^2 for $h(k_t^2)$ (dot dashed) Eq. 7.7 of chapter 7, case 1 (dotted), and case 2 (dashed) and case 4 (line) respectively.

$$\ddot{h}_i = \frac{1}{M^2}\ddot{B}_1\left[\frac{1}{\left(1+\frac{k_t^2}{\ddot{k}_0^2}\right)} + \frac{\ddot{B}_2}{\ddot{B}_1}\frac{1}{\left(1+\frac{k_t^2}{\ddot{k}_0^2}\right)^2}\right] \tag{8.20}$$

$$\breve{h}'_i = \frac{1}{M^2}\breve{B}'_1\left[\frac{1}{\left(1+\frac{k_t^2}{\breve{k}_0'^2}\right)} + \frac{\breve{B}'_2}{\breve{B}'_1}\frac{1}{\left(1+\frac{k_t^2}{\breve{k}_0'^2}\right)^2}\right] \tag{8.21}$$

which will be compared with the standard Gaussian $h(k_t^2)$ (Eq. 7.7 of chapter 7) in Fig. 8.3.

8.4 Summary

In this chapter, we have obtained the proper Froissart bound condition in Transverse Momentum Dependent Parton Distribution Functions (TMD) based on self-similarity with the sets in three magnification factors. In the previous chapter, we have already discussed TMDs with two magnification factors. In both the chapters, we have shown the k_t^2-fall in TMDs w.r.t. x and k_t^2 where one can observe that TMDs with the power law in $\left(\frac{1}{x}\right)$ in chapter 7 dominates the Froissart bound compatible TMDs with the power law in $\left(\log\frac{1}{x}\right)$.

As discussed in the earlier chapter 7, the information of TMDs in the entire x-range; $0 < x < 1$ can not be obtained in this approach as the model parameters are fitted only in a limited x-range which may be called the inherent limitation of the approach when studying the Transverse structure of the proton.

9
Conclusion and future outlook of this thesis

In this work, we have studied the structure of proton at small x by constructing the proton structure functions based on self-similarity.

In Chapter 1, we have introduced the definition of self-similarity and its application in Unintegrated Parton Distribution Functions (uPDF), Parton Distribution Functions (PDFs) and structure function of proton. We have also given outlines of the following topics in this chapter:

(1) QCD evolution equations: DGLAP and BFKL with the kinematics of DIS and SIDIS.

(2) Transverse Momentum Dependent Parton Distributions Functions (TMD) with the kinematics of DIS and SIDIS and its evolution equation.

(3) Froissart bound and its applicability in DIS.

In Chapter 2, we have introduced the model of proton structure function suggested by Lastovicka and its phenomenological ranges of validity in x and Q^2. which was fitted by HERA data [57, 58]. We have refitted the model with recently complied HERA data [59] and found the phenomenological ranges of validity nearly equal to the earlier ones. The analysis does not make any big difference with the previous one except the phenomenological range of validity enhance upto $Q^2 \leq 150$ GeV^2 instead of $Q^2 \leq 120$ GeV^2. Both the two models have got singularities at $x_0 \sim 0.019$ and $x_0'' \sim 0.012$ respectively, even though each one is outside its phenomenological range of validity.

In Chapter 3, we have removed the singularities in the models discussed in chapter 2 within the entire x-range: $0 < x < 1$ by putting an extra condition on model parameters that it should be positive definite. But an effort to make a model singularity free reduces its phenomenological range of validity drastically; $Q^2 \leq 10$ GeV^2.

In Chapter 4, we have therefore improved the earlier versions of proton structure function by generalizing the definitions of defining magnification factors in uPDF such that it has power law rise in $\log Q^2$, closer to QCD. We have found that if the defining parameters satisfy certain conditions among themselves, linear rise in Q^2 and singularity free in structure functions in models of chapter 2 and 3 can be avoided.

In Chapter 5, we have incorporated the Froissart saturation bound in the self-similarity based models of proton structure functions discussed in chapter 4. Our analysis indicates that a self-similarity based model of proton structure function with power law growth in $\frac{1}{x}$ has a wider phenomenological range of validity than one with a Froissart bound compatible slower $\log^2 \frac{1}{x}$ growth suggesting that asymptotic energy scale is not yet been reached at HERA regime.

In chapter 6, we have calculated the momentum fractions carried by quarks and gluons in the models described in chapters 2 to 5. we have also compared the results with the predictions of Perturbative QCD, Lattice QCD and Ads/QCD models.

In Chapter 7, we outline how Transverse Momentum Dependent Parton Distribution Functions (TMDs) can be introduced in the self-similarity based models of proton structure functions discussed in chapters 2 and 4. Limitations of this approach are also discussed.

In Chapter 8, we have studied how the imposition of Froissart bound on uPDF changes the corresponding TMDs form. We have also shown the k_t^2-fall in TMDs w.r.t. x and k_t^2. The difference between the power law rise in $\left(\frac{1}{x}\right)$ in TMDs as discussed in chapter 7 and that of in $\left(\log\frac{1}{x}\right)^2$ discussed in this chapter has been studied.

Let us end this section with the theoretical limitation of the present work.
Although fractality in hadron-hadron and electron-positron interactions has been well established experimentally [69] , self-similarity itself is not a general property of QCD and is not yet established, either theoretically or experimentally. In this work, we have merely used the notion of self-similarity to parametrize PDFs as a generalization of the method suggested in Ref. [1] and have shown that under specific conditions among the defining parameters, logarithmic rise in Q^2 of structure function is achievable even in such an approach and has wider phenomenological range of validity in x and Q^2. However, the model based on fractal inspired parametrization of PDFs are not comparable to QCD. Modern analyses of PDFs in perturbative QCD are carried out upto Next-to-Next-to-leading order (NNLO) [137, 138] with and without Froissart saturation using standard QCD evolution equation and corresponding calculable splitting functions in several orders of strong coupling constant and compare with QCD predictions. Instead, the present work is carried out only at the level of a parton model. In this way, the models merely parametrize the input parton distributions and their evolution in a self-similarity based compact form, which contains both perturbative

and non-perturbative aspects of a formal theory, valid in a finite $x-Q^2$ range of data. It presumably implies that while self-similarity has not yet been proved to be a general feature of strong interactions, under specific conditions, experimental data can be interpreted with this notion as has been shown in the present chapter. To prove it from the first principle is the future course of the present approach.

References

[1] T. Lastovicka, Euro. Phys. J. C **24**, 529 (2002); hep-ph/0203260.

[2] B. B. Mandelbrot, *Fractal Geometry of Nature* (W H Freeman, New York 1982).

[3] M. Glück, E. Reya and A. Vogt, Euro. Phys. J. C **5**, 461 (1998); hep-ph /9806404.

[4] Y. L. Dokshitzer, Sov. Phys. JETP **46**, 641 (1977).

[5] V. N. Gribov and L. N. Lipatov, Sov. J. Nucl. Phys. **15**, 438 (1972).

[6] G. Altarelli and G. Parisi, Nucl. Phys. B **126**, 298 (1977).

[7] E. A. Kuraev, L. N. Lipatov, and V. S. Fadin, Sov. Phys. JETP **45**, 199 (1977).

[8] V. S. Fadin, E. A. Kuraev, and L. N. Lipatov, Phys. Lett. B **60**, 50 (1975).

[9] E. A. Kuraev, L. N. Lipatov, and V. S. Fadin, Sov. Phys. JETP **44**, 443 (1976).

[10] I. I. Balitsky and L. N. Lipatov, Sov. J. Nucl. Phys. **28**, 822 (1978).

[11] L. N. Lipatov, *Perturbative QCD* (World Scientific, Singapore, 1989).

[12] J. C. Collins, Acta Phys. Polon. B **34** (2003) 3103, hep-ph/0304122.

[13] L. V. Gribov, E. M. Levin and M. G. Ryskin, Phys. Rept. **100** (1983).

[14] J. Jalilian-Marian, A. Kovner, A. Leonidov and H. Wignert, Nucl. Phys. B **504**, 415 (1997).
E. Iancu, A. Leonidov and L. D. McLerran, Phys. Lett. B **510**, 133 (2001).

[15] J. C. Collins, D. E. Soper and G. F. Sterman, Adv. Ser. Direct. High Energy Phys. **5**, 1 (1988); hep-ph/ 0409313.

[16] J. C. Collins and D. E. Soper, Nucl. Phys. B **193**, 381 (1981).
Ibid **213**, 545 (1983)

[17] J. C. Collins and D. E. Soper, Nucl.Phys. B **194**, 445 (1982).

[18] J. C. Collins, D. E. Soper, and G. F. Sterman, Nucl.Phys. B **250**, 199 (1985).

[19] M. Boglione et al., Phys. Lett. B **766**, 245 (2017); hep-ph/ 1611.10329.

[20] I. I. Balitsky, Nucl. Phys. B **463**, 99 (1996).
Y. V. Kovchegov, Phys. Rev. D **60**, 034008 (1999).
Y. V. Kovchegov, Phys. Rev. D **61**, 074018 (2000).

[21] J. C. Collins, *Foundations of perturbative QCD*, (Cambridge, UK: Univ.Pr. 2011).

[22] J. C. Collins and D. E. Soper, Nucl. Phys. B **194**, 445 (1982).

[23] J. C. Collins and D. E. Soper, Nucl. Phys. B **193**, 381 (1981).
Ibid. **213**, 545 (1983).

[24] M. Anselmino, M. Boglione, U. D'Alesio, E. Leader and F. Murgia, Phys. Rev. D **70**, 074025 (2004); hep-ph/0407100.

[25] M. Anselmino, M. Boglione, U. D'Alesio, E. Leader, S. Melis and F. Murgia, Phys. Rev. D **73**, 014020 (2006); hep-ph/0509035.

[26] M. Anselmino et al., Eur. Phys. J. A **39**, 89 (2009); hep-ph/0805.2677.

[27] M. Anselmino, M. Boglione, U. D'Alesio, S. Melis, F. Murgia and A. Prokudin, Phys. Rev. D **79**, 054010 (2009), hep-ph/0901.3078.

[28] P. Schweitzer, T. Teckentrup and A. Metz, Phys. Rev. D **81**, 094019 (2010), hep-ph/1003.2190.

[29] U. D'Alesio and F. Murgia, Prog. Part. Nucl. Phys. **61**, 394 (2008), hep-ph/ 0712.4328.

[30] S. M. Aybat and T. C. Rogers, Phys. Rev. D **83**, 114042 (2011), hep-ph/1101.5057.

[31] J. C. Collins, D. E. Soper and G. F. Sterman, Nucl. Phys. B **261**, 104 (1985),
Ibid **308**, 833 (1988).

[32] A. V. Efremov, O. V. Teryaev and P. Zavada; hep-ph/1511.01164.

[33] M. Froissart, Phys. Rev. **123**, 1053 (1961).

[34] A. Martin, Nuovo Cimento **42**, 930 (1966).

[35] A. Martin, Phys. Rev. **129**, 1432 (1963).

[36] Y. S. Jin and A. Martin, Phys. Rev. **135**, B1375 (1964).

[37] L. Lukaszuk and A. Martin, Nuov. Cimen. **52** A, 122 (1967).

[38] S. M. Roy, Phys. Lett. B **36**, 353 (1971).

[39] S. M. Roy, hep-ph/1602.03627.

[40] T. T. Wu, A. Martin, S. M. Roy, and V. Singh, Phys. Rev. D **84**, 025012 (2011); hep-ph/1011.1349.

[41] S. M. Roy, Phys. Reports, **5C**, 125 (1972);
J. Kupsch, Nuovo Cim. **71A**, 85 (1982).

[42] H. Cheng and T. T. Wu, Phys. Rev. Lett. **24**, 1456 (1970).
C. Bourrely, J. Soffer, and T. T. Wu, Phys. Rev. D **19**, 3249 (1979).
Nucl. Phys. B **247**, 15 (1984).
Z. Phys. C **37**, 369 (1988).
Eur. Phys. J. C **28**, 97 (2003).
Eur. Phys. J. C **71**, 1061 (2011).

[43] M. M. Block et al., Phys. Rev. D **60**, 054024 (1999).
M. M. Block, Phys. Reports, **436**, 71 (2006).
M. M. Block and F. Halzen, Phys. Rev. D **83**, 077901(2011).

[44] M. M. Islam et al., Int. J. Mod. Phys. A **21**, 1 (2006).

[45] Totem collaboration, G. Antchev et al, Europhys. Lett. **96**, 21002 (2011) and **101**, 21004(2013).
Phys. Rev. Lett. **111**, 012001 (2013);
Nucl. Phys. B **899**,527 (2015).

[46] CMS collaboration, Phys. Lett. B **722**, 5 (2013).

[47] Atlas collaboration, Nature Comm. **2**, 463 (2011).
Nucl. Phys. B **889**, 486 (2014).

[48] Alice collaboration, Eur. Phys. J. C **73** 2456, (2013); hep-ex/1208.4968.

[49] Pierre Auger collaboration, Phys. Rev. Lett. **109**, 062002 (2012).

[50] S. Eidelman et al., (Particle data Group) Phys. Lett. B **592**, 1 (2004) and 2005 partial update, http://pdg.lbl.gov/2005,Table 40.2.
J. Beringer et al., (Particle data Group) Phys. Rev. D **86**, 010001(2012) and 2013 partial update, http://pdg.lbl.gov/2013,Table 50.

[51] D. Greynat and E. de Rafael, hep-ph/ 1305.7045.

[52] R. G. Roberts, *The Structure of the proton: Deep inelastic scattering* (Cambridge University Press, 1994).

[53] M. M. Block et al., Phys. Rev. D **84**, 094010 (2011); hep-ph/1108.1232.

[54] M. M. Block and F. Halzen, Phys. Rev. D **72**, 036006 (2005);
Ibid **72**, 039902 (2005); hep-ph/0506031

[55] M. M. Block et al., Phys. Rev. D **88**, 014006 (2013).

[56] M. M. Block et al., Phys. Rev. D **88**, 013003 (2013); hep-ph/ 1302.6127.

[57] H1: C. Adloff et al., Euro. Phys. J. C **21**, 33-61 (2001); hep-ex/0012053.

[58] ZEUS: J. Breitweg et al., Phys. Lett. B **487**, 53 (2000); hep-ex/0005018.

[59] H1 and ZEUS Collaborations, F. D. Aaron et al., JHEP **01**, 109 (2010); hep-ex/0911.0884.

[60] L. F. Abbot, W. B. Wood and R. M. Barnett, Phys. Rev. D **22**, 582 (1980).

[61] L. N. Lipatov, Sov. J. Nucl. Phys. **20**, 94 (1975).

[62] M. Gell Mann and F. Low, Phys. Rev. D **95**, 1300 (1954).

[63] D. V. Shirkov, Sov. Phys. Dokl. **27**, 197 (1982).

[64] K. Kröger, Phys. Reports **323**, 81 (2000).

[65] Jean-Francois Gouyet, *Physics and Fractal Structures*, (Springer Verlag, 1996).

[66] Y. Baryshev and P. Teerikorpi, *Discovery of Cosmic Fractals*, (World Scientific Press, 2002).

[67] A. Bialas and R. Peschanski, Nucl. Phys. B **703**, 273 (1986).
Ibid **857**, 308 (1988).

[68] D. Ghosh et al., Phys. Rev. D **46**, (1992).

[69] Wu Yuanfang and Liu Lianshou, Int. J. Mod. Phys. A **18**, 5337 (2003).

[70] J. D. Bjorken, SLAC-PUB-**6477** (1994).

[71] I. M. Dremin and B. B. Levtchenko, Phys. Lett. B **155**, 292 (1992).

[72] D. K. Choudhury and Rupjyoti Gogoi, hep-ph/0310260;
D. K. Choudhury and Rupjyoti Gogoi, hep-ph/0503047.

[73] D. K. Choudhury and Rupjyoti Gogoi, Ind. J. Phys. **80**, 823 (2006).

[74] D. K. Choudhury and Rupjyoti Gogoi, Ind. J. Phys.**81**, 607 (2007).

[75] A. Jahan and D. K. Choudhury, hep-ph/1106.1145.

[76] A. Jahan and D. K. Choudhury, in *Proceedings of the 3rd International Workshop on Multiple Partonic Interactions at the LHC* (2012), **145** ; DOI:10.3204/DESY HUMBERG -PROC-2012-03/94.

[77] A. Jahan and D. K. Choudhury, Ind. J. Phys. **85**, 587 (2011); hep-ph/1101.0069.

[78] A. Jahan and D. K. Choudhury, Mod. Phys. Lett. A **27**, 1250193 (2012); hep-ph/1304.6882.

[79] A. Jahan and D. K. Choudhury, Mod. Phys. Lett. A **28**, 1350056 (2013); hep-ph/1306.1891.

[80] D. K. Choudhury and A. Jahan, Int. J. Mod.Phys. A **28**, 1350079 (2013); hep-ph/1305.6180.

[81] A. Jahan and D. K. Choudhury, Commun. Theo. Phys. **61** (2014), 654; hep-ph/1404.0808.

[82] A. Jahan and D. K. Choudhury, Phys. Rev. D **89**, 014014 (2014); hep-ph/1401.4327.

[83] R. Angeles-Martinez et al., Acta physica polonica B **46**, 2501 (2015).

[84] M. M. Block et al., Phys. Rev. Lett. **97**, 252003 (2006)

[85] T. Regge, Nuovo Cim. **14**, 951 (1959).

[86] R. G. Roberts, *The Structure of the proton: Deep inelastic scattering*, (Cambridge University Press, 1994).

[87] R. Devenish and A. Cooper-Sarkar, *Deep inelastic scattering*, (Oxford University Press, 2004).

[88] F. J. Yndurain, *Theory of Quark and Gluon Interactions*, (Springer Verlag, Berlin, p129 1992).

[89] Richard D. Ball, Emanuele R. Nocera and Juan Rojo, hep-ph/1604.00024.

[90] S. J. Brodsky and G. R. Farrar, Phys. Rev. Lett. **31**, 1153 (1973).

[91] J. Pumplin et al., JHEP **07**, 012 (2002), hep-ph/0201195.

[92] ZEUS and H1 Collaborations, H. Abramowicz et al., Eur. Phys. J. C **75** (2015) 580; hep-ex/1506.06042.

[93] ZEUS Collaboration, H. Abramowicz et al., hep-ex/1603.09628.

[94] David J. Gross and Frank Wilczek, *Phys.Rev. D* **9**, 980 (1974).

[95] H. D. Politzer, Phys. Rev. D **9**, 2174 (1974).

[96] G. Altarelli, Phys. Rep. **81**, 1 (1982).

[97] Xiang-Song Chen *et al.*, Phys. Rev. Lett. **103**, 062001 (2009), hep-ph/0904.0321.

[98] Xiangdong Ji, Phys. Rev. Lett. **106**, 259101 (2011), hep-ph/0910.5022.

[99] M. Deka *et al.*, Phys. Rev. D **91**, 1 (2015), hep-lat/1312.4816.

[100] R. S. Bhalerao, Phys. Lett. B **380**, 1 (1996), hep-ph/9607315.

[101] H. Navelet *et.al.*, Phys. Lett. B **385**, 357 (1996).

[102] M. Bertini Thesis, *Phenomenological study of Nucleon Structure Function*, (1995) http://www.iaea.org/inis/collection/NCLCollectionStore/_Public/27/049/27049057.pdf.

[103] A. Watanabe and K. Suzuki, Phys. Rev. D **86**, 035011 (2012).

[104] A. Watanabe and K. Suzuki, Phys. Rev. D **89**, 115015 (2014).

[105] A. Watanabe and K. Suzuki, in *Proceedings of the 10th International Workshop on the Physics of Excited Nucleons (NSTAR2015)*, hep-ph/1510.00153.

[106] D. K. Choudhury and B. Saikia, Int. J. Mod. Phys. A **31**, 1650176 (2016), hep-ph/1605.01149.

[107] D. K. Choudhury and J. K. Sarma, Pramana **39**, 273 (1992).
J. K. Sarma, D. K. Choudhury and G. K. Medhi, Phys. Lett. B **403**, 139 (1997).
D. K. Choudhury, J. Phys. Conf. Ser. IOP, **481** (2014) 012001, DOI:10.1088/1742-6596/481/1/012001, ISSN 1742-6588.

[108] D. K. Choudhury and N. N. K. Borah, Phys. Rev. D **95**, 014002, (2017).

[109] I. N. Sneddon, *Elements of Partial differential Equation* (McGraw Hill, New York, NY USA, 1957).

[110] F. E. Close, *An Introduction to Quarks and Partons* (Academic Press, p.233 1979).

[111] T. Sloan, G. Smadja and R. Voss, Phys. Rep. **162**, 45 (1988).

[112] D. K. Choudhury and P. K. Dhar, Ind. J. Phys. **81** 259 (2007).

[113] C. Lopez and F. J. Yndurain, Nucl. Phys. B **171**, 231 (1980).

[114] Tanmay Maji and Dipankar Chakrabarti, hep-ph/1608.07776.

[115] T. Gutsche, V. E. Lyubovitskij, I. Schmidt and A. Vega, Phys. Rev. D **89**, 054033 (2014).
ibid. **92**, 019902 (2015).

[116] T. Gutsche, V. E. Lyubovitskij, I. Schmidt and A. Vega, Phys. Rev. D **91**, 054028 (2015).

[117] ZEUS Collaboration, S. Chekanov et al., Phys. Rev. D **67**, 012007 (2003), hep-ex/0208023.

[118] G. P. Lepage and S. J. Brodsky, Phys. Rev. D **22**, 2157 (1980).

[119] D. K. Choudhury, B. Saikia and K. Kalita, hep-ph/1608.02771.

[120] M. Anselmino, M. Boglione, U. D'Alesio, A. Kotzinian, F. Murgia and A. Prokudin, Phys. Rev. D **71**, 074006 (2005).

[121] A. V. Efremov, P. Schweitzer, O. V. Teryaev and P. Zavada, Phys. Rev. D **80**, 014021 (2009).

[122] U. D'Alesio, E. Leader and F. Murgia, Phys. Rev. D **81**, 036010 (2010); hep-ph/0909.5650.

[123] P. Zavada, Phys. Rev. D **83**, 014022 (2011), hep-ph/0908.2316.

[124] S. J. Brodsky, D. S. Hwang, B. Q. Ma and I. Schmidt, Nucl. Phys. B **593**, 311 (2001); hep-th/0003082.

[125] M. Anselmino et al., Nucl. Phys. Proc. Suppl. **191**, 98-107 (2009); hep-ph/0812.4366.

[126] M. Anselmino et al., Phys. Rev. D **86**, 074032 (2012); hep-ph/1207.6529.

[127] M. Anselmino et al., Phys. Rev. D **75**, 054032 (2007); hep-ph/0707.1197.

[128] X. Ji, J. Ma, and F. Yuan, Phys. Rev. D **71**, 034005 (2005), hep-ph/0404183.

[129] J. C. Collins and A. Metz, Phys. Rev. Lett. **93**, 252001 (2004), hep-ph/0408249.

[130] A. Bacchetta, D. Boer, M. Diehl, and P. J. Mulders, JHEP **08**, 023 (2008), hep-ph/0803.0227.

[131] S. Catani, M. Ciafaloni, F. Hautmann, Phys. Lett. B **242**, 97 (1990).

[132] S. Catani, M. Ciafaloni, F. Hautmann, Nucl. Phys. B **366**, 135 (1991).

[133] L. P. Gamberg, G. R. Goldstein and M. Schlegel, Phys. Rev. D **77**, 094016 (2008), hep-ph/0708.0324.

[134] M. I. Gresham, Ian-Woo Kim and K. M. Zurek, Phys. Rev. D **85**, 014022 (2012), hep-ph/1107.4364.

[135] H. H. Matevosyan, A. Kotzinian and A. W. Thomas, Phys. Lett. B **731**, 208 (2014), hep-ph/1312.4556.

[136] Hrayr H. Matevosyan, Wolfgang Bentz, Ian C. Cloet and Anthony W. Thomas, hep-ph/1111.1740.

[137] S. Moch J. A. M. Vermaseren and A. Vogt, Nucl. Phys. Proc. Suppl. **116**, 100 (2003)

[138] S. Moch J. A. M. Vermaseren and A. Vogt, Nucl. Phys. B **688**, 101 (2004)

A

Momentum fractions carried by quarks and gluons in analytical approach and its limitation

A.1 Analytical Expression of $\langle \hat{x} \rangle_q$ and its limitations:

The analytical expression of $\langle \hat{x} \rangle_q$ is given as (Eq.(23) of Ref. [79]) which is corresponding to model 1 of chapter 2:

$$\langle \hat{x} \rangle_q = \frac{e^{\tilde{D_0}} Q_0^2}{D_1 M^2} e^{\left(\frac{1+D_3}{D_1}\right)(2-D_2)} \left\{ \left(1+\frac{Q^2}{Q_0^2}\right)^{D_3+1} e^{-\left(\frac{1+D_3}{D_1}\right) D_1 \log\left(1+\frac{Q^2}{Q_0^2}\right)} I_1 - I_2 \right\} \tag{A.1}$$

where the integrals I_1 and I_2 are expressible in terms of infinite series

$$I_i = \int \frac{e^{\mu_i z}}{z} dz = \log|z| + \sum_{n=1}^{\infty} \frac{\mu_i^n z^n}{n.n!} \quad , \; i = 1,2 \tag{A.2}$$

where

$$z = \frac{1+D_3}{D_1} + \log\frac{1}{x} \tag{A.3}$$

and

$$\mu_1 = D_1 \log\left(1 + \frac{Q^2}{Q_0^2}\right) + D_2 - 1 \tag{A.4}$$

$$\mu_2 = D_2 - 1 \tag{A.5}$$

In Ref. [79], only the 1st term of the infinite series is taken into account without taking into account the convergence property and their Q^2-dependence. Below, we address to this point.

A.1.1 Q^2-dependence of the convergence of the infinite series:

The integral I_1 is Q^2-dependent while I_2 is not, as can be seen from Eq. A.4 and A.5 above. Convergent condition between nth and (n-1)th term of the infinite series is

$$\frac{\mu_i^{(n-1)} . z^{(n-1)}}{(n-1).(n-1)!} \gg \frac{\mu_i^n . z^n}{n.n!} \quad ; \; i = 1,2 \tag{A.6}$$

leading to

$$z \ll \frac{n^2}{(n-1)} . \frac{1}{\mu} \tag{A.7}$$

It can be explicitly seen that if one includes more and more terms in the infinite series I_1, the convergent condition shifts to higher values of Q^2. As an illustration, the relative convergence taking respectively the ratios of the 3rd vs 2nd term, 4th vs 3rd term, 5th vs 4th, 6th vs 5th term results in the inequalities as

Table A.1 Values of $\langle \hat{x} \rangle_q$ with higher order terms in I_1 and I_2 for different Q^2

Q^2(GeV^2)	$\langle \hat{x} \rangle_q$ (n=1)	$\langle \hat{x} \rangle_q$ (n=2)	$\langle \hat{x} \rangle_q$ (n=3)	$\langle \hat{x} \rangle_q$ (n=4)	$\langle \hat{x} \rangle_q$ (n=5)
$Q^2 = Q_0^2$	3.7×10^{-2}	-1.63×10^{-1}	5.07×10^{-1}	-1.164	2.170
10	2.781×10^{-1}	-9.52×10^{-1}	2.527	-4.950	8.107
20	3.163×10^{-1}	-1.037	2.694	-5.169	8.360
40	3.582×10^{-1}	-1.112	2.830	-5.329	8.5330
60	3.750×10^{-1}	-1.150	2.897	-5.399	8.6050
80	3.911×10^{-1}	-1.176	2.939	-5.455	8.660
100	4.037×10^{-1}	-1.194	2.969	-5.467	8.672

$$\log\left(1+\frac{Q^2}{Q_0^2}\right) \ll 15.384 \tag{A.8}$$
$$\ll 45.454 \tag{A.9}$$
$$\ll 52.631 \tag{A.10}$$
$$\ll 58.823 \tag{A.11}$$

These inequalities saturates at 2.9×10^5, 3.4×10^{18}, 4.4×10^{21}, 2.1×10^{24} GeV^2 respectively, which are far above the experimentally accessible HERA range 3×10^4 GeV^2 [59]. However, it is the slow convergence of the two infinite series which makes the result highly unstable.

In column 2 of Table A.1, we record the result of Ref. [79] taking only one term of the infinite series. In the same table, we now show the corresponding results taking 2, 3, 4, 5 terms of the two infinite series. In column 3, all $\langle \hat{x} \rangle_q$ are negative. From column 4, it is seen, saturation occurs below Q^2=10 GeV^2 and in column 5, again all $\langle \hat{x} \rangle_q$ are negative while in column 6, saturation occurs even below $Q^2 = Q_0^2$ GeV^2.

A.1.2 Semi-analytical and Numerical result:

As a consequences of the limitation of the analytical method, we take recourse to semi analytical method i.e. we evaluate I_1 and I_2 numerically. Here, I_2 is Q^2-independent and is obtained as 8.249×10^{-3}

Table A.2 Values of $\langle\hat{x}\rangle_q$ with I_1 and $\langle\hat{x}\rangle_g$ for different Q^2 using semi-analytical method

$Q^2(\mathrm{GeV}^2)$	I_1	$\langle\hat{x}\rangle_q$	$\langle\hat{x}\rangle_g$
$Q^2 = Q_0^2$	1.0762×10^{-2}	1.941×10^{-4}	9.998×10^{-1}
10	6.026×10^{-2}	4.020×10^{-3}	9.959×10^{-1}
20	7.975×10^{-2}	5.527×10^{-3}	9.944×10^{-1}
40	1.059×10^{-1}	7.549×10^{-3}	9.924×10^{-1}
80	1.407×10^{-1}	1.023×10^{-2}	9.897×10^{-1}
120	1.669×10^{-1}	1.226×10^{-2}	9.877×10^{-1}
5.62×10^4	3.0558	2.355×10^{-1}	7.645×10^{-1}
3.61×10^5	9.223	7.123×10^{-1}	2.877×10^{-1}
6×10^6	12.870	~ 1	~ 0

In Table A.2, we record the numerical values of I_1 together the values of $\langle\hat{x}\rangle_q$. From above, it is seen I_1 and I_2, the two infinite series are positive definite and hence $\langle\hat{x}\rangle_q$ and $\langle\hat{x}\rangle_g$ also. Column 3 represents the $\langle\hat{x}\rangle_q$ and column 4 represents the upper limit of $\langle\hat{x}\rangle_g$. $\langle\hat{x}\rangle_q$ saturates at $Q^2 = 6\times10^5\mathrm{GeV}^2$. It is interesting to compare the corresponding saturation scale $Q^2 = 5.43\times10^6$ GeV^2 of the 1st term of the infinite series of Ref. [79] which is of course found to be unstable.

In Table A.3, we record the numerical values $\langle\hat{x}\rangle_q$ and $\langle\hat{x}\rangle_g$ of model of Ref. [1] for a few representative values of Q^2 using Eq. A.12 and A.13

$$\langle\hat{x}\rangle_q = \int_{x_a}^{x_b} aF_2(x,Q^2)dx \tag{A.12}$$

$$\langle\hat{x}\rangle_g = 1 - \langle\hat{x}\rangle_q \tag{A.13}$$

instead of Eq. A.1.

From Tables A.2 and A.3, we observe that in the present model, as Q^2 increases, $\langle\hat{x}\rangle_q$ too increases while $\langle\hat{x}\rangle_g$ decreases. However, unlike QCD, the model can not be extrapolated beyond Q_s^2=3.9×10^6 GeV^2, its saturation limit.

Table A.3 Numerical values of $\langle\hat{x}\rangle_q$ and $\langle\hat{x}\rangle_g$ for different Q^2

Q^2(GeV^2)	$\langle\hat{x}\rangle_q$	$\langle\hat{x}\rangle_g$
$Q^2 = Q_0^2$	2.114×10^{-3}	9.978×10^{-1}
10	2.158×10^{-2}	9.784×10^{-1}
20	2.595×10^{-2}	9.740×10^{-1}
40	3.094×10^{-2}	9.690×10^{-1}
60	3.426×10^{-2}	9.657×10^{-1}
80	3.662×10^{-2}	9.633×10^{-1}
120	4.038×10^{-2}	9.596×10^{-1}
580	5.831×10^{-2}	9.416×10^{-1}
3.9×10^6	~ 1	~ 0

A.1.3 Comparison with standard QCD asymptotic:

We note that in Refs. [94, 98], the asymptotic QCD predictions of $\langle x\rangle_q$ and $\langle x\rangle_g$ are:

$$\lim_{Q^2\to\infty}\langle x\rangle_q = \frac{3N_f}{2N_g+3N_f}, \tag{A.14}$$

$$\lim_{Q^2\to\infty}\langle x\rangle_g = \frac{2N_g}{2n_g+3N_f}, \tag{A.15}$$

Here, n_f and n_g represent the number of active flavors and number of gluons respectively. for SU(3)$_c$, $n_g = 8$. In Ref. [97], it has alternative asymptotic prediction:

$$\lim_{Q^2\to\infty}\langle x\rangle_q = \frac{6N_f}{N_g+6N_f}, \tag{A.16}$$

$$\lim_{Q^2\to\infty}\langle x\rangle_g = \frac{N_g}{N_g+6N_f}, \tag{A.17}$$

While Eqs. A.14 and A.15 implies that except for $N_f = 6$, $\langle x\rangle_q < \langle x\rangle_g$. Eqs. A.16 and A.17 indicates the opposite asymptotic feature $\langle x\rangle_q > \langle x\rangle_g$. In the above Eqs. A.14-A.17, $\langle x\rangle_q$ and $\langle x\rangle_g$ denotes the momentum fractions carried by quarks and gluons respectively for entire x-range $0 < x < 1$

However, still it will be interesting to calculate the momentum scale Q^2 for model 1, at which the model prediction of partial momentum fractions carried by quarks $\langle\hat{x}\rangle_q$ coincides

Table A.4 Values of momentum scale Q^2 of the model corresponds to flavored dependent asymptotic QCD predictions of $\langle x \rangle_q$

n_f	$\langle x \rangle_q$	$Q^2(\text{GeV}^2)$
3 Ref[1,2]	9/25	3.8×10^5
4 Ref[1,2]	3/7	5.5×10^5
5 Ref[1,2]	15/31	7.5×10^5
6 Ref[1,2]	9/17	9.3×10^6
3 Ref[3]	9/13	1.76×10^6
4 Ref[3]	3/4	2.13×10^6
5 Ref[3]	15/19	2.37×10^6
6 Ref[3]	9/11	2.56×10^6

with the corresponding asymptotically predicted momentum fractions $\langle x \rangle_q$ in standard QCD. This is shown in Table A.4.

Table A.4 shows the results of asymptotic values of $\langle x \rangle_q$. As an illustration, asymptotic value of $\langle x \rangle_q$= 15/19 of Ref. [97] is achieved for $\langle \hat{x} \rangle_q$ at Q^2=2.37×10^6 GeV^2.

ADDENDA

List of Publications

Papers published

1. D. K. Choudhury, Baishali Saikia and K. Kalita, *“Momentum Fractions carried by quarks and gluons in models of proton structure functions at small x"*, *Int. J. Mod. Phys. A* **32**, 1750107 (2017), ISSN: 0217-751X .

2. Baishali Saikia and D. K. Choudhury, *“An improved singularity free self-similar model of Proton Structure Function"*, accepted in *Communication in Theoretical Physics*, Commun. Theor. Phys. **67**, 61 (2017), ISSN: 0253-6102 .

3. D. K. Choudhury and Baishali Saikia, *“Parton Distribution Functions and models of proton structure functions with self-similarity"*, *Int. J. Mod. Phys. A* **31**, 1650176 (2016), ISSN: 0217-751X .

4. D. K. Choudhury and Baishali Saikia, *“A re-analysis of momentum fractions carried by quarks and gluons in a model of proton structure function at small x"* J. Assam Sc. Soc. **56**, 112 (2015), ISSN: 0587-1921 .

Papers submitted

1. D. K. Choudhury and Baishali Saikia, *“Froissart bound and self-similarity based models of proton structure functions"*, hep-ph/1704.03235,
- under review (International Journal of Modern Physics A).

2. Baishali Saikia and D. K. Choudhury, *“Froissart Bound and Transverse Momentum Dependent Parton Distribution Functions (TMDPDF) with self-similarity"*, hep-ph/1710.04911,
- under review (Communication in Theoretical Physics).

Conference Proceedings

1. Baishali Saikia and D. K. Choudhury, *“A self-similarity based model of proton structure function at large and small x with logarithmic rise in Q^2"*, p7 (2017), ISBN: 978-93-86256-85-0, Excel India Publishers.

Conference attended

1. Presented a poster entitled *“A model of proton structure function $F_2(x,Q^2)$ with self-similarity at small x"* at National Conference on Theoretical Physics (NCTP) held at Tezpur University, Tezpur during February 8-12, 2013.

2. Presented a poster entitled *“An improved self-similar model of Proton Structure Function at small x"* at IXth National conference of Physics Academy of North East (PANE) held at North Eastern Regional Institute of Science and Technology (NERIST), Nirjuli, Arunachal Pradesh during December 18-20, 2014.

3. Presented a poster entitled *“A singularity free self-similar model of Proton at small x and analysis of quarks and gluons momentum fractions"* at National Conference on Current Issues in Cosmology, Astrophysics and High Energy Physics (CICAHEP) held at Dibrugarh

University, Assam during November 2-5, 2015.

4. Presented oral entitled *“A re-analysis of momentum fractions carried by quarks and gluons in a model of proton structure function at small x"* at 61th Annual Technical Session of Assam Science Society held at Department of Physics, Goalpara College, Goalpara on January 23, 2016.

5. Presented oral entitled *“A self-similarity based model of Proton structure function at large and small x with logarithmic rise in* Q^2*"* at Xth biennial conference of Physics Academy of North East (PANE) held at St. Anthony’s College, Shillong during November 10-12, 2016.

School/Meeting/Workshop attended

1. Preparatory Level SERC School in Theoretical High-Energy Physics held at Tezpur University, Tezpur during June 17- July 13, 2013.

2. Discussion Meeting on EWSB and Flavor Physics held at Indian Institute of Technology, Guwahati (IIT-G) during February 20-22, 2014.

3. Workshop on Nonlinear Dynamics and Application (NDA 2014) held at Tezpur University, Tezpur during March 14-15, 2014.

4. Introductory Workshop on Relativistic Astrophysics held at Gauhati University in collaboration with Inter University Centre for Astronomy and Astrophysics (IUCAA), Pune during August 21-23, 2014.

5. Inter-University Accelerator Centre (IUAC) Acquaintance Program on Accelerator based multi-disciplinary scientific research held at Department of Physics, Gauhati University on 16th November, 2015.

6. School cum workshop on Collider Physics : Events, Analysis and QCD held at Department of Physics, Indian Institute of Technology Guwahati (IIT-G) during March 27-31, 2017.